Harkers Island Bridge Replacement: Material Characterization and Structural Performance

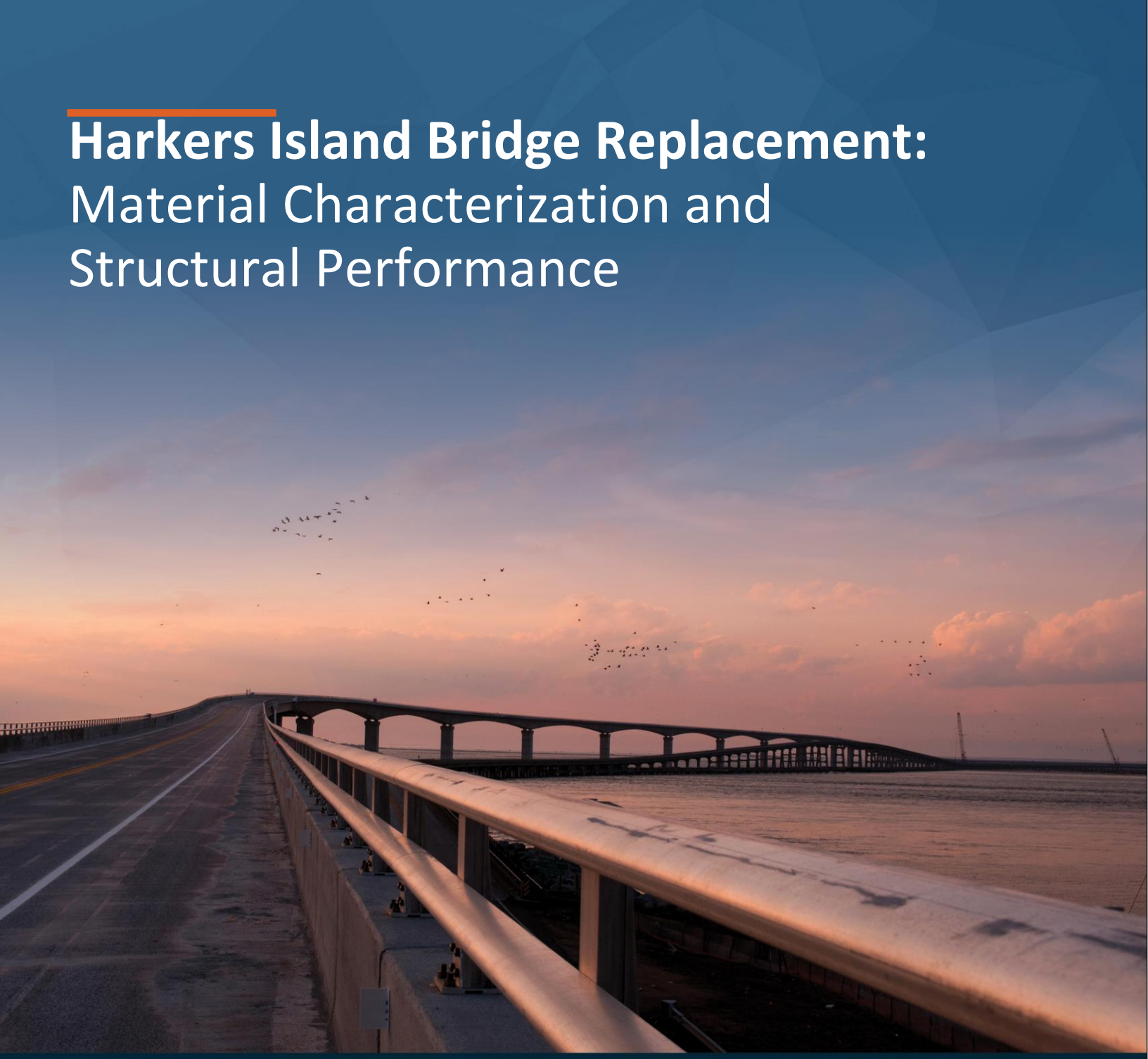

NCDOT Project 2022-08
FHWA/NC/2022-08
March 2026

Paul Acuña
Rudolf Seracino, Ph.D.

Department of Civil, Construction, and Environmental Engineering
North Carolina State University

RESEARCH & DEVELOPMENT

Harkers Island Bridge Replacement: Material Characterization and Structural Performance

FINAL REPORT

Submitted to:
North Carolina Department of Transportation
Office of Research
(Research Project No. RP2022-08)

Submitted by

Principal Investigator	Dr. Rudolf Seracino
Research Assistant	Paul Acuña

Department of Civil, Construction, and Environmental Engineering
North Carolina State University
Raleigh, NC

March 2026

Technical Report Documentation Page

1. Report No. **FHWA/NC/2022-08**	2. Government Accession No.	3. Recipient's Catalog No.	
4. Title and Subtitle **Harkers Island Bridge Replacement:** **Material Characterization and Structural Performance**		5. Report Date **March 2026**	
		6. Performing Organization Code	
7. Author(s) **Paul Acuña** (https://orcid.org/0009-0006-1997-7155) **Rudolf Seracino, Ph.D.** (https://orcid.org/0000-0003-2821-3633)		8. Performing Organization Report No.	
9. Performing Organization Name and Address **Department of Civil, Construction, and Environmental Engineering** **North Carolina State University** **915 Partners Way** **Raleigh, NC 27606**		10. Work Unit No. (TRAIS)	
		11. Contract or Grant No.	
12. Sponsoring Agency Name and Address **North Carolina Department of Transportation** **Research and Development Unit** **1549 Mail Service Center** **Raleigh, North Carolina 276699-1549**		13. Type of Report and Period Covered **August 2021 – December 2025**	
		14. Sponsoring Agency Code **RP2022-08**	
15. Supplementary Notes			
16. Abstract The Harkers Island Bridge replacement is North Carolina's first bridge in which all primary load-carrying components use internal fiber-reinforced polymer (FRP) reinforcement. The project combines carbon FRP (CFRP) prestressing strands and spirals with glass FRP (GFRP) bars in piles, girders, substructure, and deck. This companion research program documents bridge construction, characterizes the FRP materials, and develops practical recommendations for project-level quality assurance/quality control (QA/QC), detailing, and future code development. An extensive material-testing program showed that all CFRP strands from 73 production lots exceeded the specified minimum strength and tensile modulus. Bent bar tests on CFRP spirals confirmed substantial strength reduction at bends, while GFRP bar tests verified compliance with ASTM D7957 but exposed gaps in sampling and traceability. Statistical analyses indicate that 2 to 5 tension tests per lot can provide acceptable confidence levels for project-level QA/QC. Field observations informed recommendations on end-region detailing, lifting systems, handling practices, and tagging. Overall, the project demonstrates that all-FRP reinforced, prestressed concrete bridges are technically feasible within conventional schedules and highlights where specifications, standards, and QA/QC practices must evolve to support broader implementation.			
17. Keywords **Fiber-Reinforced Polymer (FRP), Carbon FRP, Glass FRP, Prestressed Concrete Bridges, Quality Assurance, Quality Control**		18. Distribution Statement	
19. Security Classif. (of this report) **Unclassified**	20. Security Classif. (of this page) **Unclassified**	21. No. of Pages **165**	22. Price

Form DOT F 1700.7 (8-72) **Reproduction of completed page authorized**

DISCLAIMER

The contents of this report reflect the views of the authors and are not necessarily the views of North Carolina State University. The authors are responsible for the facts and the accuracy of the data presented herein. The contents do not necessarily reflect the official views or policies of the North Carolina Department of Transportation at the time of publication. This report does not constitute a standard, specification, or regulation.

AUTHORSHIP NOTE

Portions of this report may be used verbatim in the Ph.D. dissertation of Paul Acuna, as part of his doctoral work at North Carolina State University. The author has contributed directly to the content presented herein.

ACKNOWLEDGEMENTS

The research team gratefully acknowledges the financial support of the North Carolina Department of Transportation (NCDOT) and the guidance provided by the Steering and Implementation Committee throughout this project. The Steering and Implementation Committee included:

Trey Carroll, Chair
Randy Hall
Darin Waller
Cabell Garbee
Gordy Eure
Daniel Muller (FHWA)
Boyd Tharrington
Todd Whittington
Mustan Kadibhai
Curtis Bradley

The authors also wish to thank Balfour Beatty, the principal contractor for the Harkers Island Bridge, for their support and collaboration. In particular, the assistance of Peter Distefano (Project Manager) and Will Janning (Project Engineer) is gratefully acknowledged. They consistently welcomed the research team at monthly progress meetings and during site visits, facilitated access to the work areas, and generously shared their experience and observations on the use of FRP materials in construction.

Appreciation is extended to Coastal Precast Systems (CPS) for accommodating multiple visits during the production of piles and girders. The team is especially thankful to Josh Ross (Operations Manager) for coordinating access, adjusting production schedules to allow data collection, and answering numerous technical questions, and to Joe Rose (CPS President) for supporting the ongoing production of full-scale girders to be tested in shear and for providing plant space and logistical assistance.

The research team also thanks Elbert Pittman of Gannett Fleming, serving as an inspector on behalf of NCDOT, for his time and effort during field visits. His detailed explanations of ongoing construction activities and willingness to walk the site with the research team were invaluable for documenting constructability issues and solutions.

In addition to the Steering and Implementation Committee, several NCDOT staff members provided essential assistance. Jason Civils helped coordinate logistics for plant and site visits and supported material procurement. Cabell Garbee and Joshua Law, from the Materials and Tests Unit, coordinated sample delivery, discussed testing protocols, and provided valuable feedback on QA/QC procedures. Trey Carroll, Ashvin Patel, and Ahmad Ighwair contributed design- and construction-oriented perspectives during meetings and site visits and responded to technical questions throughout the project.

The authors gratefully acknowledge the contributions of undergraduate research assistants Sam Valmassoi, Juniper Walter-Eger, Marissa Osansky, and Emily Boldor, whose extensive efforts in preparing and testing hundreds of CFRP strands, GFRP bars, and CFRP spirals were critical to the material characterization program.

At NC State University's Constructed Facilities Laboratory, Dr. Greg Lucier (Laboratory Manager), and Johnathan McEntire (Laboratory Technician) provided indispensable support with test setup design, specimen preparation, and execution of the experimental program.

Finally, the research team thanks Tokyo Rope USA for their technical collaboration, including multiple meetings to discuss material properties, the sharing of internal test data that enabled extended statistical analyses, and the supply of additional materials for supplementary testing. Their openness and willingness to engage in detailed technical discussions greatly strengthened the outcomes of this project.

EXECUTIVE SUMMARY

The Harkers Island Bridge replacement project provided North Carolina with its first bridge in which all primary load-carrying components use internal fiber-reinforced polymer (FRP) reinforcement. Located in a harsh coastal environment, the new 3,200-ft-long structure replaces two deteriorated steel-prestressed cored-slab, conventionally reinforced concrete bridges that had experienced significant corrosion since their construction in the 1970s. To support NCDOT in evaluating this technology and guiding future applications, this companion research program documented the construction of the bridge, characterized the mechanical properties and variability of the CFRP and GFRP reinforcement used, evaluated constructability at full bridge scale, and developed practical recommendations for quality assurance/quality control (QA/QC), detailing, and future code development.

The bridge employs 0.6 in. seven-wire carbon FRP (CFRP) prestressing strands in piles and Florida I Beam (FIB) girders, CFRP spirals as transverse reinforcement in piles, and glass FRP (GFRP) bars as non-prestressed reinforcement in pile caps, pier columns, girders, and deck. Throughout construction (September 2021 – December 2023), the research team attended monthly progress meetings and conducted more than 20 site and plant visits, documenting constructability challenges and solutions and photographing all major stages: trestle construction, pile driving, substructure and superstructure work, and opening. Additional visits following completion focused on salvaging prestressed piles from the demolished bridge for future testing and observing early in-service performance of the new bridge.

A significant component of the project was an extensive material-testing program. For CFRP strands, tension tests were performed on a large, project-scale dataset of 0.6 in. strands sampled from 73 production lots. Because direct gripping of CFRP strands is not feasible due to their low transverse strength and braided geometry, specimens were prepared with steel pipe end anchors filled with expansive grout and tested in accordance with ASTM D7205, with anchor lengths modified to accommodate the constraints of the universal tensile machine (UTM) used. Axial strains were measured with an extensometer up to approximately 50% of the expected rupture load to establish reliable stress–strain curves and calculate tensile modulus.

The results show that the CFRP strands exhibited high tensile strength with low variability. All lots exceeded the project's minimum guaranteed tensile strength (60.7 kips), with an average rupture load of approximately 82.3 kips. The mean tensile modulus was 22,400 ksi, above the minimum 21,000 ksi required by the special provisions, although some individual specimens fell below the manufacturer's guaranteed modulus of 21,800 ksi. This discrepancy does not compromise the material's suitability for the project, but it highlights that reported tensile modulus values are sensitive to the method used to calculate the modulus, particularly the choice of strain range, treatment of machine compliance, and assumptions about the effective cross-sectional area for 7-wire CFRP strands with PET wraps. A consistent, standardized procedure for determining modulus will be essential to ensure that values reported by manufacturers, laboratories, and owners are comparable and suitable for use in design specifications.

To assess the performance of CFRP transverse reinforcement, 0.28 in. uni-strand CFRP spirals used in the piles were tested at their bend locations following an adapted version of ASTM D7914 (due to the geometry of the spirals used in the project). The tests demonstrated a substantial reduction in bend strength relative to straight companion samples, with average bend strength 41% of the straight bar rupture strength. The data also revealed considerable scatter and sensitivity to specimen geometry and alignment, reinforcing the need for bend-strength test methods that are both practical and representative. The project highlights the advantages of L-shaped bend test configurations, similar to those adopted in CSA S807, which are more easily matched to production geometries and are under active consideration by the ASTM D30.10 Committee.

Tension tests were also conducted on GFRP bars sampled from straight legs of L-, U-, and C-shaped bars used in the project. All tested bars met the tensile-strength requirements of ASTM D7957, confirming the adequacy of the GFRP reinforcement at the material level. However, QA/QC efforts were limited by how materials were supplied and labeled: not all lots were delivered to the lab, some bundles were mis-tagged or lacked traceable lot identifiers, and no dedicated bent-bar specimens were provided, so only a subset of the GFRP lots in the bridge could be directly tied to test data.

Using large datasets on CFRP strands and spirals, statistical tools were applied to determine appropriate replicate counts for project-level QA/QC. Given the relatively low variability observed, the analysis indicates that the replicate counts required by current standards may be higher than necessary for acceptance testing in a single project, particularly when external laboratories perform tests. The report therefore recommends prioritizing tensile tests of CFRP strands and GFRP bars, and bend-strength tests for CFRP spirals and bent GFRP bars, while relying on product-qualification programs (such as the AASHTO Product Evaluation & Audit Solutions program, supported by the FRP Institute) and prior durability research for secondary and durability properties.

Field observations during pile and girder production and erection revealed several constructability issues that informed design and detailing recommendations. Early production stages exhibited end-region cracking in CFRP-prestressed piles and FIB girders, attributed to transfer-length and bursting effects at relatively low concrete strengths, as well as to incomplete confinement of the outer strands. These issues were mitigated by delaying detensioning and field cutting to allow higher concrete strength gain, and by revising confinement details to enclose all bottom strands. Lifting loops also emerged as a critical challenge: NCDOT's preference for eliminating conventional steel led to the exploration of several non-ferrous options, but schedule constraints ultimately required the use of stainless-steel strand bundles as a pragmatic interim solution, highlighting the need for dedicated research on FRP-based lifting systems and clearer guidance on acceptable interim practices. Contractors also reported handling challenges with GFRP bars (splintering and itching), manufacturing limitations on bent-bar geometries, and recurring issues with bar tagging and unit conventions, all of which informed practical recommendations on PPE, bar coatings, standardized shapes, and documentation.

Looking ahead, the report outlines an experimental program to test three full-scale 54 in. deep FIB girders in shear, each providing two tests (one per end), covering different combinations of CFRP versus steel prestressing, GFRP versus steel stirrups, stirrup spacing, and GFRP bar manufacturer. Unlike many academic studies that intentionally exclude beam ends from the test region to isolate shear behavior, the planned tests will maintain realistic support locations and reinforcement details closely aligned with the Harkers Island bridge, thereby providing a complementary dataset to ongoing research efforts that have examined shear behavior in FRP-prestressed members from a more academic, idealized perspective. The findings from this research task will be presented in a separate report once the girders are tested.

The report concludes with recommendations for NCDOT on project-level QA/QC protocols, sampling and replicate counts, detailing of end regions and lifting loops, improved tagging and handling practices, and next steps for implementation and training. Taken together, the Harkers Island Bridge and its companion research program demonstrate that all-FRP reinforced, prestressed concrete bridges are technically feasible and constructible within standard schedules, while also revealing where codes, specifications, and acceptance procedures must evolve to make such projects routine, efficient, and widely adoptable.

TABLE OF CONTENTS

LIST OF FIGURES

LIST OF TABLES

Chapter 1. INTRODUCTION

1.1 Background

Bridges are essential components of modern transportation networks. They connect communities, support regional and national economies, and provide access to education, healthcare, and emergency services. Their performance and reliability directly affect social equity, resilience, and long-term economic development.

In coastal and marine environments, reinforced and prestressed concrete bridges are particularly vulnerable to deterioration (see Figure 1). Conventional systems rely on internal steel reinforcement, either passive mild steel or high-strength prestressing strands, which are susceptible to corrosion when exposed to chlorides. Once corrosion initiates, the cross-sectional area and mechanical properties of the steel are progressively reduced, leading to cracking, spalling, loss of prestress, and ultimately a reduction in structural capacity and service life.

Experience in coastal North Carolina (NC) indicates that steel-reinforced concrete bridges can require major repairs or complete replacement after only a few decades in service, significantly shorter than the current 75-year design life expected for new bridge construction. Field investigations and laboratory testing of deteriorated prestressed cored slabs, which have historically been among the primary structural systems used in NC's bridge structures, have documented extensive corrosion of strands and stirrups, widespread patching and delamination, and uncertainties in load ratings for bridges that had been in service for less than 40 years. This recurring pattern has prompted the North Carolina Department of Transportation (NCDOT) to explore more durable alternatives for both new construction and rehabilitation of existing structures.

Figure 1. Corroded steel-reinforced concrete structural elements

1.2 Coastal Bridge Deterioration in North Carolina

Prestressed cored slab bridges have been widely used in NC since the late 1960s for spans of approximately 40–70 ft. Many of these structures are in coastal regions, where exposure to saltwater, tidal fluctuations, and airborne chlorides accelerates the deterioration of internal steel reinforcement. Research sponsored by NCDOT on two cored-slab bridges in Carteret County (Bridge No's. 150035 and 150039) documented severe corrosion of bottom prestressing strands and stirrups, accompanied by spalling, rust staining, and delamination of the concrete cover [1].

Complementary research on replacement options studied cored slabs prestressed with carbon fiber-reinforced polymer (CFRP) strands and reinforced with glass fiber-reinforced polymer (GFRP) stirrups as a direct, corrosion-free substitute for traditional steel-prestressed units [2]. Full-scale testing showed that, when properly detailed and manufactured, these FRP-reinforced cored slabs satisfy NCDOT serviceability criteria and achieve flexural and shear capacities comparable to or greater than those of steel control specimens.

In parallel, NCDOT has investigated mechanically fastened FRP (MF-FRP) systems to restore the structural capacity of deteriorated prestressed concrete beams in existing bridges [3]. These systems use prestressed FRP plates bolted to the concrete girder stems to provide external flexural and shear strengthening, thereby allowing damaged members to safely remain in service while replacement projects are planned and implemented.

Collectively, these research efforts have highlighted both the vulnerability of traditional steel-reinforced systems in aggressive coastal environments and the potential of FRP-based solutions, either as internal reinforcement in new construction or as external strengthening systems for existing bridges, to provide more durable infrastructure for NC's coastal communities.

1.3 Fiber-Reinforced Polymer Reinforcement for Coastal Bridges

FRP composites combine high tensile strength, low weight, and corrosion resistance, making them appealing alternatives to steel reinforcement in environments where durability is a primary concern. FRP products can be manufactured in forms similar to conventional ferrous-based reinforcing bars and prestressing strands (see Figure 2), allowing the use of established concrete design practices while overcoming the long-term durability limitations of steel.

Figure 2. Reinforcement bar types

In the United States (US), FRP has been used extensively for the repair and strengthening of existing structures since the 1970s. Its use as the primary internal reinforcement in new bridges, however, has expanded more gradually. Early demonstration projects, such as the first entirely FRP-reinforced bridge in Michigan [4], constructed in 2001, provided critical performance data and informed the development of design guidelines by organizations such as ACI and AASHTO. To date, several state DOTs have successfully implemented FRP-reinforced decks, girders, and piles, particularly in regions where corrosion has led to repeated maintenance interventions.

Within North Carolina, NCDOT's transition to FRP reinforcement has been carefully studied and planned. Initial efforts included using GFRP bars in selected bridge decks to compare their performance against adjacent steel-reinforced decks under similar exposure conditions [5]. Subsequent NCDOT-funded research programs examined (i) the performance of prestressed cored slabs with CFRP strands and GFRP stirrups as direct replacements for steel-reinforced cored slabs, (ii) the application of MF-FRP systems to retrofit deteriorated prestressed concrete cored slabs and C-channel beams, and (iii) the durability of CFRP strands, including creep, bond, and environmental exposure effects.

The positive outcomes from these studies, combined with the growing body of national and international experience developed over recent years, created a foundation of confidence that enabled NCDOT to pursue the design and construction of a fully FRP-reinforced, prestressed concrete bridge at a scale that had not previously been attempted in the US.

1.4 Harkers Island Bridge Replacement Project

1.4.1 Project Context

Harkers Island is situated in Carteret County, North Carolina, within the Cape Lookout National Seashore (Figure 3). The island, home to approximately 1,200 permanent residents, depends heavily on fishing, boat building, tourism, and related industries. Consequently, reliable bridge access is essential for the community's daily life and economic well-being.

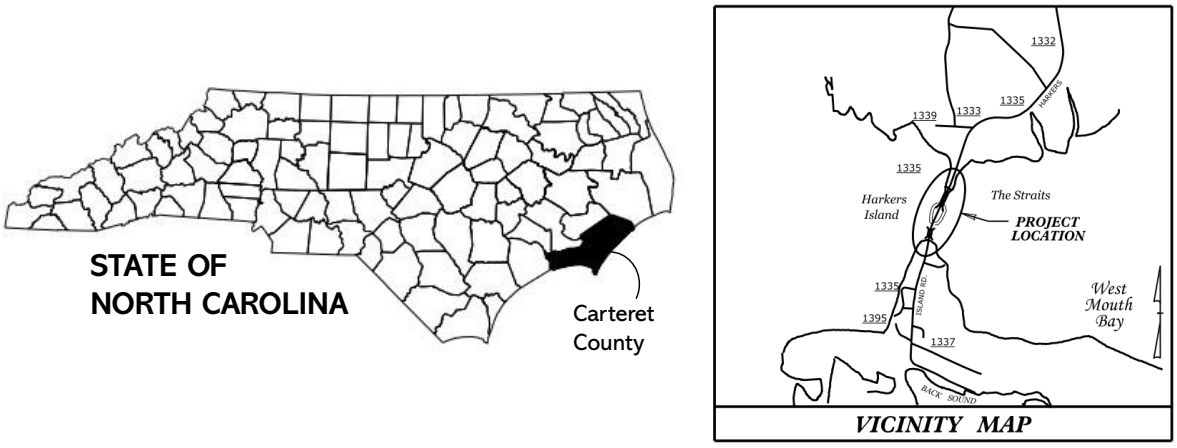

Figure 3. Project location

The island was originally connected to the mainland by two timber bridges constructed in 1941 (Figure 4). These structures were later replaced by two concrete bridges: Bridge No. 73 (Earl C. Davis Memorial Bridge) and Bridge No. 96, constructed with steel prestressed cored slabs supported by octagonal prestressed concrete piles. Over decades of service, both bridges experienced extensive corrosion of internal reinforcement, leading to spalling, cracking, load postings, and frequent partial closures despite repeated repair interventions.

Figure 4. The first bridge connecting Harkers Island, built in 1941

By the early 2010s, inspection findings and load-rating issues at these and other coastal bridges clearly showed that a long-term replacement plan was needed. Therefore, NCDOT initiated the Harkers Island Bridge replacement project to create a robust, low-maintenance connection that could reliably serve the community for many decades without the severe deterioration observed in earlier structures.

1.4.2 New Bridge Configuration and Use of FRP

The new Harkers Island Bridge is a 28-span, 3,200 ft. long fixed-span structure with a vertical navigational clearance of 45 ft. (Figure 5). It was delivered as a design-bid-build project with an estimated construction cost of $60 million. The new bridge eliminates maintenance issues associated with the previous steel swing span and provides a wider, safer crossing for vehicles.

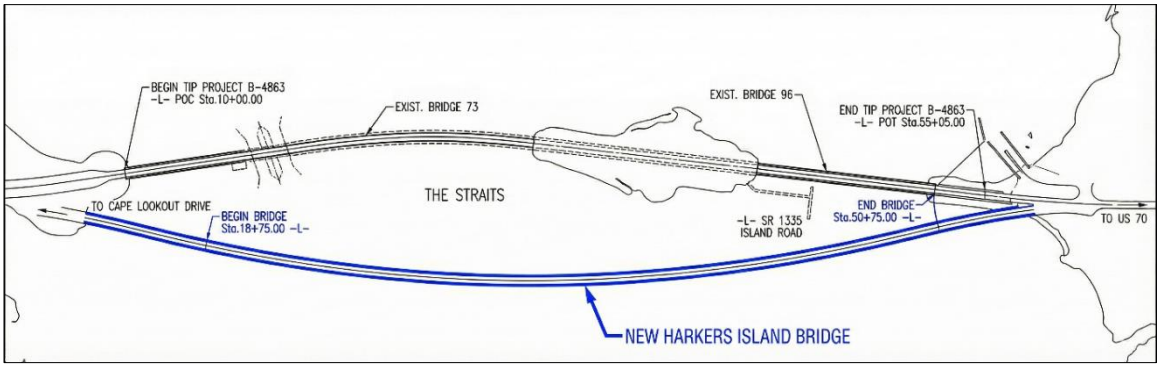

(a) Horizontal profile

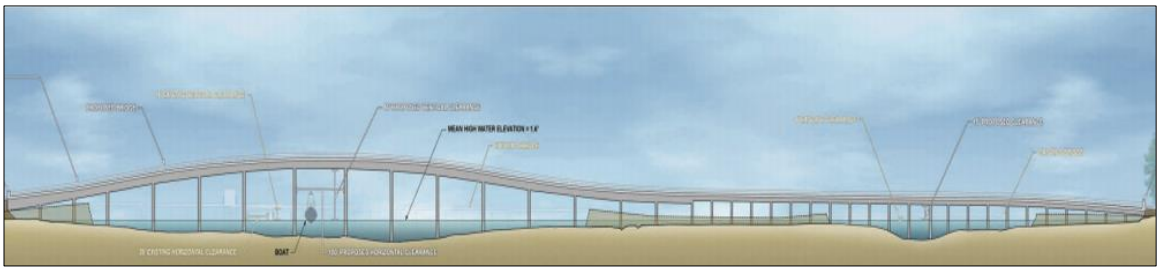

(b) Vertical profile

Figure 5. Bridge layout

All major structural components of the new bridge are reinforced or prestressed with FRP materials as follows:

- **Precast, prestressed piles**: square concrete piles prestressed with seven-wire CFRP strands and confined with CFRP spirals.
- **Precast, prestressed girders**: Florida I-beam (FIB) girders prestressed with CFRP strands and transversely reinforced with GFRP bars and stirrups.
- **Cast-in-place substructure and superstructure elements**: pile caps, columns, and deck reinforced exclusively with GFRP bars.

Approximately 975,000 linear ft. of CFRP prestressing strand and a similar quantity of GFRP reinforcement were used in the project, making it the longest bridge in the US to rely on FRP as the primary source of reinforcement for all major structural elements. Construction began in September 2021 and was completed in December 2023, approximately ten months ahead of the original schedule, despite an annual six-month annual moratorium on in-water work. The project, therefore, represents not only a significant technological milestone for NCDOT but also a demonstration of the constructability and schedule feasibility of large-scale FRP-reinforced bridge projects.

1.5 Research Project Objectives and Scope

Recognizing the unique opportunity presented by the Harkers Island Bridge replacement project, NCDOT sponsored a companion research program titled "Harkers Island Bridge Replacement: Material Characterization and Structural Performance" (Research Project No. 2022-08) to be conducted at North Carolina State University (NCSU). The overarching goal of this research is to document and evaluate the performance of FRP materials and FRP-reinforced structural systems used in the project, and to develop practical recommendations for future FRP bridge projects in NC and beyond.

The research program was organized into seven primary tasks: literature review; field observation and documentation; material characterization; instrumentation and monitoring; analytical modeling; full-scale testing; and the development of recommendations. Within this framework, specific objectives include:

1. Synthesize relevant literature and prior research on FRP reinforcement in bridges, with emphasis on durability, structural performance, and code provisions applicable to coastal infrastructure.
2. Document the design and construction of the Harkers Island Bridge, including key structural details, FRP material specifications, construction sequencing, and issues encountered during fabrication and erection.
3. Characterize the mechanical properties of the FRP materials used in the project through an extensive series of tension and bent-bar tests on CFRP strands, CFRP spirals, and GFRP bars, and perform statistical analyses to determine appropriate design values and the optimal number of replicate tests for quality control.
4. Investigate the performance of FRP-reinforced members at critical locations, including the strength reduction at bent regions of spirals and stirrups, and the behavior of full-scale FIB girders in shear, accounting for size effects and FRP-specific failure modes.
5. Develop analytical and numerical models to interpret experimental observations, study cracking behavior in FRP-prestressed piles and girders, and evaluate design provisions for FRP-reinforced bridge components.
6. Formulate recommendations and implementation guidelines for NCDOT and other agencies regarding FRP material acceptance criteria, quality-control testing protocols, detailing of FRP reinforcement, and shear and flexural design of FRP-reinforced girders and piles, informed by both the Harkers Island experience and prior NCDOT projects.

1.6 Organization of the Report

The remainder of this report is organized as follows:

Chapter 2: FRP Material Testing Program

Describes the CFRP strands and GFRP bars used in the project, outlines the acceptance testing protocols suggested by NCDOT, and presents the material test results.

Chapter 3: Experimental Investigation of Bend Locations in CFRP Spirals

Summarizes the laboratory program on CFRP spirals, focusing on the effects of bend diameter, surface treatment, and test configuration. Implications for design are also discussed.

Chapter 4: Statistical Evaluation of Material Properties and Sample Sizes

Presents the statistical analyses performed on the tension and bent-bar test data to establish representative design values and to determine efficient testing strategies for future projects.

Chapter 5: Full-Scale Shear Tests of CFRP-Prestressed FIB Girders

Presents the planned large-scale tests on FIB girders, together with analytical and numerical models developed to interpret and extend the experimental results.

Chapter 6: Summary of Findings and Conclusions

Summarizes the main outcomes of the research, discusses limitations, identifies areas for future work, and highlights the broader implications of the Harkers Island Bridge project for the adoption of FRP technology in coastal bridge infrastructure.

Chapter 7: Recommendations, Implementation, and Technology Transfer

Consolidates findings from the previous chapters into practical guidance for NCDOT and other agencies contemplating the use of FRP reinforcement in new bridge construction or rehabilitation projects.

Table 17 and Table 18 summarize recommended special provisions for 0.6 in. CFRP strands and GFRP bars, respectively.

Appendices A-H:

In addition to the seven chapters, a set of eight appendices provides a comprehensive literature review, project description, construction highlights, as well as supporting experimental details, data, and visual documentation that complement the main text:

- Appendix A – Literature Review: Summarizes national and international experience with FRP-reinforced and prestressed concrete bridges, with particular emphasis on past case studies, durability, flexural and shear behavior, and acceptance testing of FRP materials. It also reviews key findings from previous NCDOT projects on deteriorated cored slabs, CFRP-prestressed cored slabs, MF-FRP retrofits, and CFRP strand durability and material tests.

- Appendix B – Harkers Island Bridge Description: Provides a detailed description of the project characteristics, structural system, material specifications, and construction sequence for the new bridge, including observations from site visits and field documentation.
- Appendix C – Construction Photo Documentation: Chronological photographic record of key construction stages, from existing conditions and trestle construction through piles, substructure, superstructure, and opening, including post-completion visits.
- Appendix D – Supplementary Area and Water Absorption Tests on 0.6 in. CFRP Strands: Summary of measured cross-sectional area and water-absorption tests on 0.6 in. CFRP strands, illustrating the influence of PET wrap removal and highlighting why these tests are not practical as routine project-level QC.
- Appendix E – Rationale for Using Tensile Modulus in Sample Size Determination: Additional explanation of why tensile modulus, rather than measured area or tensile strength, was selected as the primary basis for the statistical sampling and number of replicates recommended in Chapter 4.
- Appendix F – Preparation of FRP Tension Tests: Detailed procedures, photographs, and notes on specimen preparation, anchorage, and early premature failure modes for CFRP strands (and selected GFRP bars), expanding on the summary presented in Chapter 2.
- Appendix G – Supplementary Bend Tests on CFRP Spirals: Results from additional bent-bar tests on CFRP spirals with different bend radii and surface treatments, providing further context for the findings in Chapter 3.
- Appendix H – Statistical Tables: Tabulated Z-values for the normal distribution and other statistical parameters used in the sampling and confidence-interval calculations in Chapter 4.

Chapter 2. FRP MATERIAL TESTING PROGRAM

2.1 Purpose and Scope of the Tension Testing Program

The Harkers Island Bridge relies solely on FRP reinforcement for its main structural components: CFRP strands for prestressing, CFRP spirals for confinement in piles, and GFRP bars for passive reinforcement in girders, substructure elements, and deck. In this context, evaluating the material properties of CFRP and GFRP products used in the project is key.

However, given the breadth of potential FRP material properties to be assessed (e.g., tensile strength, modulus of elasticity, bond, creep, relaxation, glass transition temperature, fiber content, etc.), it is neither realistic nor necessary to measure every property for every production lot on a single project. Many of these properties have already been extensively studied in national and international research programs [6], [7], [8], [9], [10], [11], [12], and are incorporated into design provisions adopted by ACI [13], AASHTO [14], [15], and CSA [16], [17]. Therefore, the material testing framework for this project focuses on properties that directly control structural design and can be measured consistently on a project-by-project basis. For completeness, the material properties included in NCDOT's special provisions for the CFRP products used in Harkers Island are listed in Table 1.

Since tensile properties govern the design strength used in flexural and shear checks and directly influence serviceability behavior, this chapter focuses on the tension-testing program implemented as part of the Harkers Island research project. The objectives are twofold:

1. At the project level, it functions as a quality-assurance and quality-control (QA/QC) tool, providing an independent verification of the tensile strength and stiffness of the CFRP seven-wire prestressing strands and GFRP reinforcing bars delivered to the bridge, and to assess whether their behavior is consistent with manufacturer certifications and applicable product standards.
2. At the research level, it generates a sufficiently large dataset of tension test results across multiple production lots to support the statistical evaluations presented in Chapter 4 and to inform practical recommendations for future FRP bridge projects.

No QA/QC tension tests were performed on straight segments of the CFRP spiral used for pile confinement, because the project specifications did not require the manufacturer to supply companion straight samples made in the same process and lots as the spirals. To compare the straight and bent behavior of the spiral product, the research team relied on tension data from the manufacturer's internal QA/QC. Some additional straight spiral samples were later supplied for future research, but those specimens do not correspond to the specific lots used in the Harkers Island piles. They are therefore not treated as project-level QA/QC data in this report.

For each product tested in tension, this chapter describes the lot definition, sampling strategy, specimen preparation (including end anchorage and, where applicable, removal of protective wraps), test setup, and key measured quantities such as ultimate tensile strength and modulus. In addition, auxiliary measurements, such as cross-sectional area by Archimedes' principle and water absorption for selected CFRP strand specimens, are documented to illustrate both the consistency of the material and the practical limits of what can reasonably be incorporated into project-level QA/QC. Due to space constraints, the latter is included in Appendix D.

Table 1. Physical and mechanical property requirements for CFRP materials

Test No.	Property	Test Method	Requirement	Specimens per Lot
1	Fiber Mass Content	ASTM D2584 or ASTM D3171	≥ 70%	10
2	Short-Term Moisture Absorption	ASTM D570, Procedure 7.1; 24 hours immersion at 122°F	≤ 0.25%	10
3	Long-Term Moisture Absorption	ASTM D570, Procedure 7.4; immersion to full saturation at 122°F	≤ 1.0%	10
4	Glass Transition Temperature (Tg)	ASTM D7028 (DMA) or ASTM E1356 (DSC; Tm)/ASTM D3418 (DSC; Tmg)	≥ 230°F (D7028) ≥ 212°F (E1356/D3418)	3
5	Total Enthalpy of Polymerization (Resin)	ASTM E2160	Identify the resin system used for each strand size and report the average value of three replicates for each system	-
6	Degree of Cure	ASTM E2160	≥ 95% of total polymerization enthalpy	3
7	Measured Cross-Sectional Area	ASTM D7205	Within -5% to +10% of nominal values listed in Table 2	10
8	Guaranteed Tensile Strength		≥ Value listed in Table 2	
9	Tensile Modulus		≥ 21,000 ksi	
10	Alkali Resistance with Load	ASTM D7705, 3 months test duration at 140 ± 5°F. Apply sustained tensile stress to induce 3000 microstrain, followed by a tensile test per ASTM D7205	Tensile strength retention ≥ 70% of UTS	5
11	Creep Rupture Strength	ASTM D7337, 3-month test duration at laboratory conditions. Apply a sustained tensile load equivalent to 75% UTS, followed by tensile test per ASTM D7205	Equivalent sustained load ≥ 75% UTS AND Tensile strength retention ≥ 90% UTS	3

Bent-bar and spiral bend behavior, including the project-specific tests on CFRP spirals and the limitations of existing bent-bar test methods for GFRP stirrups, are treated separately in Chapter 3. The combined datasets from Chapter 2 and Chapter 3, along with manufacturer tension data where appropriate, form the basis for the statistical evaluation of mechanical properties and the development of acceptance criteria presented in Chapter 4.

2.2 FRP Products Used in the Harkers Island Bridge

The three main FRP products reinforcing the Harkers Island Bridge are summarized below, and their material properties are listed in Table 2.

- 0.6 in., seven-wire CFRP prestressing strands for prestressing in piles and FIB girders.
- 0.28 in., single-wire CFRP spirals for confinement in prestressed piles.
- GFRP bars for all passive reinforcement in girders, substructure elements, and deck.

Table 2. FRP material properties

FRP Material	Bar Designation No.	Nominal Diameter (in)	Nominal Area (in^2)	Minimum Guaranteed Ultimate Tensile Force (kip)	E (ksi)
GFRP	3	0.375	0.11	13.2	6,500
	4	0.500	0.20	21.6	
	5	0.625	0.31	29.1	
	6	0.750	0.44	40.9	
	8	1.000	0.79	66.8	
CFRP	7-wire strand	0.600	0.179*	66.2**	21,800
	Uni-strand	0.280	0.05*	13.1	23,200

* *Once the PET wrap has been removed.*
** *Current value reported by manufacturer. At the time of the bridge design, it was 60.7 kip.*

2.2.1 CFRP Seven-Wire Prestressing Strands

The primary prestressing reinforcement for the Harkers Island Bridge consists of 0.6 in. diameter seven-wire CFRP strands manufactured by Tokyo Rope USA, located in Canton, Michigan. These strands are used as direct replacements for conventional steel prestressing strands in:

- 24 in. square precast piles, and
- 54, 72, and 78 in. FIB girders.

The strands are composed of high-strength carbon fibers embedded in a polymer matrix and are supplied in continuous coils (see Figure 6a). They include a surface treatment and wrapping system (PET wrap) intended to protect the strand and improve handling during fabrication and prestressing operations. The PET wrap is shown in Figure 6b. In the precast plant, these CFRP strands were stressed using conventional multistrand jacks with appropriate hardware and splice connectors, as discussed in Appendix B, and shown in Figure A - 19b. The tension tests performed in this project provide an independent check of the tensile strength and stiffness of the strands delivered to Harkers Island, while Archimedes-based area measurements and water absorption tests were carried out on a subset of specimens to evaluate the consistency of these material properties and to compare them with manufacturer data (see Appendix D).

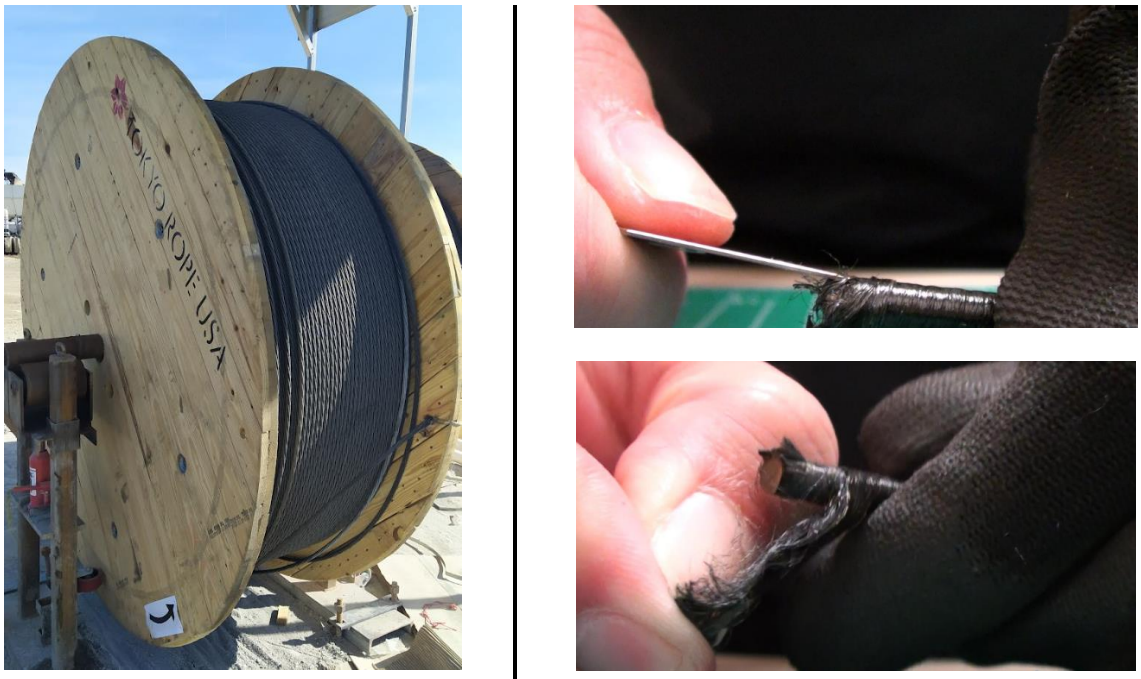

(a) Coils of CFRP strands

(b) PET wrap in CFRP products

Figure 6. CFRP Seven-Wire Prestressing Strands

2.2.2 CFRP Spirals for Pile Confinement

Confinement in the 24 in. square piles is provided by CFRP spirals formed from a 0.28 in., single-wire CFRP strand. The spirals are pre-formed with a specific bend radius and are installed in the pile forms prior to casting, as depicted in Figure 7a. These spirals are critical for both pile drivability and structural performance under axial load, bending, and shear. It must be noted that the bend radius at corners (see Figure 7b) significantly influences the strength at bends and is therefore a key test to be performed on spiral segments.

(a) CFRP spirals before casting

(b) Close-up view of the spiral bend

Figure 7. Single-wire CFRP spirals

From a material perspective, it would be desirable to characterize both the tensile behavior of companion straight portions of the spiral strand and the strength at bends, where stress concentrations are highest. However, for the Harkers Island project, the specifications did not require Tokyo Rope USA to provide

additional straight spiral samples manufactured using the same process and from the same lots as the spirals supplied for the piles. As a result, no project-level tension tests were performed on straight 0.28 in. single-wire strands.

2.2.3 GFRP Bars for Passive Reinforcement

All passive internal reinforcement in the bridge's cast-in-place elements and in the transverse reinforcement of the FIB girders consists of GFRP bars supplied by Owens Corning, based in Concord, NC. The GFRP bars must be compliant with ASTM D7957 [18], which specifies minimum tensile and bend-strength requirements, along with associated test methods, for product qualification. Within the bridge, GFRP bars are used in the following roles:

- FIB girders (stirrups and secondary bars),
- Pile caps, columns, and bent caps (longitudinal and transverse reinforcement), and
- Deck slab (mats of reinforcement).

For project-level tension testing, an additional practical constraint arose: the specifications did not require the manufacturer to provide dedicated straight-bar specimens produced using the same process and from the same lots as the stirrups and bent bars used in the bridge. In practice, the research team obtained adequate straight specimens only because certain L-, C-, or U-shaped GFRP bars delivered for the project had straight legs long enough to be cut into straight specimens for tension tests.

While this "fortunate geometry" enabled tension tests on GFRP bars representing the actual production lots, it also highlights a limitation and a lesson for future projects. Unless specifications explicitly require extra straight and bent samples from each lot, project-level tension and bend testing may not be feasible or representative.

The GFRP tension tests described in Section 2.4 provide measured tensile strengths, tensile modulus, and failure modes for these straight portions. The bend behavior of GFRP stirrups themselves was not evaluated at the project level; the reasons for this and the implications for quality control and test standards are discussed in Chapter 3.

2.3 Tension Tests on CFRP Seven-Wire Prestressing Strands

This section describes the experimental program used to characterize the tensile behavior of the CFRP strands supplied to the project.

2.3.1 Lots and Sampling Strategy

CFRP strands were delivered to the precast plant in multiple production lots, each accompanied by manufacturer certifications that report the nominal area, guaranteed tensile strength, and tensile modulus. For project-level QA/QC, NCDOT and the research team defined strand lots based on the manufacturer's production identifiers and shipment information.

From each lot used on the project, a set of six, 7 ft. long, strand specimens was selected for tensile testing. Sampling was carried out on randomly selected lengths from full-size coils or cut lengths intended for production, ensuring the tested specimens were representative of the material used in piles and girders. In addition to the six specimens delivered to NCSU, three companion 7 ft. long specimens from each lot were delivered to NCDOT's Materials and Tests Unit to allow independent verification testing if needed. This report focuses on the results obtained from the six specimens per lot tested at NCSU only.

2.3.2 Specimen Preparation and End Anchorage

Directly gripping CFRP prestressing strands in a testing machine is impractical due to their low transverse strength and the intertwined seven-wire geometry. Unlike steel, which is isotropic and can tolerate high localized clamping pressures, CFRP strands are highly anisotropic: they are robust and stiff along the fiber direction but relatively weak perpendicular to it. Direct mechanical gripping concentrates transverse stresses in the outer wires and crushes the matrix, damages the fibers, and induces uneven load sharing among the wires, leading to premature, nonrepresentative failures.

Several alternative anchorage systems have been proposed in the literature for CFRP strands [19], including specialized wedge-type anchors and proprietary mechanical grips designed to distribute stress more uniformly. For this project, the research team followed the anchorage procedure recommended in ASTM D7205 [20], using steel pipe end anchors filled with expansive grout to develop the strand capacity in tension. The detailed specimen preparation procedure, including the sequence of cutting, pipe installation, grouting, and curing, is provided in Appendix F together with observations from early unsuccessful trial specimens. Nonetheless, typical stages of the specimen preparation are illustrated in Figure 9.

A practical hurdle is that the anchor and clear gauge lengths currently recommended in ASTM D7205 [20] (Figure 8) were developed with older universal testing machines in mind, many of which allowed significantly long specimens to pass through a hollow frame. For example, a No. 5 CFRP bar, which has a diameter similar to a 0.6 in. CFRP strand, implies an anchor length (*La*) of 30 in. at each end (60 in. of anchor length in total) following ASTM guidance. Besides, a clear length (*L*) equal to the larger of 15 in. or 40 times the effective bar diameter. For a 0.6 in. strand, this corresponds to 24 in., resulting in a total specimen length (*Lt*) of 84 in. (7 ft.).

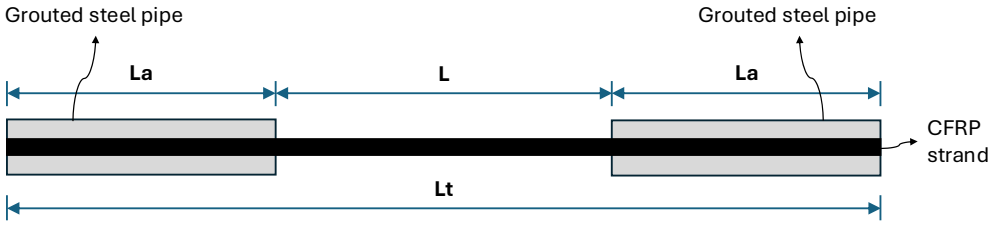

Figure 8. Anchor and clear lengths as per ASTM D7205

This requirement motivated the sampling of 7 ft. long strand specimens for Harkers Island. However, the universal testing machine (UTM) available at the Constructed Facilities Laboratory (CFL) (Figure 10a), where the experimental tests for this project were conducted, could only accommodate approximately 53 in. long specimens in the configuration required for 0.6 in. strands. This constraint is likely shared by many modern machines that lack a long pass-through opening beneath the grips.

Moreover, in older testing frames, the grips were located near the top of the anchor, and the specimen could extend freely through the frame (Figure 10c), making long anchors less problematic. In contrast, the current machine grips the specimen near the bottom of the anchor, over a limited length of 5 in. (Figure 10b). The remaining portion of the anchor relies entirely on bond and friction between the strand and the grout to transmit the tensile force. This introduces multiple interfaces that may influence the measured response.

(a) Steel pipes *(b) Centering plastic cap*

(c) Expansive grout *(d) Aligned strands* *(e) Alignment fixture*

Figure 9. Tension test preparation

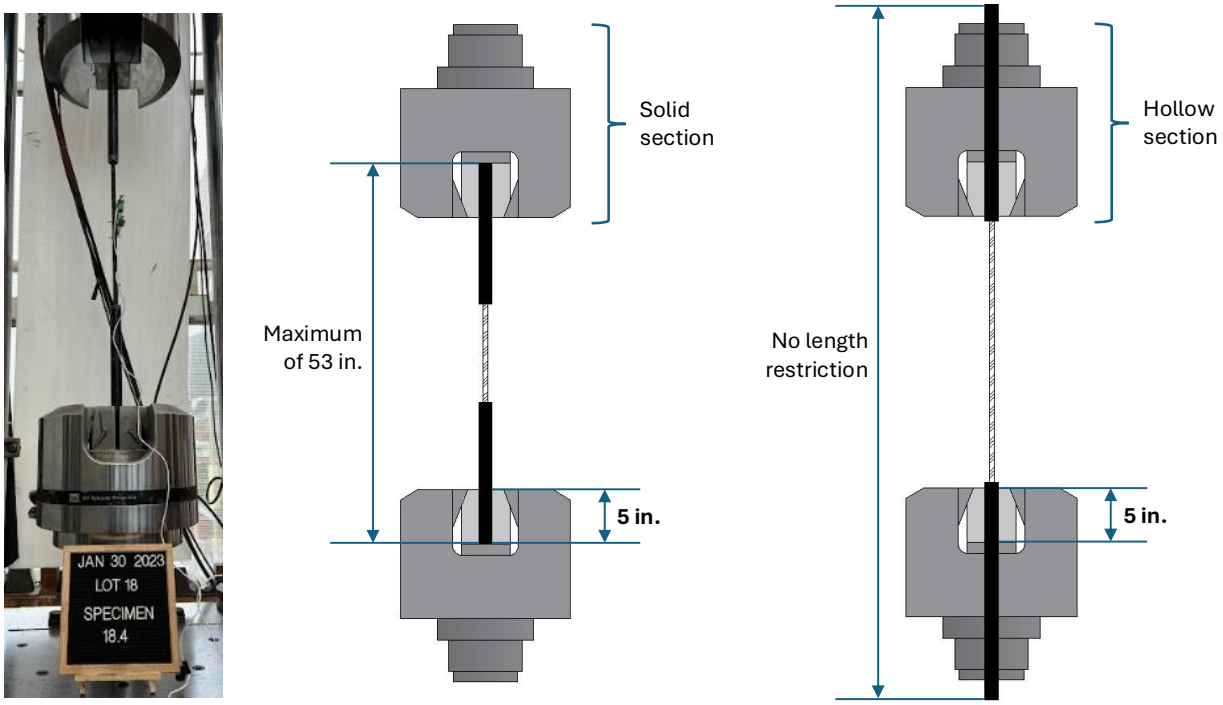

(a) UTM at CFL *(b) Solid UTM (at CFL)* *(c) Hollow UTM*

Figure 10. Types of Universal Tensile Machines

Because of these geometric limitations, the project team could not fully adhere to the anchor and gauge lengths specified in ASTM D7205 [20]. After a series of trial tests, an anchor length of 18 in. per end was adopted as a practical compromise that fit within the test frame capacity and consistently allowed the specimens to reach strand tensile rupture, with failures occurring away from the grips and generally near mid-height of the free length.

Strictly speaking, this means that the clear gauge length did not meet the ASTM-recommended value for all specimens. However, as long as failures occurred in the central portion of the specimen and not within the anchors, the test results were considered representative of the strand's tensile behavior for this project. A systematic study of the interaction between anchor length, gauge length, machine geometry, and failure mode for CFRP strands is beyond the scope of this report. Still, the experience gained here suggests that existing ASTM provisions may need to be revisited and updated to better reflect the constraints of modern test frames and to facilitate routine project-level testing.

These practical considerations have direct implications for quality control: the combination of grout-filled pipe anchors, long preparation times, and machine-length constraints places an upper bound on the number of strand specimens that can realistically be tested per lot within a reasonable timeframe. This issue is revisited in Chapter 4, where recommended test numbers and strategies for future FRP bridge projects are discussed. The test setup configuration used to test the CFRP strands, as well as a strand right after failure, is shown in Figure 11.

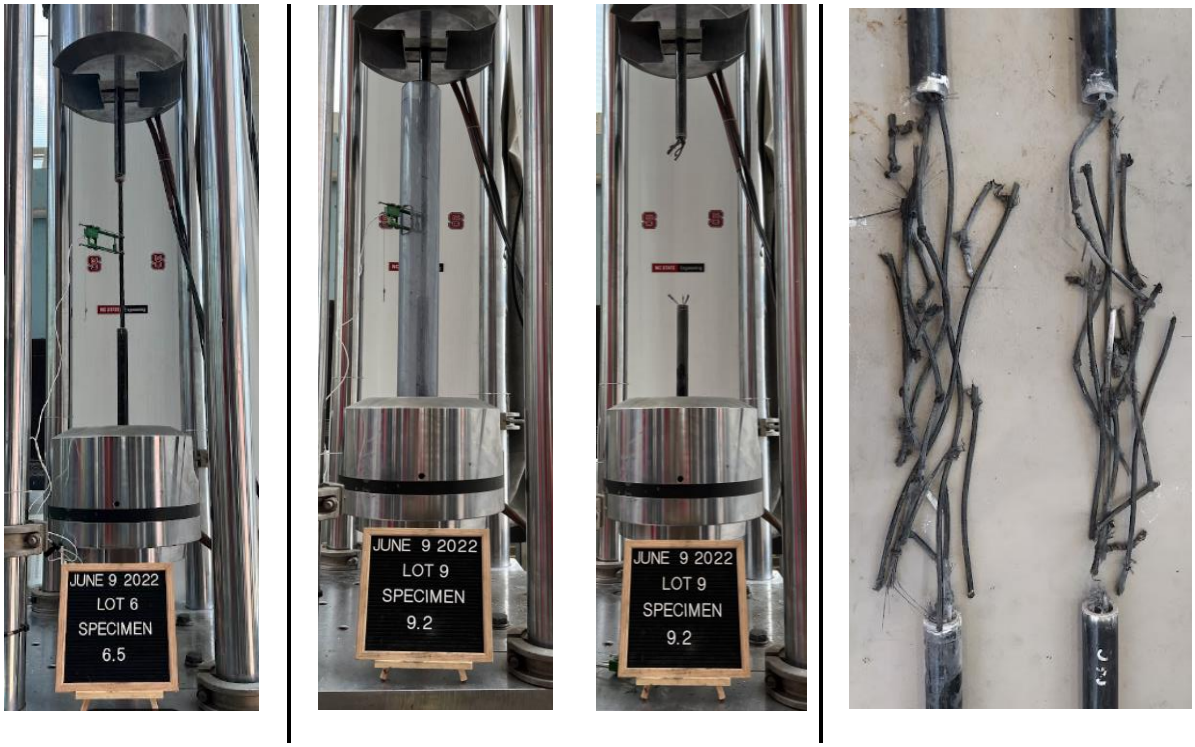

(a) Tension test setup *(b) CFRP strand tested to rupture* *(e) Brittle failure*

Figure 11. CFRP strand tension test

2.3.3 Test Setup and Procedure

Tension tests were conducted in a 200-kip servo-controlled UTM, allowing them to reach the ultimate rupture load of 0.6 in. CFRP strands (82.3 kip on average). The general test configuration included:

End support and gripping:

The steel pipe anchors at each end of the specimen were mechanically gripped in the UTM using contoured grips with an indentation matching the round geometry of the steel pipe. This configuration provided line contact along the pipe circumference and helped maintain axial alignment, thereby minimizing unintended bending within the gauge length. Lateral grip pressure is critical for preventing slip at the interface between the steel pipe and the grips. For this project, the grip pressure was set to 3,500 psi, selected based on the expected maximum tensile load in the CFRP strands and the monotonic loading conditions. This pressure was sufficient to avoid slip without deforming the pipe or inducing localized damage that could affect the behavior in the free length.

Gauge length and instrumentation:

A clear gauge length of 16 to 18 in. was defined between the two pipe anchors. Axial deformation was measured with a 2 in. gauge-length clip-on extensometer attached directly to the strand within this clear region. The extensometer was used to obtain the stress–strain response in the initial linear range, enabling accurate determination of the tensile modulus.

For safety and to avoid damaging the extensometer, it could not be left in place until failure. Consistent with the guidance in ASTM D7205 [20] for FRP bars, which recommends evaluating modulus over a strain range of 0.001-0.006, or up to 50% of the ultimate strain for materials that fail below 0.012, the extensometer was removed well before rupture. For the CFRP strands used in this project, the expected tensile strain at failure was approximately 2% (0.02, or 20,000 με). Accordingly, the extensometer was typically removed when the specimen reached approximately 50% of the expected breaking load (40 kips for an anticipated ultimate load of ~80 kips), corresponding to a strain of approximately 10,000 με.

This procedure provided a sufficiently large strain interval to compute a reliable modulus of elasticity while minimizing risk to the operator and to the extensometer, a sensitive and fragile device. After the extensometer was removed, loading continued under machine displacement, with global displacement used only to track the remaining portion of the test.

Loading protocol:

All tests were conducted under monotonic tension in accordance with the general requirements of ASTM D7205 [20]. The standard recommends setting the test speed to produce failure within 1 to 10 minutes from the start of loading, using either a nearly constant strain rate of 0.01 min^{-1} or an equivalent crosshead speed equal to 0.01 times the specimen's free length when strain control is not available. Since the UTM used in this project lacked strain control, a displacement-controlled protocol was adopted. Based on the minimum clear gauge length, the crosshead speed was set to 0.15 in./min (0.01 × 15 in.), consistent with the ASTM D7205 [20] recommendation. At this loading rate, CFRP strand specimens ruptured in tension within the 1–10-minute window specified by the standard.

Nonetheless, not all CFRP strand specimens were tested to rupture. Because the material behaves in a brittle manner, tensile failure is sudden and violent, sending debris and fibers outward from the fracture zone (see Figure 11). Therefore, testing to rupture required additional safety measures, including installing a protective enclosure around the specimen, clearing personnel from the immediate area as the load approached failure, and thoroughly cleaning up debris after each test. These steps significantly increased the total test time per specimen, with full-rupture tests taking around 45 minutes from setup to post-test cleanup. Given the number of strands to be tested, it was not realistic to load every specimen to failure, particularly since the project specifications required only demonstrating that the minimum guaranteed tensile strength was exceeded, not measuring the ultimate capacity of every strand.

To balance safety, scheduling, and project requirements, the typical approach was to load only a subset of specimens per lot (two strands whenever possible) to failure in tension to document ultimate strength. In contrast, the remaining specimens were loaded monotonically beyond the minimum guaranteed tensile strength of 60.7 kips specified in the NCDOT special provisions for 0.6 in. CFRP strands. Once this force level had been exceeded without signs of anchorage slip or other anomalies, the specimen was unloaded and removed from the machine. In this way, the tests satisfied the acceptance criteria in the specifications while limiting the number of full-rupture events required.

Consequently, these are the properties that can be obtained from a tension test:

- **Maximum tensile load** recorded (rupture force, if achieved).
- **Modulus of elasticity** (slope of the stress–strain response).
- **Tensile strength** (obtained by dividing the maximum load by the nominal cross-sectional area of the strand).

2.3.4 Results

A total of 326 CFRP strands from 73 different production lots were tested between March 2022 and July 2024. All the specimens tested sustained loads exceeding 60.7 kips. Thus, all CFRP strand lots used on the project met the minimum tensile strength requirement in the NCDOT special provisions. The latter shows the consistency of material properties. For subsequent analysis, a filtered dataset of 290 specimens from 52 lots was retained. The remaining tests were excluded for at least one of the following reasons: (i) no strain data were recorded, (ii) the specimen failed within the anchorage due to a preparation issue, or (iii) the specimen was damaged locally during transportation or preparation. The entire tension-test dataset, including specimens with incomplete information, was transmitted to NCDOT's Materials and Tests Unit in July 2024 for their records.

2.3.4.1 Stress–Strain Behavior

The CFRP strands exhibited an expected linear-elastic response throughout loading. A representative stress–strain curve for a single specimen is shown in Figure 12a. The initial sag in the curve at lower strains corresponds to seating of the strand in the anchors and grips, and engagement of the seven wires as they twist and straighten upon loading. Beyond this seating stage, the response is essentially linear until the extensometer is removed, as discussed in Section 2.3.3.

To illustrate the overall consistency of the material, Figure 12b overlays the stress–strain curves for the 290 specimens for which strain data were available. The curves cluster closely, indicating relatively small stiffness variability and confirming linear-elastic behavior. The few curves that extend to higher stress and strain levels correspond to specimens in which the extensometer was left in place longer, closer to ultimate.

As noted in Section 2.3.3, the extensometer was not left in place until rupture for safety reasons and to protect the instrument. Moreover, for the modulus calculation, a strain interval of 6,000-10,000 με was used. The underlying rationale is that 10,000 με corresponds to approximately 50% of the expected rupture strain (≈ 0.02 or 20,000 με) for the 0.6 in. CFRP strands. At this strain level, the axial force is on the order of 40 kips, which is comparable to the jacking force applied during prestressing operations in piles and girders. Therefore, this strain range provides a meaningful basis for estimating the modulus of elasticity in the stress range relevant to prestressing while remaining within the safe operating range for the extensometer.

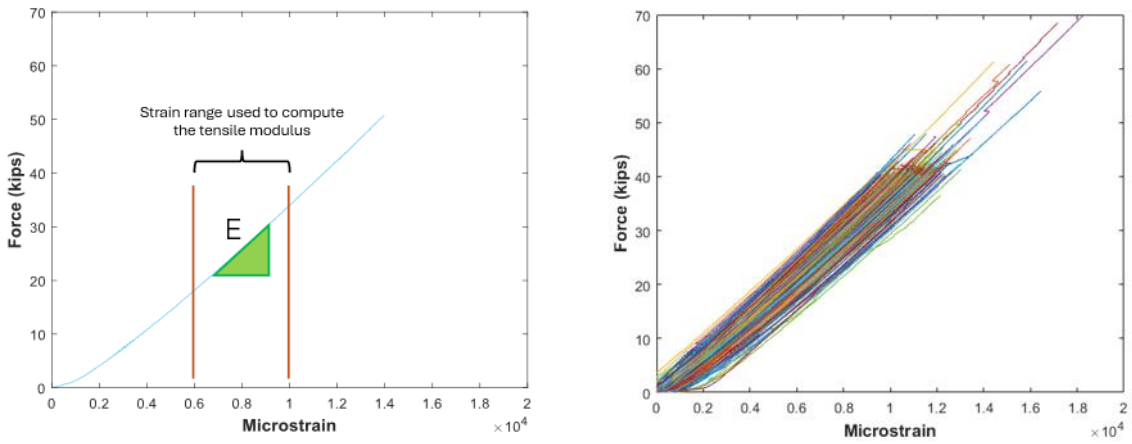

(a) Single-strand response *(b) 290 strands plotted altogether*

Figure 12. Stress-strain response for CFRP strands tested in tension

2.3.4.2 Tensile Rupture Load

A total of 95 strands were tested to rupture. All of them failed in a brittle manner. The average rupture force was 82.3 kips, with a standard deviation of 2.6 kips. Other descriptive statistics are summarized in Table 3 and a plot showing the distribution of rupture loads is shown in Figure 13, where the solid horizontal line indicates the mean value. The manufacturer does not openly report the average rupture force, which is usual. Instead, the minimum guaranteed value is given. The average rupture force exceeds the project's guaranteed value of 60.7 kips. Also, a common practice is to use the mean minus three standard deviations as a lower bound for strength; in this case, this corresponds to 74.4 kips and is shown as a dashed line. At any rate, a prestressing jacking force of around 40 kips appears to be a safe lower limit.

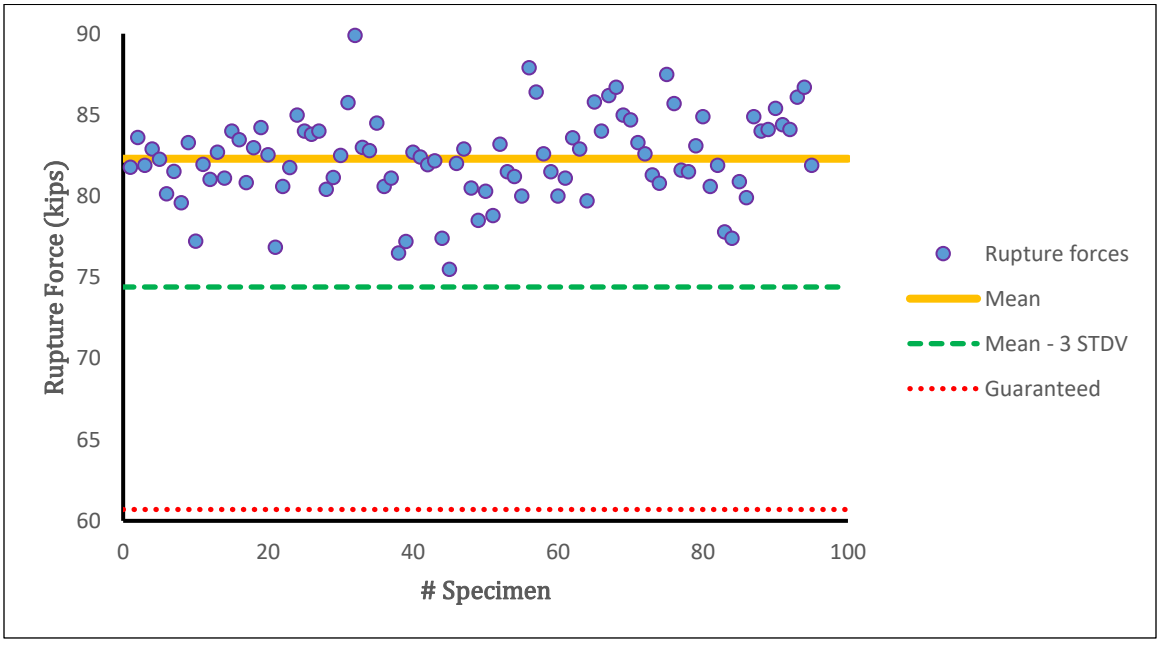

Figure 13. Data dispersion for the rupture force of 0.6 in. CFRP strands

Table 3. Descriptive parameters for the CFRP strands tested to rupture

Parameter	n	$\bar{x}$	Min	Max	Mode	Median	Range	s
Rupture force	95	82.3	75.5	89.9	84.0	82.4	14.4	2.6

2.3.4.3 Modulus of Elasticity

The modulus of elasticity, E, was calculated for each specimen with valid strain data using the strain interval between 6,000 and 10,000 με described above. This choice is consistent with ASTM D7205 [20], which recommends evaluating modulus over a strain range in the lower portion of the stress–strain curve, provided that the strain does not exceed an estimated 50% of the ultimate strain. This range also avoids the initial seating effects, which may lead to unrepresentative conclusions. Using this procedure, the mean modulus of elasticity for the filtered dataset of 290 strands was 22,424 ksi, with a standard deviation of 807 ksi. A distribution of modulus values is shown in Figure 14, and a summary of the most common descriptive statistics is presented in Table 4.

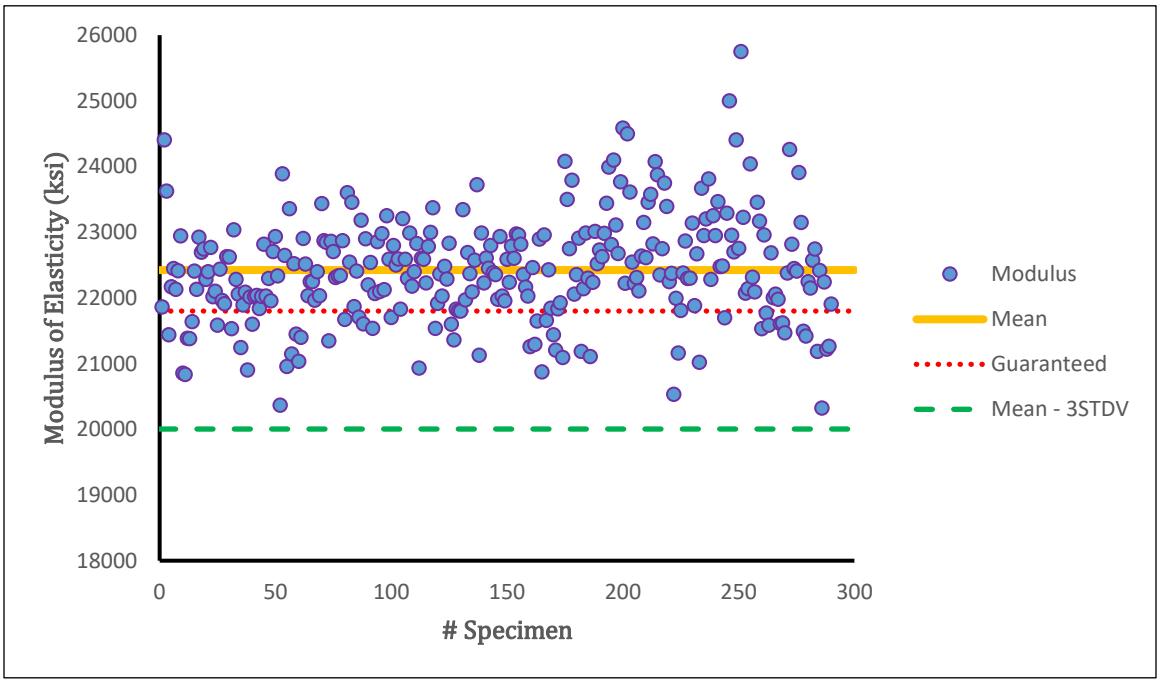

Figure 14. Data dispersion for the tensile modulus of 0.6 in. CFRP strands

Table 4. Descriptive parameters for the modulus of elasticity of CFRP strands

Parameter	n	$\bar{x}$	Min	Max	Mode	Median	Range	s
Tensile Modulus	290	22,424	20,322	25,749	22,446	22,381	5,427	807

The minimum guaranteed modulus required by the NCDOT special provisions is 21,000 ksi. Hence, not all specimens met this requirement; however, the average for each lot exceeded the threshold, resulting in the material's acceptance. Conversely, the manufacturer reports an elastic modulus of 21,800 ksi in its technical datasheets (dotted line in Figure 14), which might appear inconsistent with the experimental data obtained in this work. The latter could raise concerns about the appropriate modulus to use. If the common practice of mean minus three standard deviations were to be used, the guaranteed modulus based on the collected data would be approximately 20,000 ksi (dashed line in Figure 14). Nonetheless, since the tensile modulus is typically used to gauge the applied force based on each strand's elongation during prestressing operations, setting that lower bound might be detrimental since forces higher than expected could be introduced. Also, it should be noted that the modulus of elasticity has direct implications for serviceability checks, as deflections may be overestimated with a lower modulus. This discrepancy in the minimum guaranteed values of the modulus of elasticity warrants attention. These are the kinds of aspects that may be overlooked when standards or specifications are defined, but they become important in practice when QA/QC policies must be implemented on large-scale projects.

It is essential to recognize, though, that the measured modulus is not purely a material property. The test configuration also influences it. As discussed earlier, the modulus in this project was evaluated over a strain interval of 6,000–10,000 με, which is consistent with ASTM D7205 but not identical to the exact 5,000 με window suggested. Based on the collected data, it was observed that the higher the strain range, the higher the modulus. However, exceeding a strain of 10,000 με would not be compatible with field strain levels. In addition, the UTM used here employs free-rotating heads, which can slightly reduce the apparent stiffness of the specimen compared with older machines that constrain rotation more. In frames with more constrained head rotation, the same CFRP strand might yield somewhat higher values of tensile modulus.

A systematic comparison of CFRP strand stiffness measured in different test frames, with varying lengths of anchorage and head-rotation conditions, as well as the assessment of multiple strain ranges, is beyond the scope of this project. However, the experience gained here suggests that machine compliance and rotation should be explicitly considered when interpreting modulus data and developing future standardized procedures for FRP, especially CFRP strands, given their intertwined wires. In other words, part of the observed discrepancy between manufacturer-guaranteed values and the experimental results obtained here may be attributable to differences in test-frame behavior and modulus-calculation conventions, rather than to variability in the material alone. This reinforces the need for statistically based acceptance criteria that are grounded in realistic testing conditions, as discussed further in Chapter 4.

2.3.4.4 Tensile Strength Versus Cross-Sectional Area

Strictly speaking, tensile strength is defined as the ratio of ultimate load to the cross-sectional area of the strand. For CFRP strands, however, the area used should correspond to the effective area after PET wrapping is removed, as the PET wrapping does not contribute to strength or stiffness. Measurements of the area of CFRP samples, with and without PET wrap, are presented in Appendix D.3.1. It should be noted that determining the effective area in a project setting is nontrivial, as it requires removing the PET wrap and measuring its volume by displacement through Archimedes' principle or similar techniques. This process is time-consuming and may be impractical to implement on a large number of specimens as part of routine QA/QC.

Moreover, for specimens intentionally unloaded once they exceed 60.7 kips, reporting tensile strength would be misleading, as the recorded value corresponds only to the stress at the unloading point, not to the actual strength at failure. To assess compliance with the NCDOT special provisions, which specify a minimum guaranteed tensile load rather than a minimum stress, the project team primarily used the measured maximum load and the manufacturer-reported nominal area.

2.4 Tension Tests on GFRP Bars

Since the project specifications did not require the supplier to provide dedicated straight-bar samples from each production lot, the GFRP specimens for tension tests were obtained from bent bars, from which sufficiently long straight segments could be cut. This section describes the resulting test program, the practical constraints imposed by bar geometry, and the main observations relevant to later statistical analysis and future quality-control recommendations.

2.4.1 Bar Sizes, Lots, and Available Straight Specimens

GFRP bars were supplied in five different diameters (see Table 2). Each bar size was produced in multiple lots, and the supplier provided documentation demonstrating compliance with ASTM D7957 [18] at the product level. Since most lots corresponded to bent bars, and no extra straight bars were explicitly manufactured for QA/QC, the only viable option for project-level tension testing was to cut specimens from the straight legs of L-, U-, or C-shaped bars sampled at the precast plant and in the field. However, not all bar sizes and lots could be tested in tension. Only shapes with straight legs long enough to satisfy both the minimum clear length of 40 d_b and the 18 in. anchorage length at each end could be used. The number of lots and specimens tested per bar diameter is summarized in Table 5.

Compared with the CFRP strand program, the GFRP sampling process was less complete. Not all GFRP lots used on the project were sent to NCSU for testing, and several bars arrived at the lab without lot identification tags. From a QA/QC standpoint, this created traceability issues: only 36 out of 59 GFRP lots could be confidently identified and associated with test specimens. In total, 50 GFRP bar specimens were tested and could be correlated with specific project lots. Additional bars (primarily No. 5 bars) were also tested, but since they could not be linked to a particular lot, their results were used only in global statistical summaries, not in lot-by-lot evaluations. All GFRP test results were compiled and shared with NCDOT's Materials and Tests Unit in July 2024.

Table 5. Test matrix for GFRP bars

Material	Diameter	Lots tested	Specimens Tested
GFRP	No. 3	4	7
	No. 4	2	2
	No. 5	29	40
	No. 6	0	0
	No. 8	1	1
	∑	36	50

This sampling strategy, while practical given the project's constraints, highlights a clear limitation and an important lesson for future FRP bridge projects. If project-level tension and bend testing are expected to inform lot-by-lot acceptance, specifications should (i) explicitly require the supplier to provide additional straight and bent samples from each lot with geometries tailored to standard test methods, and (ii) enforce lot traceability so that every tested bar can be unambiguously linked to its production lot.

2.4.2 Specimen Preparation and End Anchorage

The GFRP bar specimens were prepared as straight segments, typically cut from the legs of bent bars (Figure 15). When selecting cut locations, care was taken to avoid regions near bends or hooks, thereby ensuring that the clear gauge length fully represented straight-bar behavior.

End anchorage was provided using steel pipe anchors filled with expansive grout (Figure 15d), following the same general approach used for the CFRP strands, but adapted to each GFRP bar diameter. The detailed procedure, including pipe dimensions, preparation, grout placement, and curing, is provided in Appendix F.

(a) C- and L-shaped

(b) U-shaped

(c) Straight

(d) GFRP bar specimens ready to test

Figure 15. Preparation of GFRP bars for tension tests

2.4.3 Test Setup and Procedure

Tension tests on GFRP bars were conducted in the same UTM used for the CFRP strands. The test setup was broadly similar:

End support and gripping:

The steel pipe anchors were held in contoured grips that matched the pipe curvature, ensuring adequate friction and axial alignment while minimizing bending in the gauge length. The grip pressure was selected to prevent slip at the anchor–grip interface without deforming the pipe. Further details are presented in Appendix F.

Gauge length and strain measurement:

As with the strand tests, an extensometer with a 2 in. gauge length was used over the clear gauge length to capture axial deformation in this region. Once more, the extensometer was used only over the initial portion of the loading history to determine the modulus of elasticity. It was removed before failure to protect the instrument from the sudden, brittle rupture of GFRP bars.

Loading protocol:

Tests were performed under displacement control in monotonic tension, with a crosshead speed selected in accordance with ASTM D7205 [20] to ensure specimen failure occurred within the recommended 1–10-minute window. Out of the 50 bars tested, only 5 bars were tested up to rupture: 4 – No. 5 bars, and 1 – No. 8 bar.

2.4.4 Results

A total of 50 GFRP bars from 36 different production lots were tested between June 2023 and July 2024. All the specimens tested sustained loads exceeding the minimum guaranteed tensile forces shown in Table 2, which vary based on bar diameter. Thus, all the tested GFRP bar lots used on the project met the minimum tensile strength requirement in the NCDOT special provisions. Although not every lot used in the project could be tested, these results demonstrate the consistency of GFRP bar material properties.

2.4.4.1 Tensile Rupture Load

The GFRP bar tests exhibited the expected linear-elastic behavior throughout loading. When loaded to failure, bars fractured in a brittle manner within the gauge length, characterized by fiber shattering (Figure 16). For the No. 5 and No. 8 bars tested up to failure, the average rupture forces were 44.7 and 95 kips, respectively, which are 1.54 and 1.42 times their respective minimum guaranteed forces.

Figure 16. GFRP bars after failure

2.4.4.2 Modulus of Elasticity

The modulus of elasticity, E, was calculated using the same procedure as for the CFRP strands, but with a strain interval of 1,000-6,000 με, as recommended by ASTM D7205 [20]. Since the GFRP bars act as passive reinforcement, the strains they are expected to experience are much lower. Therefore, the range stipulated in ASTM D7205 [20] is a good fit. Using this procedure, the mean modulus of elasticity for the 56 tested GFRP bars (including six extra specimens for which the lot identification was unavailable) was 8,096 ksi, with a standard deviation of 1,237 ksi. It must be noted that the stiffness defined by E does not depend on bar diameter. Thus, the modulus of elasticity should remain constant. The most critical statistical descriptive parameters for these results are presented in Table 6, whereas the data dispersion is shown in Figure 17. The standard deviation for these results is relatively high, indicating significant dispersion. However, all specimens exceeded the minimum threshold of 6,500 ksi indicated in the special provisions.

Table 6. Descriptive parameters for the modulus of elasticity of GFRP bars

Parameter	n	$\bar{x}$	Min	Max	Mode	Median	Range	s
Tensile Modulus	56	8,096	6,531	11,300	8,766	7,627	4,769	1,237

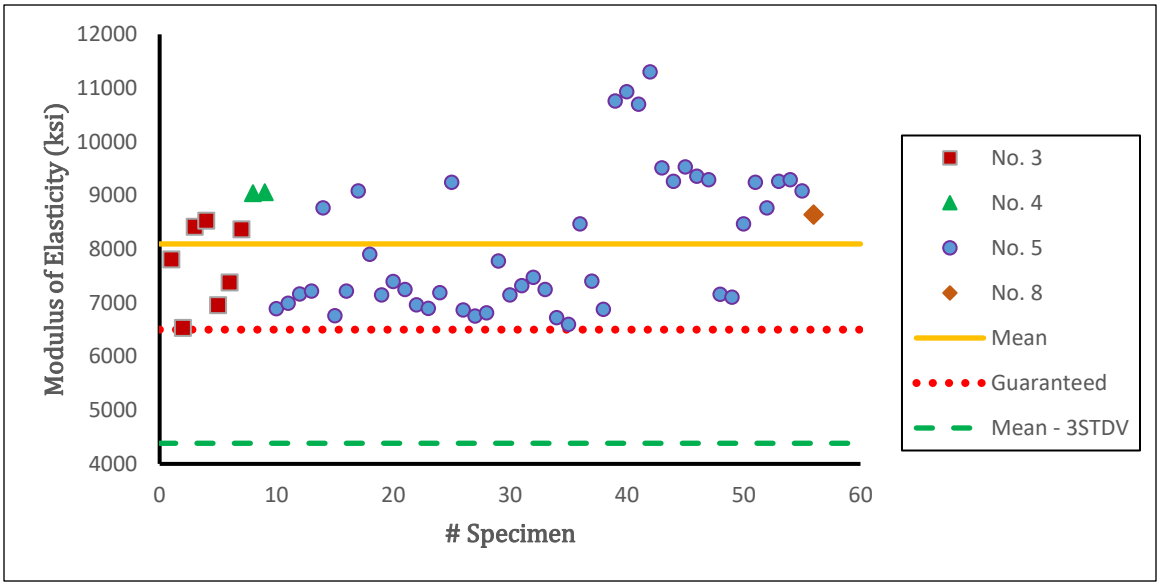

Figure 17. Data dispersion for the tensile modulus of GFRP bars

2.4.4.3 Tensile Strength Versus Cross-Sectional Area

For GFRP bars, the relationship between tensile strength and cross-sectional area is less critical than for the 0.6 in. CFRP strands discussed in Section 2.3.4.4. The GFRP bars have a solid, nominally circular cross section, so their area can be determined reliably from the effective diameter using simple caliper measurements. However, since most specimens were unloaded once they exceeded the minimum guaranteed tensile load, reporting tensile strengths would also be misleading, as the recorded value corresponds only to the stress at the unloading point, not the actual strength at failure. Once again, the nominal areas and minimum guaranteed tensile load, rather than minimum stress, have been used to assess compliance.

Chapter 3. EXPERIMENTAL INVESTIGATION OF BEND LOCATIONS IN CFRP SPIRALS

3.1 Introduction and Scope

As described in Appendix B, the 24 in. square piles used in the Harkers Island Bridge rely on CFRP spirals to provide transverse confinement, contribute to shear strength, and support drivability during installation. In these members, the spiral is not merely a secondary detail; it plays a central role in maintaining concrete integrity under driving stresses, service loads, and ultimate demands. Because the spiral follows the perimeter of the pile cross-section, its bends at the corners become natural points of stress concentration and potential weakness.

For FRP reinforcement, this issue is crucial. Unlike steel, which is ductile and can tolerate localized yielding at bends, FRP composites are brittle and anisotropic. Fibers are aligned primarily along the bar or wire axis, and any change in direction, such as a bend, introduces fiber misalignment and local stress concentrations. As a result, the strength at bends may be significantly lower than that of straight segments, and this reduction must be understood and accounted for in both design and quality control.

This chapter focuses on the experimental evaluation of bend behavior for the 0.28 in. CFRP spiral used in the Harkers Island piles. The objectives are to:

- Quantify the strength at the spiral bends for the specific product and geometry used in the project.
- Compare the measured bend strength to available straight-wire tension data to estimate a bend-strength ratio.
- Assess whether the spiral detailing adopted in the piles is consistent with expected performance and with the assumptions implicit in current design provisions.

It is also important to emphasize the scope and limitations of this chapter:

- The experimental program covers only the CFRP spiral product.
- No project-level bend tests were performed on GFRP stirrups or bent bars, due to geometry and specification constraints, as explained in Section 3.2.
- The results presented here focus on one spiral product and one nominal bend radius, tailored to the Harkers Island pile details.

3.2 GFRP Bent Bars: Project Limitations and Future Work

Although GFRP bars were used extensively in the Harkers Island Bridge, no project-level bend tests were performed on GFRP bent bars or stirrups as part of this research program. This was mainly due to a combination of geometric constraints and specification provisions that limited the scope of testing that could be conducted using available standards and specimens.

The GFRP reinforcement for the bridge was supplied in project-specific shapes (straight, L-, U-, and C-shaped bars) designed to meet the detailing requirements for the girders and substructure. The project

specifications required that these products be qualified under ASTM D7957 [18], which includes both tensile and bend-strength requirements. However, the special provisions did not require the manufacturer to fabricate additional bars with geometries tailored to the bend-test configuration prescribed in ASTM D7914 [21] (Figure 18a).

As a result, all GFRP shapes delivered to the project exhibited bent regions and leg lengths that were not compatible with the ASTM D7914 [21] test setup. Even when straight legs were long enough to cut tension specimens (as presented in Chapter 2), the remaining geometry did not permit constructing specimens that met the dimensional requirements for bend testing. No extra companion bent bars were manufactured for QA/QC bend tests, so there was no straightforward way to generate a representative, standard-compliant bend-test matrix for the GFRP bars used in the bridge.

From an acceptance standpoint, upon discussion with the Steering and Implementation Committee, it was concluded that project-level QA/QC efforts would focus on tension tests of straight segments cut from delivered shapes (where geometry allowed), as described in Chapter 2, to verify tensile strength and stiffness for the lots used in Harkers Island. Since there is a governing standard for GFRP bars (ASTM D7957 [18]), it was assumed that if bars met the tensile strength requirements, they would also meet the bend strength requirements, as the standard requires a certain bend radius and strength retention for bent portions.

Looking ahead, there is a clear opportunity to improve both testing practice and specifications. Alternative bend-test configurations, notably the L-shaped test adopted in CSA S807 [17] (Figure 18b), are more easily adapted to project-specific geometries. As long as sufficient straight length is available beyond the bend, L-shaped specimens can often be prepared from actual stirrups and bent bars. The ASTM D30.10 Committee is actively considering similar modifications, moving away from the more restrictive configuration of ASTM D7914 [21] toward an L-shaped setup that more readily accommodates bar shapes typically used in construction practice.

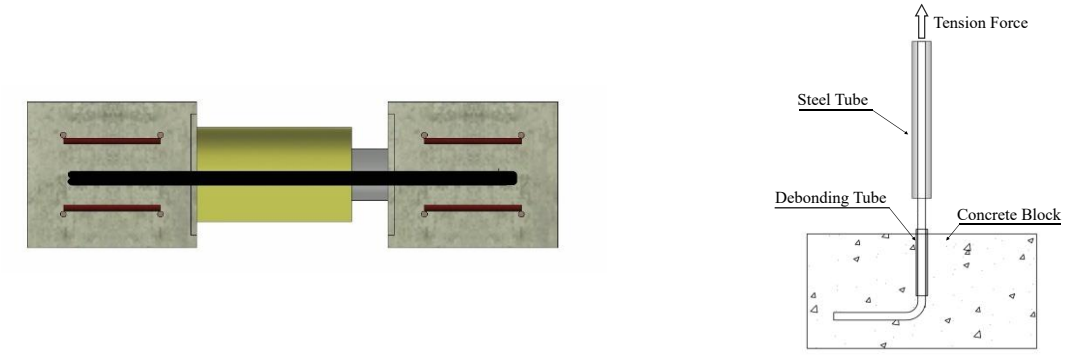

(a) ASTM D7914 configuration *(b) CSA S807 configuration*

Figure 18. Strength at bend locations test setup configuration

For future FRP bridge projects where project-level bend testing is desired, specifications should:

- Require the manufacturer to provide additional bent samples from each lot, with geometries suitable for standardized bend tests (U- or L-shaped, as appropriate); and
- Ensure that lot traceability is maintained so that bend test results can be meaningfully linked to the material installed in the bridge.

In summary, this chapter focuses on the CFRP spiral bent behavior because it was the only FRP product for which a practical, project-relevant bend test program could be implemented within the constraints of the Harkers Island project. The behavior of GFRP bent bars remains an important topic for future work, and lessons learned from the CFRP spiral program directly inform the design and specification of future testing.

3.3 Experimental Program for CFRP Spiral Bend Tests

3.3.1 Specimen Selection and Test Matrix

The CFRP spiral used in the 24 in. square piles was supplied as continuous coils from the manufacturer. To generate test specimens, full spiral coils were unwound and cut into segments containing a single representative lap. Each specimen included a target bend region and two straight legs of sufficient length to transfer load between the two concrete blocks without premature failure away from the corner. Since this test was not part of the special provisions for CFRP spirals, only one specimen per lot, across 20 lots, was prepared to obtain a representative sample. All spirals had a 0.28 in. diameter and a bend radius-to-bar diameter ratio (r/d) of 2.2, which is lower than the minimum r/d ratio of 3.0 specified by ASTM D7957 [18] for GFRP bars.

3.3.2 Test setup

The specimens were prepared by embedding the straight portions of the CFRP spirals in concrete blocks to replicate the conditions experienced in a reinforced concrete member (Figure 19a). The straight portions of one side of the spirals were debonded on the continuous end to ensure that failure would occur at one of the bends on that side (Figure 19b). Specifically, the straight portion was covered with plastic sheathing, typically used to debond prestressing strands, and secured with silicone and duct tape. This configuration successfully prevented the concrete from adhering to the FRP material. Figure 19c shows a typical specimen before casting, where a steel wire mesh or carbon grid prevents the concrete blocks from prematurely cracking or splitting.

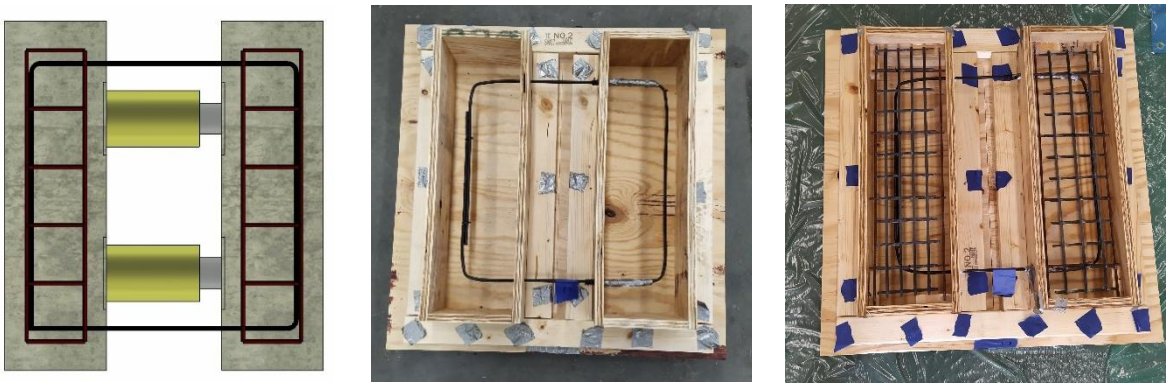

(a) Test concept *(b) Debonded spiral (right)* *(c) Carbon grid*

Figure 19. Bent bar test preparation

This setup is consistent with the requirements of ASTM D7914 [21] and is similar to the B.5 test method stated in the ACI PRC-440.3-12 Guide [22]. The concrete block dimensions were nominally 24 × 7 × 6 in. The concrete had a target compressive strength of 35 MPa, which was ordered from a local supplier.

The two concrete blocks were then monotonically pushed apart using a hydraulic jack actioned by a hand pump until one of the FRP bent legs failed. Due to geometric constraints, two hydraulic jacks connected in parallel were used to apply the tensile load, reducing potential eccentricities. An additional hydraulic jack was connected in parallel with a load cell to record force values in real time. Therefore, the bend strength measured by ASTM D7914 [21], f_b [ksi], can be estimated by Eq. 1, where F_u is the rupture load [kip], and A is the FRP nominal cross-sectional area [in.^{2}]. Further, the strength reduction factor due to an FRP bend, χ, can be estimated through Eq. 2, where f_{fu} is the ultimate strength of the straight portion of the FRP bar. This nomenclature is consistent with former publications on this topic [23], [24].

$$f_b = \frac{F_u}{A} \tag{1}$$

$$\chi = \frac{f_b}{f_{fu}} \tag{2}$$

Additionally, the concrete block containing the debonded portion of the bar was supported on rollers to minimize friction and permit free movement. In contrast, steel profiles support the other block. Steel plates, steel tubes, and rubber pads were used to ensure proper, even load application. Two extensometers and two strain gauges were used to record axial strains on the CFRP spiral legs. Also, two LDTs were attached to each side of the blocks to monitor their relative displacement. The loading rate was set to ensure a failure within 10 minutes, as recommended by ASTM D7914 [21]. A typical test setup before and after failure is shown in Figure 20.

(a) Concrete blocks cast

(b) Instrumentation

(c) Failure mode

Figure 20. Bent bar test setup

3.3.3 Results and Discussion

The CFRP spirals exhibited a mean rupture force of 6.5 kip, with a standard deviation of 1.1 kip, and a coefficient of variation (COV) of 17%. An apparent rupture in the bent portion of the spirals characterized the failure mode. For each specimen tested, only one of the two spiral legs failed. This behavior was expected due to the variable bend quality and inherent eccentricities within the test setup. In other words, predicting which leg would fail from the outset was not feasible. As the strains on both legs were monitored throughout the test, it was observed that the leg with slightly higher strains consistently ruptured, as expected. Nonetheless, the strains on each leg remained relatively close, indicating proper alignment. Figure 21 presents the load-displacement experimental curves.

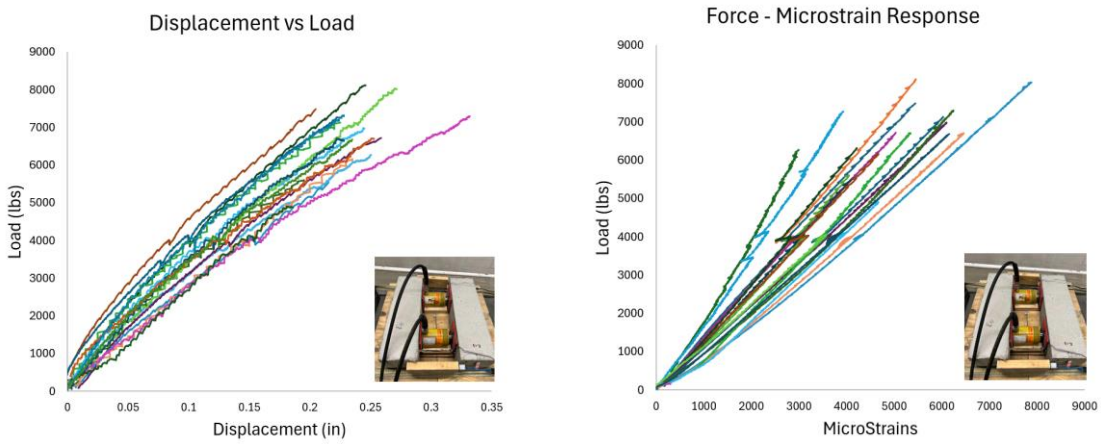

(a) *(b)*

Figure 21. Load-displacement curves for CFRP spirals at bend locations

The rupture values obtained indicate that the mean ultimate bend strength is approximately 41% of the ultimate tensile strength of a straight companion CFRP specimen from the same lot, tested to rupture by the manufacturer in accordance with ASTM D7205 [20]. This reduction percentage aligns with findings from other research efforts [24], [25]. Moreover, considering the small bend diameter (r/d = 2.2), a capacity of 41% of the ultimate tensile strength might not be an undesirable outcome. Historically, Eq. 3 presented by JSCE [26] has been used as a reference to estimate the strength of a bent FRP bar based on its bend radius and bar diameter. Applying Eq. 3 to the experimental results of this project yields an exact correlation with the experimental findings ($\chi_{JSCE}/\chi_{exp} = 1$).

$$\chi_{JSCE} = 0.05\frac{r}{d} + 0.30 \quad (3)$$

However, the recently released ACI CODE 440.11-22 [13] references ASTM D7957 [18], which specifies a minimum r/d of 3.0 for GFRP bars used in FRP-RC design. This ratio is notably higher than the one used for the CFRP spirals. Alternatively, ACI CODE 440.11-22 [13] allows the use of experimental data to determine the guaranteed tensile strength at the bend as the mean ultimate strength minus three standard deviations. If this latter approach is applied, the guaranteed bend strength suggested by the experimental data would be only 3.3 kip, which corresponds to 21% of a straight companion portion's ultimate tensile strength.

This lower bound may hinder the widespread adoption of CFRP as an alternative to shear and transverse reinforcement. Therefore, a second phase of bent bar tests was conducted on 0.28 in. CFRP spirals to investigate whether increasing the bend diameter to at least the current minimum criteria stated by ASTM D7957 [18] for GFRP bars would significantly improve the strength at the bend. Additionally, this data will contribute to the development of a carbon-oriented standard currently being undertaken by the ASTM D30.10 Committee on Composite Materials. The results of this examination are presented in Appendix G.

Chapter 4. STATISTICAL EVALUATION OF MATERIAL PROPERTIES AND SAMPLE SIZES

4.1 Introduction and Scope

As documented in earlier chapters, corrosion of conventional steel reinforcement remains one of the most critical durability challenges for coastal bridge infrastructure. FRP materials offer a viable alternative, particularly in highly aggressive environments, but their widespread implementation depends not only on design provisions and codes, but also on practical, efficient acceptance and QA/QC procedures at the project level. Material testing programs must therefore be calibrated to reliably confirm the quality of FRP products without imposing unnecessary costs or disruption to construction.

The Harkers Island Bridge represents a landmark project as the first fully FRP-reinforced bridge in North Carolina. However, the project relied on special provisions similar to those used by other DOTs along the U.S. East Coast, many of which were adapted from steel-oriented specifications and early FRP guidance. As a result, some prescribed tests and sample sizes may not fully align with the actual behavior and variability of FRP materials. At the same time, most existing product standards focus on GFRP bars, and there is still no ASTM standard explicitly dedicated to CFRP bars or strands, which can hinder the broader adoption of CFRP as a primary prestressing material.

Within this context, this chapter uses the Harkers Island material database to develop a statistical framework for CFRP acceptance testing. The analysis focuses on two key CFRP products used in the bridge: (1) 0.6 in. seven-wire CFRP prestressing strands, used in piles and girders, tested in tension; and (2) 0.28 in. uni-strand CFRP spirals, used as transverse reinforcement in the driven piles, tested at their bent regions.

For both products, the chapter examines the distribution of measured properties. It evaluates how many replicate tests are realistically needed to (i) validate material quality and design assumptions with an acceptable confidence level, and (ii) support the development of future CFRP-specific standards.

In summary, the goal of this chapter is to translate the Harkers Island test results into practical guidance on sample sizes and acceptance criteria for CFRP strands and spirals. The findings are intended to inform DOTs, manufacturers, designers, and end users as they prepare contractual documents for all-FRP-reinforced structures, and to help bridge the gap between design, construction, and inspection by suggesting a more efficient, statistically grounded QA/QC protocol.

4.2 Statistical Methods

The following section summarizes the data collected and the foundational theory underlying the statistical approach. First, the origins of the available datasets are discussed in more detail. Then, fundamental equations and key concepts are introduced. Lastly, an alternative method to estimate an appropriate sample size is presented.

4.2.1 Test Groups

In this chapter, three distinct types of datasets are used. Two of them are associated with tension tests on 0.6 in. CFRP strands according to ASTM D7205 [20] (see Chapter 2). The remaining dataset was obtained by testing the bent portion of 0.28 in. CFRP spirals as per ASTM D7914 [21] (see Chapter 3). Therefore, all data used in this document are experimental. Moreover, because all experiments were conducted under the same conditions, the data points are expected to be independent and identically distributed (*iid*). The latter characteristic makes it reasonable to assume that all samples (x) follow a standard normal distribution (N) with mean, μ, and standard deviation, σ, shown in Figure 22, and numerically expressed in Eq. (4). It is worth mentioning that the assumption of normality was further validated before proceeding with the calculations.

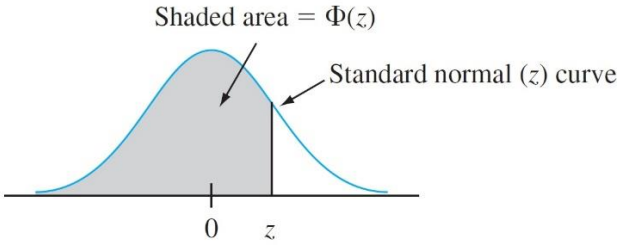

Figure 22. Standard normal distribution (Taken from [27])

The three datasets under study are summarized in Table 7. Two datasets (NCSU-T and NCSU-B) were experimentally collected as part of this work. In contrast, the third dataset (TR-T) was obtained from manufacturer-internal QA/QC tests conducted on 0.6 in. CFRP strands from January 2022 through February 2023. Additionally, although appropriate comparisons between NCSU-T and TR-T data are presented later in this report, the datasets were treated separately, resulting in different sample estimates.

Table 7. Available datasets

Dataset	Material	Number of tests	ASTM Standard
NCSU-T	0.6 in. CFRP Strand	290	ASTM D7205
TR-T		1260	
NCSU-B	0.28 in. CFRP Spiral	19	ASTM D7914

4.2.2 Sample Size Estimation Procedure

Equations (4) to (11) summarize the calculations required to estimate an appropriate sample size (number of test replicates), based on a specific confidence interval and margin of error, and the data collected following a normal distribution. Firstly, Eqs. (4) to (7) define the key parameters to determine from each of the available datasets. The hat symbol refers to the best estimate of the parameter based on the data collected (e.g., $\hat{\sigma}$ is the estimator for the population standard deviation, which is the sample standard deviation, s).

$$X_1, \dots, X_n \sim iid\ N(\mu, \sigma) \tag{4}$$

and

$$\hat{\mu} = \bar{x} \tag{5}$$

and

$$\widehat{\sigma^2} = \frac{1}{n-1}\sum_{i=1}^{n}(x_i - \bar{x}^2) \tag{6}$$

and

$$\hat{\sigma} = \sqrt{\sigma^2} = s \tag{7}$$

Once the estimated parameters have been determined, a confidence interval at a specified confidence level can be defined using *Z*-scores from a normal distribution. The *Z*-scores are provided in Appendix H. For example, a $100(1-\alpha)\%$ confidence interval for the mean, μ, of a normal population when the value of σ is known is given by Eq. (8).

$$\hat{\mu} \pm Z_{\alpha/2} \cdot \frac{\hat{\sigma}}{\sqrt{n}} \tag{8}$$

and

$$E = Z_{\alpha/2} \cdot \frac{\hat{\sigma}}{\sqrt{n}} \tag{9}$$

Where $Z_{\alpha/2}$ is a factor linked to the confidence level (CL) adopted (e.g., 90%, 95%, 99%, etc.), and *E* corresponds to the margin of error associated with the CL. Further, if *E* is given as an absolute value, Eq. (9) could be used directly to obtain the required sample size as shown in Eq. (10). However, the margin of error is typically expressed as a percentage, *e*. In that case, it is necessary to rewrite Eq. (9) by normalizing the standard deviation with respect to the sample mean ($COV = s/\bar{x}$). Then, the sample size can be estimated by Eq. (11).

$$n = \left(Z_{\alpha/2} \cdot \frac{s}{E}\right)^2 \tag{10}$$

or

$$n = \left(Z_{\alpha/2} \cdot \frac{COV}{e}\right)^2 \tag{11}$$

One more time, the main difference between Eq. (10) and Eq. (11) is that the former uses an absolute, numerical value, E, for the margin of error, whereas the latter expresses it as a percentage, e. This report will primarily use Eq. (11) to estimate the sample sizes for each dataset. It can be noted that Eq. (11) makes it easier to calculate the sample size for different values of $Z_{\alpha/2}$ and e. Hence, results will be tabulated for each case.

To summarize, this work employed conventional statistical techniques to analyze the data obtained. First, descriptive statistics were used to show the data dispersion and the most representative statistical parameters. The data were assessed for normality to determine whether conventional inferential procedures were appropriate for this project. To that end, histograms and box plots (also known as box-and-whisker plots) were elaborated.

Finally, sample sizes for each parameter of interest were estimated under the assumption of normality. Given the large amount of data collected, the analyses were conducted on Microsoft Excel. However, the use of automated functions was limited to the extent possible to ensure accurate application of statistical principles. The latter was the primary reason not to adopt more advanced statistical software at this stage.

On a separate note, the minimum guaranteed strength of a material is typically defined as the mean minus three standard deviations of the experimental results, which sets a conservative lower bound. By adopting this criterion, it is expected that at least 99.7% of the experimental values will be covered. This is a valid approach, as obtaining large amounts of data may not always be feasible, which increases uncertainty in the results. However, when a lesser degree of certainty is desired, or at least tolerable, a smaller multiplier may be used. The $Z_{\alpha/2}$ values for different CLs are depicted in Table 8, which are consistent with ASTM E122 [28].

Table 8. Standard normal percentiles and critical values

	Percentiles (%)			
	90	**95**	**99**	**99.7**
α (tail area)	0.1	0.05	0.01	0.003
$\boldsymbol{Z_{\alpha/2}}$	1.64	1.96	2.56	3.0

4.3 Results and Discussion

This section is divided into two parts, each focusing on a different material under study: 0.6 in. CFRP strands and 0.28 in. CFRP spirals. For each subsection, the data distribution and descriptive parameters are first presented. When necessary, specific details about experimental procedures or data-collection methods are also included. Next, the assumption of normality was examined. Finally, a sample size estimate was calculated for each dataset. Additionally, detailed discussion and comments accompany each set of data and results.

4.3.1 CFRP Strands

As mentioned earlier, there are two datasets related to this material: NCSU-T and TR-T. The first dataset, NCSU-T, comprises material characterization tests conducted at the CFL at NCSU as part of the Harkers Island Bridge project. A detailed review of this dataset was presented in Chapter 2.

On the other hand, the TR-T dataset was collected directly by Tokyo Rope as part of their internal QA/QC campaign. This dataset comprises 1,260 strands from 252 different lots, tested between January 2022 and February 2023. Notably, the number of lots and specimens tested by Tokyo Rope is much higher because it encompasses all the material produced by the manufacturer during that period. Additionally, a key difference between the two datasets is that in TR-T, all specimens were tested to failure, whereas in NCSU-T, only 95 of 290 strands were tested to failure.

Not testing all NCSU-T data entries to rupture is due to three main reasons: (i) safety measures in the lab, which is a shared academic space used by several students, faculty, and staff; (ii) the large amount of debris generated upon failure, which could affect the normal function of the UTM pressurized hoses and grips; and (iii) exceeding the minimum guaranteed tensile strength of 60.7 kips was enough to validate

each specimen according to the special provisions, so most strands were unloaded after surpassing this value to speed up the testing process. Notably, the first two reasons pertain to the material's brittleness, underscoring another challenge in the use of FRP technology. In all cases, two strands per lot were tested to rupture whenever possible.

It should be noted that the 0.6 in. CFRP strands were tested in tension in accordance with ASTM D7205 [20]. These tests determine three key parameters: (i) measured cross-sectional area, (ii) guaranteed tensile strength, and (iii) tensile modulus. While a sample size can be estimated based on the results for each parameter, this work primarily focuses on the tensile modulus, which has been identified as the most sensitive and inconsistent among the three outcomes of ASTM D7205 [20]. This also makes the tensile modulus the most critical parameter to evaluate before validating a lot. Further explanation on why the other two parameters obtained from ASTM D7205 [20] were not used to estimate the sample size are summarized in Appendix E.

4.3.1.1 Data Distribution and Descriptive Parameters

Figure 23 depicts the dispersion of results for the modulus of elasticity from the TR-T dataset. The dispersion for the NCSU-T dataset was previously shown in Figure 14. In both cases, the mean value is represented by a solid line behind the data points. Notably, the TR-T values are less scattered, indicating a lower standard deviation. Table 9 summarizes the most representative descriptive parameters for each dataset.

Table 9. Descriptive parameters for the NCSU-T and TR-T series

Dataset	n	$\bar{x}$	Min	Max	Mode	Median	Range	s
NCSU-T	290	22,424	20,322	25,749	22,446	22,381	5,427	807
TR-T	1,260	22,159	21,430	23,289	22,467	22,158	1,858	234

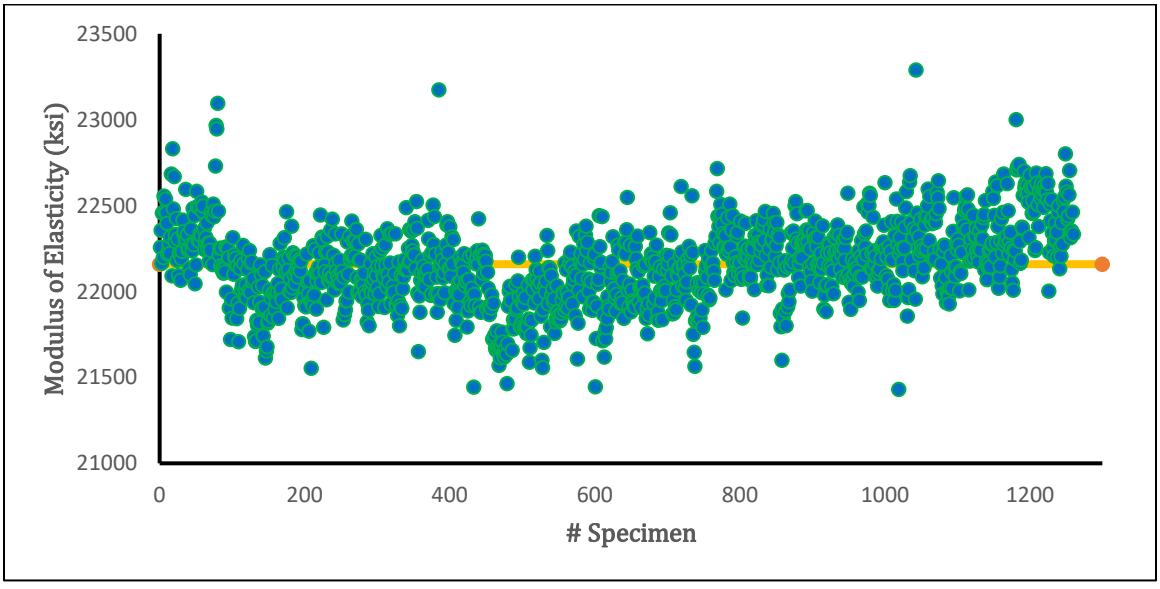

Figure 23. Data dispersion for tensile modulus in the TR-T series

The two datasets are consistent with each other. For example, the NCSU-T mean is just 1.2% higher than TR-T's, and both datasets have similar modes, which is a positive sign given the significant difference in the number of data entries between the two series. This indicates that the material under study is sufficiently consistent for its descriptive parameters to converge even with smaller samples. Additionally, the similarity between the mean and median (0.2% and 0.005% relative differences for NCSU-T and TR-T, respectively) indicates that the data are symmetrically distributed. The only concern is the substantially higher standard deviation in NCSU-T, which is consistent with a broader range, including more extreme minimum and maximum values. The high standard deviation of NCSU-T will be further discussed in the following sections.

4.3.1.2 Normality Assessment

Before estimating the sample size using the method described in Section 4.2.2, which assumes normality, it is crucial to verify whether this assumption is reasonable. Figure 24 and Figure 25 show the histograms obtained for the NCSU-T and TR-T series, respectively. NCSU-T was divided into 13 equal-width classes, each measuring 430 ksi. Due to the larger number of datapoints, TR-T was divided into 25 classes, each 76 ksi wide. A smaller class width more accurately captures the data distribution of the 1,260 specimens comprising the TR-T dataset.

The two histograms show a clear normal distribution with a single peak. Additionally, they both appear slightly skewed to the left (more points on the right side, toward the upper tail). The latter is expected, as manufacturers tend to overshoot the strength of their products rather than fall short, thereby justifying more values beyond the mean. Nonetheless, this skewness is not sufficiently pronounced to distort the graph or disrupt its symmetry. This is also expected, given the consistency between the mean and median values for both groups (see Table 9).

In addition to the histograms shown above, boxplots were also created for each dataset. These boxplots (also called box-and-whisker plots) are an excellent resource for identifying outliers and assessing the symmetry of normally distributed data. Figure 26 shows a conceptual boxplot, where the box indicates the range between the first and third quartile ($Q1$ and $Q3$, respectively). This range encompasses 50% of the data collected. An intermediate line inside the box represents the median. The lines extending out of the central box (whiskers) define the minimum and maximum values as $Q1 - 1.5IQR$ and $Q3 + 1.5IQR$, respectively. IQR is the interquartile range, obtained by finding the length of the box as $Q3 - Q1$. Any value beyond these whiskers is considered an outlier. Additionally, the symmetry of a dataset is indicated by the even distribution of lines and boxes on both sides of the graph.

Figure 27 illustrates the boxplots for both the NCSU-T and TR-T series. An "x" inside the box represents the mean value. These box-and-whisker plots visually summarize the descriptive statistics discussed earlier. For example, NCSU-T displays more dispersed data, indicated by a thicker box and longer whiskers that cover a wider range. It is also clear that NCSU-T has more data points beyond the median value, with boxes that differ slightly in size. However, both datasets display good symmetry and a correlation between their mean and median values. Therefore, it is reasonable to assume normality in both datasets and proceed with sample size estimation. Interestingly, both datasets show almost the same number of outliers below and above the median. In this work, the datasets have been processed as-is; however, some extreme outliers may warrant further investigation in future work.

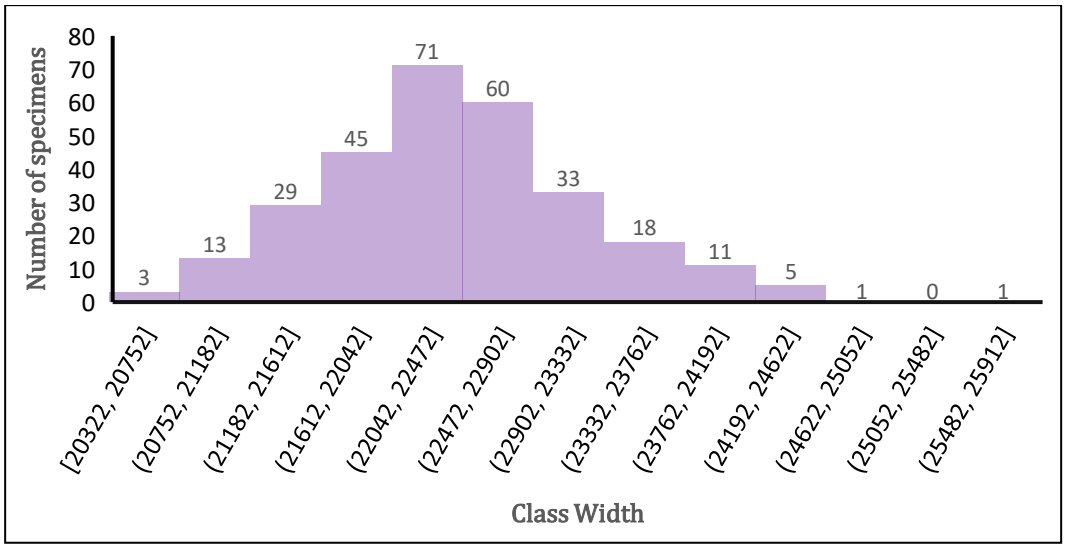

Figure 24. Data distribution in the NCSU-T series

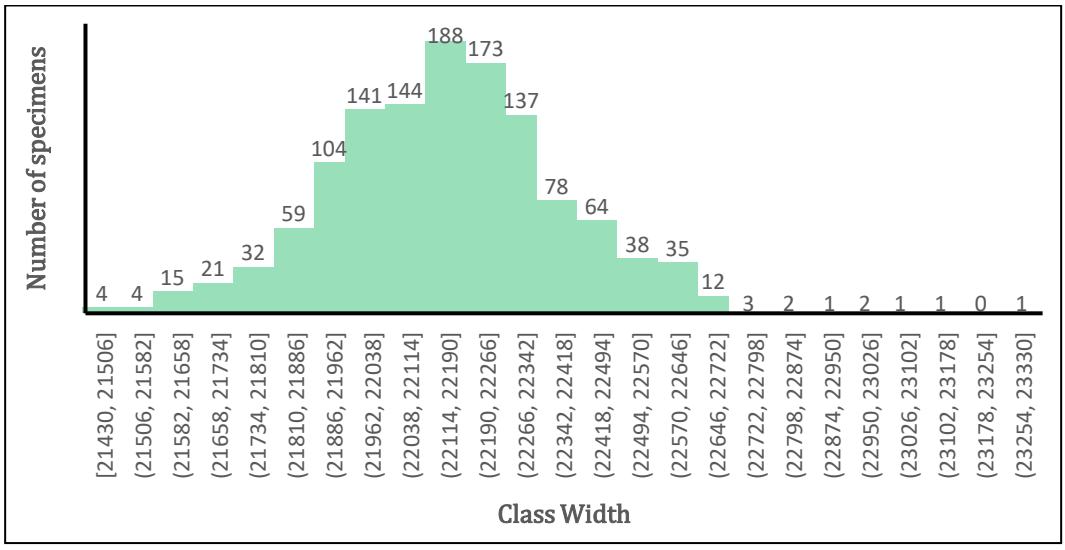

Figure 25. Data distribution in the TR-T series

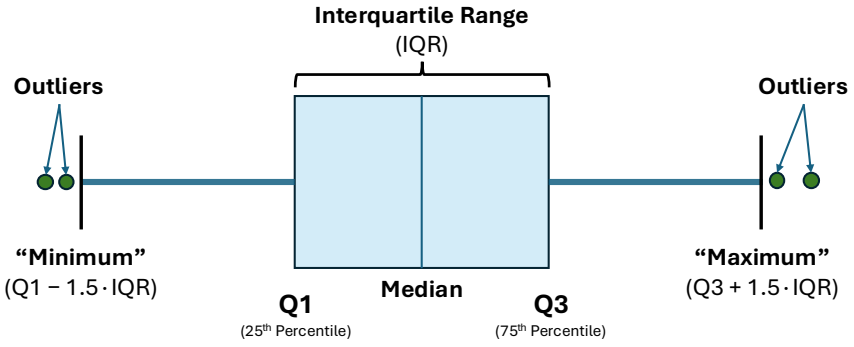

Figure 26. Boxplot graph representation

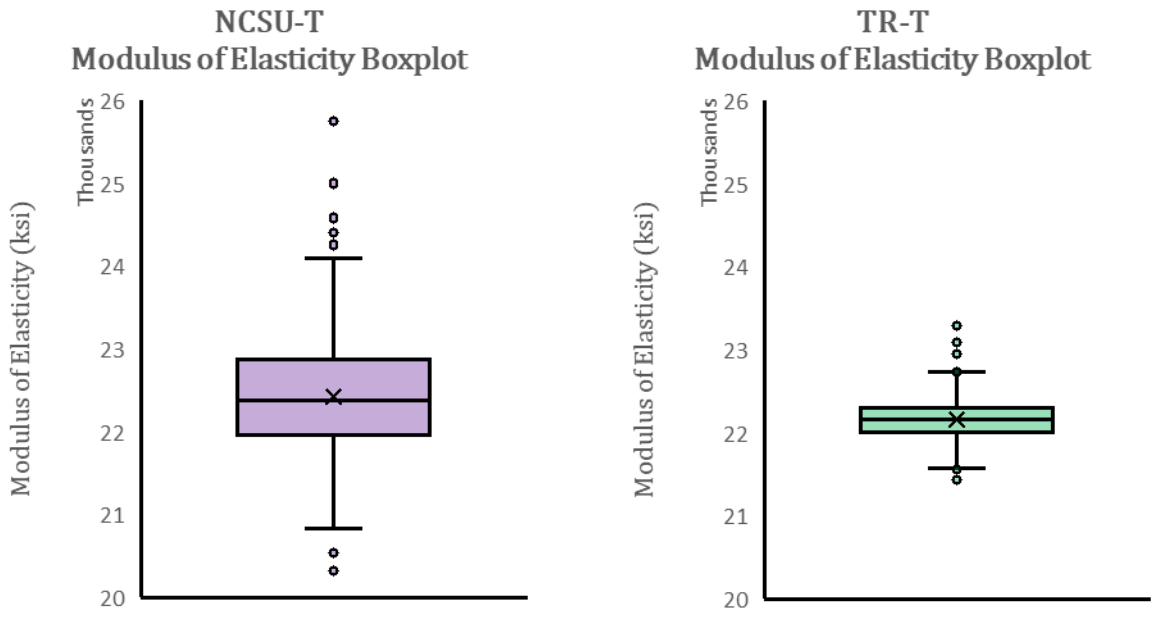

(a) NCSU-T series *(b) TR-T series*

Figure 27. Data symmetry and outliers' identification

4.3.1.3 Sample Size Estimation

Once the normality assumption has been confirmed, Eq. 11 can be used to estimate the sample size for various confidence levels (CLs). It should be noted that the selected CL will be expressed as a $Z_{\alpha/2}$ value. The margin of error, *e*, was maintained at 5%. This is standard practice and enables examination of how choosing a different CL, the most influential parameter in determining a sample size, affects the results. The exact sample size calculated was rounded up to the nearest higher integer. Table 10 summarizes the values obtained. The COVs for the NCSU-T and TR-T series were 3.6% and 1.1%, respectively.

Table 10. Sample size estimation based on 0.6 in. CFRP strands' tensile modulus (*e*=5%)

		NCSU-T		**TR-T**	
CL (%)	$Z_{\alpha/2}$	$n_{calculated}$	n_{final}	$n_{calculated}$	n_{final}
90	1.64	1.39	**2**	0.12	**1**
95	1.96	1.99	**2**	0.17	**1**
99	2.56	3.39	**4**	0.29	**1**
99.7	3.00	4.66	**5**	0.40	**1**

The estimated sample sizes differ significantly across datasets. This was expected given the much lower standard deviation of the TR-T series, which, in turn, leads to fewer replicates. The latter occurs because the data are so consistent that the mean can be estimated even with a few tests, and the CL does not increase the sample size. This behavior suggests that the TR-T mean is essentially equal to the population mean. By contrast, the NCSU-T data are significantly more dispersed, as evidenced by a higher standard deviation and coefficient of variation, necessitating more replicates to achieve the same CL.

On the other hand, it is notable that the dataset is highly consistent (with minimal variation). Therefore, since every specimen in the TR-T series was tested to failure, the ultimate strength was also analyzed for comparison. For completeness, the 95 specimens tested to failure in NCSU-T were also examined. After conducting the same process as with the modulus of elasticity, the sample size estimations based on ultimate strength are presented in Table 11.

Table 11. Sample size estimation based on 0.6 in. CFRP spirals' rupture strength (*e*=5%)

		NCSU-T		**TR-T**	
CL (%)	$Z_{\alpha/2}$	$n_{calculated}$	n_{final}	$n_{calculated}$	n_{final}
90	1.64	1.11	**2**	1.47	**2**
95	1.96	1.59	**2**	2.11	**3**
99	2.56	2.71	**3**	3.59	**4**
99.7	3.00	3.72	**4**	4.93	**5**

Interestingly, the dispersion of ultimate strength obtained from NCSU-T is lower than that for TR-T, resulting in a smaller sample size. The latter seems reasonable given the smaller number of data points in NCSU-T, but it contradicts the observed tensile modulus dispersion, in which TR-T was much more consistent despite having more data points. Nonetheless, the most notable observation from Table 11 is that the sample sizes are consistent across datasets and, more importantly, align with the modulus-based sample sizes for NCSU-T previously shown in Table 10. The latter may suggest a misleading estimate of sample size when using TR-T's modules.

It has been noted that the modulus of elasticity is a sensitive parameter whose value depends on other variables and criteria. Based on the results obtained, it is suspected that the modulus of elasticity in TR-T was calculated from displacements directly reported by the testing machine, rather than from the actual strains developed in the specimen as the tensile load was applied. This would explain the perfect consistency in its values, with the sample sizes held constant across different CLs. Of course, this is just an assumption, and verification is needed. Further insights are provided in Chapter 6.

To establish recommended minimum sampling requirements, the sample sizes determined using TR-T, based on the tensile modulus as the parameter of analysis, are now disregarded. Consequently, the conservative number of replicates should be 2, 3, 4, and 5 for CLs of 90, 95, 99, and 99.7%, respectively. Any of these sample sizes would significantly improve upon the specifications for the Harkers Island bridge, which required up to 10 replicates. Notably, the number of replicates could be halved even with the highest level of confidence.

Furthermore, it is crucial to note that increasing the CL, particularly beyond the 90% CL range, does not necessarily enhance the accuracy of the results. Following the law of large numbers, a higher CL will increase the number of replicates required to guarantee that the average falls into that broader confidence interval associated with a higher CL. Moreover, given the bell shape of a normal distribution, which flattens out near its tails on each side (see Figure 22), a significant increase in replicates will be required as the CL approaches 100%, which may not even be statistically attainable. ASTM E122 [28] refers to this issue by denominating a 99.7% CL as practical certainty. The latter justifies taking the mean minus three standard deviations (i.e., 99.7% CL) as the minimum guaranteed value, given the lack of more extensive data.

Based on these preliminary results, the suggested sampling campaign and QA/QC protocol for an FRP-reinforced project would be:

i. Randomly select five specimens from each lot to achieve a 99.7% confidence level in the material collected.
ii. Test two specimens per lot in tension according to ASTM D7205 up to the minimum guaranteed tensile strength while recording strains at least until reaching 50% of the expected ultimate (rupture) capacity. Spot check the diameter of each specimen tested and confirm it does not exceed the maximum diameter specified in the special provisions and/or applicable ASTM standard.
iii. Calculate the modulus of elasticity using the nominal area and confirm that the average for each lot exceeds the minimum guaranteed tensile modulus specified by the special provisions.
iv. In the unlikely event of non-compliance, test one more specimen of the same lot until the average of all tested specimens exceeds the minimum guaranteed tensile modulus required by the special provisions. No more than five specimens per lot should be tested. If the stiffness requirement is not met after testing five specimens, the lot should be rejected.
v. If any of the specimens tested fail before reaching the minimum guaranteed tensile strength, the lot should be rejected once it has been verified that the premature failure did not occur due to a preparation issue (i.e., pipe crushing, anchor slippage, previously damaged specimen).

4.3.2 CFRP Spirals

Due to reduced strength at the bent portion, it is especially notable that the strength at the bend locations tested in accordance with ASTM D7914 [21] was not included in the special provisions. This test should be of utmost importance when bends are present in FRP bars, since the strength of a straight portion may not control the acceptance criteria.

Therefore, as part of the material characterization, 20 spirals with the same geometry (18 x 18 in.) as those used in the square piles were tested (see Chapter 3 for test details). One spiral was excluded due to issues with the Data Acquisition System (DAQ), resulting in 19 data points for analysis in this section. Each tested spiral belonged to a different lot. Additionally, the CFRP spirals had a bend radius-to-bar diameter (r/d) ratio of 2.2. This ratio is considered the most critical parameter affecting strength reduction due to bends [29]. However, it is lower than the minimum r/d ratio required for GFRP bars according to ASTM D7957 [18]. It is important to note that there is currently no ASTM standard specifically addressing CFRP.

On a separate note, unlike the ASTM D7205 [20] tension test described previously, where the tensile modulus (stiffness) is measured, the ASTM D7914 [21] test does not include this parameter. Instead, the focus is solely on strength at the bend location. Therefore, the ultimate (rupture) strength at the bend will be used as the criterion to determine an appropriate sample size. Also, this dataset was named the NCSU-B series.

All tested spirals exhibited the same failure mode, characterized by a clear rupture in the bent section of the spirals within the concrete blocks. For each specimen tested, only one of the two spiral legs failed, maintaining data consistency. It is also noteworthy that the manufacturer did not provide a value for strength reduction in their datasheets. This reduction is typically expressed as a percentage of the ultimate strength of a similar straight specimen tested in tension.

Since the NCSU-B dataset contains only 19 entries, a normal distribution is no longer appropriate. Instead, a student's T-distribution provides a suitable alternative. A T-distribution is a slight variation of a normal distribution and is more appropriate for smaller samples, typically fewer than 40. The methodology and calculation process remain the same as those outlined in 4.2.2, but the Z-score values will differ because the areas under the T-distribution curve change (Figure 28). In this case, the Z-score is replaced by a $t_{\nu,\alpha/2}$ score, where ν represents the degrees of freedom (taken as n-1), and α is a factor related to the selected confidence level. A student's T-distribution table is included in Appendix H, and the corresponding values for NCSU-B are provided in Table 12. It should be noted that the factors listed in Table 12 are higher than those in Table 8, primarily because the uncertainty is greater with fewer data.

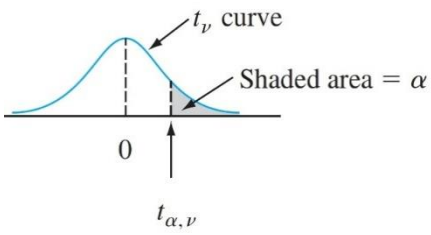

(a) standard curve

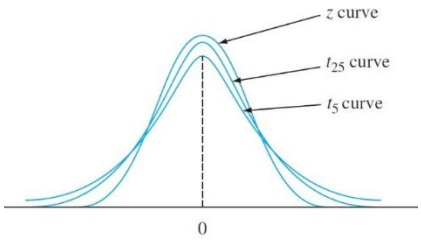

(b) curve for different degrees of freedom, where z curve is the standard normal curve

Figure 28. Student t distribution (Taken from [27])

Table 12. T-Student percentiles and critical values

	Percentiles (%)			
	90	**95**	**99**	**99.7**
α (tail area)	0.1	0.05	0.01	0.003
$t_{\nu,\alpha/2}$	1.734	2.101	2.878	3.610

4.3.2.1 Data Distribution and Descriptive Parameters

Figure 29 shows the dispersion of the results obtained for ultimate strength. Once again, the mean value is represented by a solid line. Table 13 summarizes the most representative descriptive parameters for the NCSU-B dataset. It is interesting to see such a difference between the maximum and minimum values. Nonetheless, the mean appears reasonably close to the median, which is a positive sign overall. Moreover, the mean ultimate strength of the bent spirals turns out to be 41% of the average ultimate strength of a straight portion (15.9 kips).

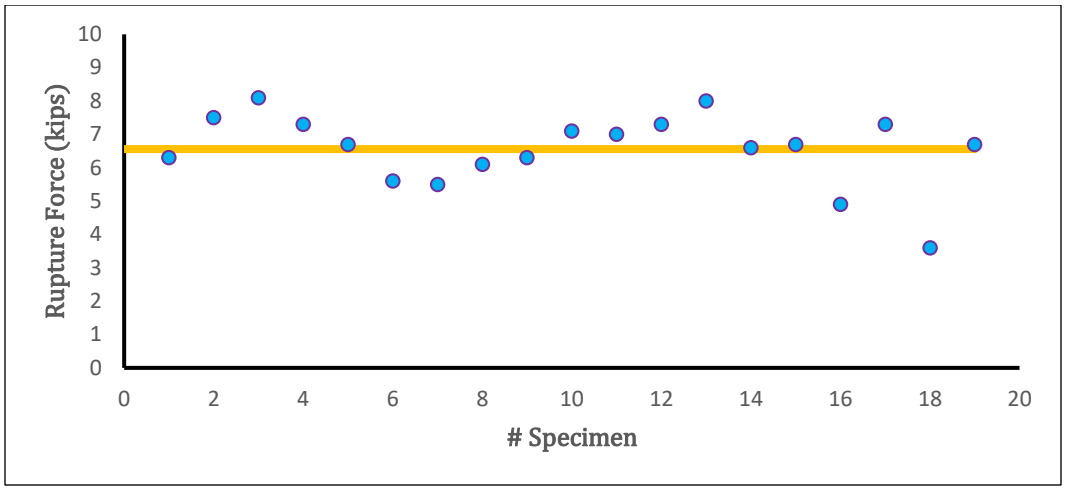

Figure 29. Data dispersion in the NCSU-B series

Table 13. Descriptive parameters for the NCSU-B series

Dataset	n	$\bar{x}$	Min	Max	Mode	Median	Range	s
NCSU-B	19	6.56	3.6	8.1	7.3	6.7	4.5	1.09

4.3.2.2 Normality Assessment

A histogram for the NCSU-B series is shown in Figure 30. A constant class width of 1.4 kips was used. The data is slightly skewed to the right (with more values on the lower tail). However, given the limited number of data points, it is reasonable to assume the data follows a normal distribution under a Student's T-distribution. The T-distribution already accounts for reduced data, allowing the sample size estimate to proceed.

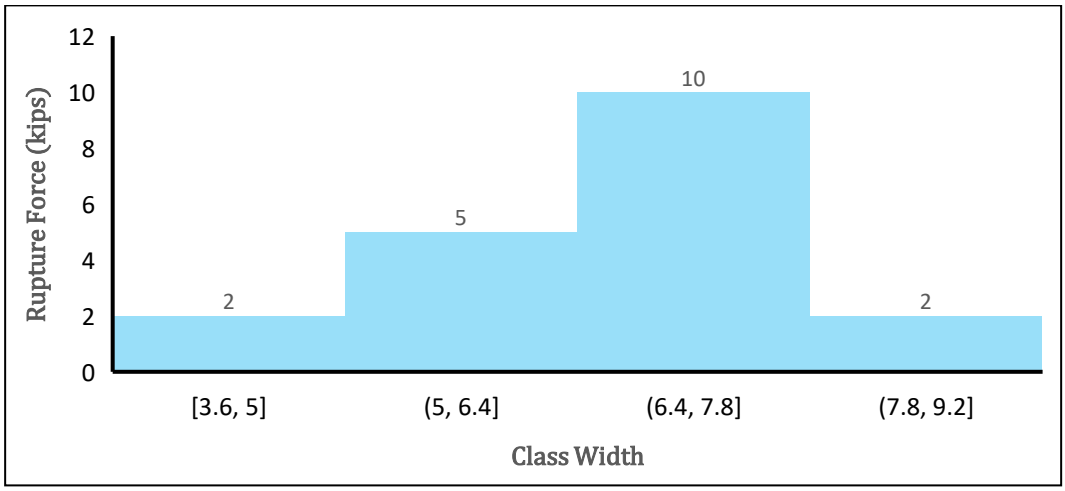

Figure 30. Data distribution in the NCSU-B series

Furthermore, a boxplot was created and is shown in Figure 31. The boxplot indicates good symmetry both within the box and along the whiskers. Notably, there is only one outlier on the lower end. This outlier may also warrant further investigation. Nevertheless, all data were included in this work. It can also be observed that the mean does not precisely match the median, which is slightly higher. Both the reduced data and the outlier influence this difference. In any case, a T-distribution is a suitable fit for the data and will be used next.

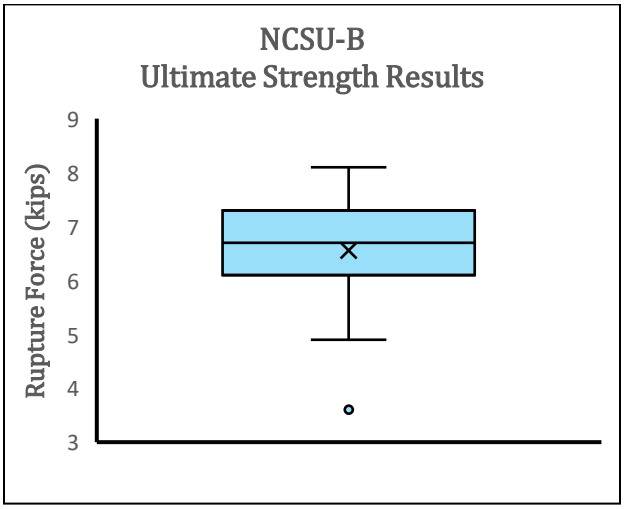

Figure 31. Data symmetry and outliers' identification: NCSU-B series

4.3.2.3 Sample Size Estimation

The sample size was estimated using Eq. (11) by substituting $\boldsymbol{Z_{\alpha/2}}$ with the $\boldsymbol{t_{v,\alpha/2}}$ score listed in Table 12. The margin of error was maintained at 5% and the exact sample size calculated was rounded up to the nearest higher integer. Table 14 summarizes the values obtained. The COV for the NCSU-B series was 16.6%, which is quite concerning and likely the main reason for the large sample size estimate.

Table 14. Sample size estimation based on 0.28 in. CFRP spirals' ultimate strength (*e*=5%)

		NCSU-B	
CL (%)	$\boldsymbol{t_{v,\alpha/2}}$	$\boldsymbol{n_{calculated}}$	$\boldsymbol{n_{final}}$
90	1.734	33.3	**34**
95	2.101	48.9	**49**
99	2.878	91.7	**92**
99.7	3.610	144.3	**145**

The sample size estimation presented in Table 14 does not represent a realistic scenario. Testing the bent portion of FRP materials according to ASTM D7914 [21] is already time-consuming, making it essentially impossible to test such a large number of specimens per lot. However, validating this parameter is critical, necessitating suitable alternatives. First, it would be ideal to have more data to verify

whether these results are consistent with others. Nonetheless, as part of additional work (presented in Appendix G), more specimens have been tested, and similar results (average and standard deviation) have been obtained. Then, the options are reduced to two:

(i) The CFRP spirals evaluated are not being produced with the same quality, hence their results vary so much among them that setting a lower bound would almost be unrealistic due to the excessive variation.
(ii) The ASTM D7914 [21] test incorporates so many uncertainties and misalignments that it is not a reliable option. Several authors have encountered this problem with this test [23], [24], and some have proposed an alternative test method that is already included in the CSA S807:19 specifications [17], [30]. They have reported lower COVs ranging from 3.8% to 7.2%.

Alternatively, instead of using conventional approaches to estimate sample size, which are primarily based on the mean and standard deviation as initial parameters (required for a normal distribution), a more complex statistical process could be implemented. The primary option is bootstrapping, where the standard deviation plays a lesser role, and the focus is on the median and normally distributed data. Throughout this report, the data for tension tests of strands and bent-bar tests of CFRP spirals are consistent at the central location, as indicated by symmetric box-and-whisker plots. This consistency could be used to analyze how the sample size estimate varies in future work.

Therefore, given the results for the CFRP spirals, neither a sampling protocol nor QA/QC guidelines will be recommended at this time, as it is impractical to determine an appropriate procedure based solely on these results. Additionally, given the current uncertainty and potential issues associated with CFRP bends, their use as stirrups and transverse reinforcement is not recommended until clear manufacturing requirements and testing procedures are established.

Chapter 5. FULL-SCALE SHEAR TESTS OF CFRP-PRESTRESSED FIB GIRDERS

5.1 Motivation and Context

As discussed in Appendix A, the research community has invested substantial efforts into understanding the behavior of concrete bridge girders prestressed with CFRP strands, most notably through NCHRP Project 12-97 [8], which focused on flexural behavior and prestress-related issues, and the ongoing NCHRP Project 12-121, which targets the role of FRP auxiliary reinforcement (transverse, skin, confinement, etc.) in CFRP-prestressed girders. Together, these projects are expected to serve as the technical basis for future AASHTO provisions governing all-FRP-reinforced/prestressed concrete bridge beams.

However, several gaps remain, particularly around shear behavior in large, realistic bridge girders that are both prestressed with CFRP and transversely reinforced with GFRP stirrups:

- Many existing experimental programs use relatively small or moderate girder depths and shorter spans, which may not fully capture size effects that are relevant for modern bridge structures.
- Test setups often overhang the specimen beyond the support to intentionally exclude the influence of transfer lengths and end-zone reinforcement, creating a clean academic shear problem but not an entirely realistic representation of in-service conditions.
- There are relatively few tests on I-shaped (such as an FIB-type) girders prestressed with CFRP and reinforced with GFRP stirrups that are detailed and built using the same materials and practices used in actual bridges.

The Harkers Island Bridge provides a unique opportunity to address part of this gap. The 54 in. FIB girders used in the bridge are prestressed with CFRP strands and reinforced with GFRP stirrups, and they represent the most common girder depth used in the project. Testing full-scale girders with the same cross-section, prestressing layout, and (in one case) the same stirrup configuration as the Harkers Island design creates a direct link between experimental data and field practice.

5.1.1 Evolution of the Experimental Plan

A full-scale testing component was included in the Harkers Island research proposal from the outset. However, the specific specimens and test configuration were not defined from the very beginning. Early in construction, the first set of 54 in. FIB girders produced for the bridge exhibited extensive end-region cracking and spalling after detensioning, resulting in their rejection. At that time, the research team considered transporting these girders to the CFL at NCSU for testing.

Nevertheless, several practical and technical considerations led to a different strategy:

- The affected girders were approximately 100 ft long, which would have required oversized load permits, police escorts, and lifting capacities beyond the existing cranes at the CFL.
- The research questions associated with those specific girders were not yet well defined; testing them without a clear focus risked investing time and resources in not-so-meaningful data.

As the literature review and project experience matured, it became clear that the most impactful role for the full-scale research component of this project would be to complement, not duplicate, the ongoing work of NCHRP 12-121 on the evaluation of shear behavior of all-FRP-reinforced girders, emphasizing the role and contribution of GFRP stirrups. Since NCHRP 12-121 constitutes a comprehensive study of several variables (e.g., shear reinforcement ratio, pretension vs post-tension, type of FRP reinforcement, shear span to depth ratio, and prestressing level), this project focuses on a targeted shear testing program on three deep FRP-prestressed FIB girders that are:

- Closer in scale and detailing to actual Harkers Island girders; and
- Tested under realistic support conditions, without overhanging the ends to isolate the shear span from end reinforcement.

5.2 Research Objectives and Scope

The planned experimental program on 54 in. FIB girders was designed to address the following questions:

1. Shear capacity and conservatism of current design provisions
   - How do the measured shear capacities of deep, CFRP-prestressed, GFRP-reinforced FIB girders compare with predictions from existing shear design approaches (e.g., existing steel-oriented codes, truss analogy, Modified Compression Field Theory (MCFT)-based methods)?
2. Influence of transverse reinforcement ratio and spacing
   - How does increasing stirrup spacing (and thus reducing transverse reinforcement ratio) affect the shear behavior and failure mode of CFRP-prestressed FIB girders?
   - What is a realistic upper bound on stirrup spacing for this type of girder, considering both strength and crack control?
3. Effect of GFRP stirrup manufacturer and surface characteristics
   - For a fixed stirrup spacing and overall geometry, do different GFRP stirrup products (surface treatment, manufacturer) result in meaningfully different shear behavior?
4. Comparison with steel-reinforced control girders
   - How does the shear response of an all-FRP-reinforced FIB girder compare with an otherwise similar steel-prestressed, steel-reinforced control girder?
   - To what extent do differences in stirrup stiffness or bond affect shear strength and crack patterns?
5. Realistic boundary conditions and size effects
   - How do deeper sections (54 in.) with supports located near the girder ends (field representative) behave in shear, compared with the smaller, overhung girders commonly used in prior research?

The scope of this chapter is limited to the planned experimental program and analytical framework. At the time of writing, the design and production at CPS Wilmington have been completed. The GFRP bars and stirrups were donated by Mateenbar (formerly known as Owens Corning) and MST Bar. Similarly, the CFRP strands were donated by Tokyo Rope USA. The production of the three 50 ft. long, 54 in. FIB-CFRP prestressed girders took place from Feb 13-18. The results, data analysis, and design recommendations emerging from the FIB girder tests will be documented in a future companion report.

During production, the two top strands ruptured because of a shift in the steel bulkhead template, which delayed the original schedule as the strands were removed and construction restarted from scratch. The latter highlights the material's brittleness, which poses a safety hazard, particularly for construction workers during prestressing operations. Given that a similar event occurred during pile production for the Harkers Island Bridge, it would be valuable to develop procedures to visually identify surface damage to the PET wrap covering the CFRP strands, thereby reducing the likelihood of premature failure.

5.3 Specimen Design and Test Matrix

5.3.1 Girder Geometry and Prestressing

All test specimens will use the 54 in. FIB cross-section adopted in the Harkers Island Bridge (Figure 32). Each girder will be 50 ft long, representing a practical balance between (i) a sufficiently long span to achieve a shear span-to-depth ratio (a/d) greater than 3 (to avoid arching effects), and (ii) the lifting and handling capacities available at the CFL.

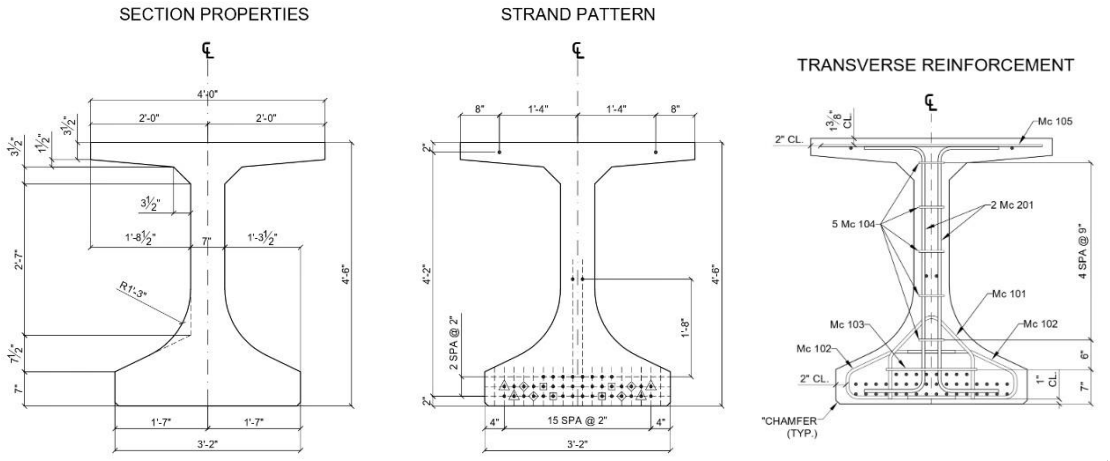

Figure 32. 54 in. FIB cross-section

The prestressing layouts are identical to those used in the Harkers Island Bridge. A 0.6 in. CFRP strand will be used as the primary prestressing reinforcement for two girders, and 0.6 in. conventional carbon high-strength steel (Grade 270) for the third girder. All specimens will be fabricated simultaneously in the same prestressing bed. The 50 ft. length also corresponds to the maximum length at which the girder would not be considered an oversized load. Therefore, no additional permits or police escorts would be required.

It should be noted that no composite deck will be cast over the girders. The tests will focus on the girder alone, simplifying interpretation of shear behavior while preserving the realistic girder geometry and prestressing arrangement.

5.3.2 Shear Span and Support Conditions

To reflect bridge-like support conditions, the reaction support will be located 8.5 in. away from the girder end, consistent with field practice. A concentrated load will be applied at a fixed distance from the support to achieve an a/d ratio of approximately 3.1 in all tests. This ratio is intentionally selected to keep the critical tested area in the B-region (beam-like behavior) rather than in the D-region (disturbed behavior due to arching effects, in which plain sections no longer remain plane and strut-and-tie methods should be used). Each girder will provide two test regions (one at each end). During testing of one end, the opposite end will likely be externally strengthened to prevent local damage before being tested. Figure 33 shows the test setup.

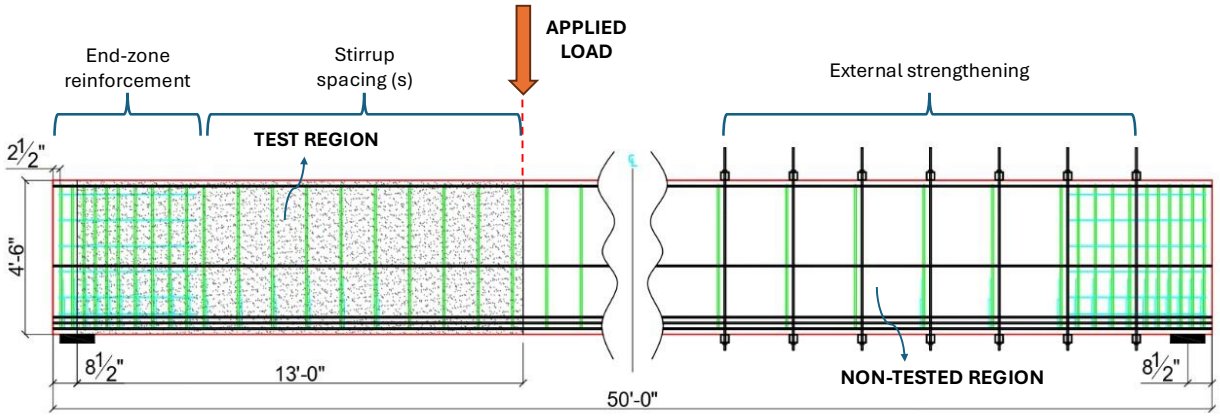

Figure 33. Test setup schematic view

5.3.3 Test Matrix and Variables

The test matrix consists of three 54 in. FIB girders, each providing two shear tests, for a total of six tests (Table 15). The main variables are shown below:

- Transverse reinforcement material: GFRP vs steel stirrups.
- Stirrup spacing: Harkers Island practice (6 and 10 in.) vs increased spacing (12 in. and 24 in.).
- GFRP stirrup manufacturer: same as Harkers Island vs an alternative supplier.

Table 15. Test matrix for FIB girders

Girder	Prestressing	End	Stirrup material	Spacing (in.)	Notes
G1	CFRP	A	GFRP (Mateenbar)	Harkers Island (6 and 10)	Direct comparison to bridge detailing
		B		12	
G2		A		24	Effect of spacing and manufacturer
		B	GFRP (MST Bar)	12	
G3	Steel	A	Grade 60 steel	Harkers Island (6 and 10)	Steel control for direct comparison
		B		12	

The best flexural and shear strength estimates for the six configurations listed in Table 15 were obtained through a combination of AASHTO guide specifications [15] and recommendations from other researchers based on similar experimental work [31], [32]. These results were validated by a cross-sectional analysis in RESPONSE [33], which indicated good agreement. The nominal and shear moment capacities for each end of the three 54 in. FIB girders are shown in Table 16. The forces required to achieve a flexural failure (P_{flex}) or a shear failure (P_{shear}) have also been included. These values are critical because they may constrain the range of tests that can be conducted with the available lab equipment.

In all cases, P_{flex} exceeded P_{shear}, indicating that shear failure was the governing mechanism. However, as the P_{flex}/P_{shear} ratio approaches unity, an interaction between flexure and shear, instead of a pure shear failure, should be expected. From a design standpoint, the latter might be preferred, as the failure mode should be more ductile. Ends G1-A and G3-A, corresponding to the Harkers Island configuration, should fall into this category. Figure 34 and Figure 35 show the variation of P_{shear} and P_{flex}/Ps_{hear} ratio, respectively, when the stirrup spacing changes.

Table 16. Nominal capacities

Girder End	Mn (kip-ft)	Vn (kip)	P_{flex} (kip)	P_{shear} (kip)	P_{flex}/P_{shear}
G1-A	7,400	440	777	580	1.3
G1-B		380		508	1.5
G2-A		302		397	2.0
G2-B		403		535	1.5
G3-A	7,200	500	758	650	1.2
G3-B		423		562	1.4

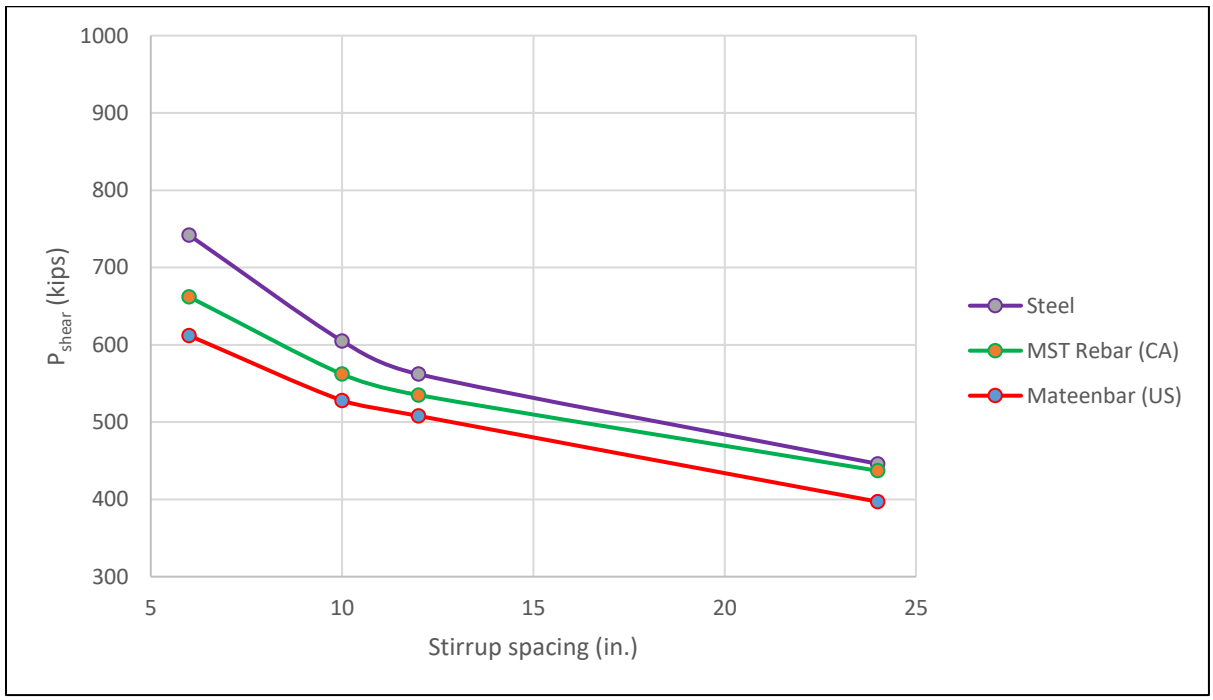

Figure 34. Variation of P_{shear} with the spacing of stirrups

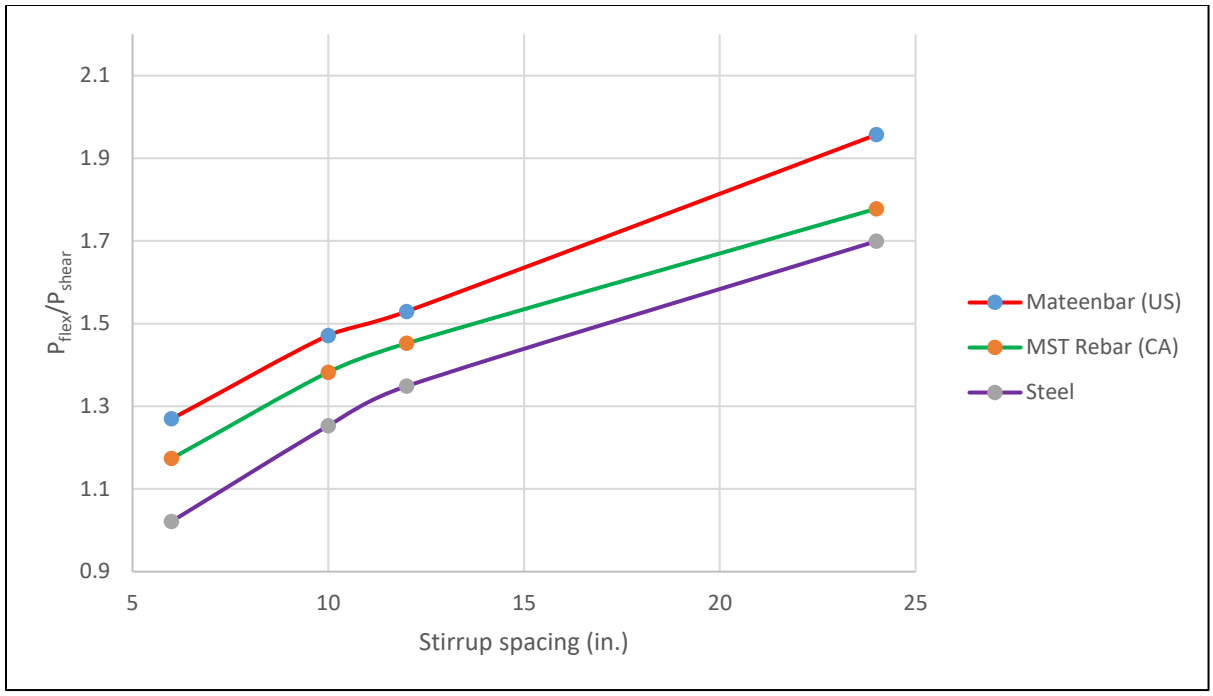

Figure 35. Variation of the P_{flex}/P_{shear} ratio with the spacing of stirrups

5.4 Loading and Instrumentation (Planned)

Tests will be conducted under monotonic loading until failure. A single-point loading arrangement, as presented in Figure 33, will be adopted. The latter configuration prevents flexural failure. Therefore, the failure mode is expected to be shear or shear-flexure. Instrumentation details will be finalized before testing, but are expected to include:

- Load cells to measure applied load.
- LVDTs along the span to quantify deflections.
- Digital Image Correlation (DIC) to obtain a full-field view of each test and document shear crack initiation and propagation.

Given the brittle nature of FRP, appropriate safety measures, such as protective screens and restricted access during peak loading, will be implemented. The research team will inform the NCDOT Steering and Implementation Committee once a test date has been set so they can attend the test in person. Alternatively, a livestream option can be made available.

Chapter 6. SUMMARY OF FINDINGS AND CONCLUSIONS

The Harkers Island Bridge is North Carolina's first bridge in which all primary load-carrying components use internal FRP reinforcement, delivering a corrosion-resistant solution in a harsh marine environment to replace two deteriorated steel-prestressed cored-slab bridges. The companion research program documented the bridge's configuration and construction, characterized CFRP strands, CFRP spirals, and GFRP bars through extensive testing, analyzed constructability at full bridge scale, and developed practical recommendations for acceptance testing and detailing to inform future FRP bridge projects for NCDOT. Overall, the findings confirm that FRP reinforcement can be implemented successfully at the scale of a 3,200 ft. long coastal bridge, but they also reveal gaps in current specifications, test methods, and acceptance procedures that must be addressed to enable routine and efficient use of FRP systems.

6.1 Key Material-Level Findings

The 0.6 in. seven-wire CFRP strands exhibited high tensile strength with low variability. All 73 production lots tested exceeded the project's minimum guaranteed tensile strength, and the average rupture load (~82.3 kips) was substantially above the 60.7-kip acceptance threshold. Additionally, all lots exceeded the minimum guaranteed tensile modulus (mean ≈ 22,400 ksi); however, some specimens reported moduli below the manufacturer's guaranteed value of 21,800 ksi. This does not undermine the material's adequacy for the project, but it underscores the importance of basing guaranteed design values on statistically robust datasets that reflect realistic test conditions, rather than relying solely on supplier information. Specimen preparation for tension tests with steel pipe/grout anchors is sensitive and labor-intensive; anchor lengths prescribed by ASTM D7205 [20] may be difficult to accommodate in modern testing frames, and careful control of grip pressure is required to prevent slip without damaging the anchors.

CFRP spirals (0.28 in. uni-strand) exhibited significant strength reduction at bends, with a mean bend strength that was ~41% of that of a straight companion portion. Moreover, the data showed notable scatter when tested in accordance with ASTM D7914 [21], highlighting the potential need for alternative test methods, such as an L-shaped bar setup. Bend strength is significantly influenced by the bend radius and bar diameter (r/d ratio) and by test-method alignment. The lack of a CFRP-specific standard is a considerable limitation, but the ASTM D30.10 Committee is actively working to publish one soon. Data produced in this project will aid its development. Given the current uncertainty and potential issues associated with CFRP bends, their use as stirrups or transverse reinforcement is not recommended until clear manufacturing requirements and testing procedures are established.

For GFRP bars, the tension tests conducted on straight bars and specimens cut from the straight legs of L-, U-, and C-shaped bars showed compliance with ASTM D7957 [18] strength requirements. Nonetheless, the QA/QC program was constrained by the manner in which materials were supplied and labeled: not all lot samples were sent to NCSU, there were no companion bent-bar specimens, and some bundles lacked clear identification. As a result, only a subset of the GFRP lots used in the project could be tied directly to test data. This experience confirms that the logistics of sampling and traceability are just as necessary as the test methods themselves.

The statistical evaluation in Chapter 4 indicates that the number of replicate tests required by current specifications may be higher than necessary for product validation within a project, given the relatively low variability observed in the Harkers Island data. In practice, testing every material property for every lot at the replicate counts implied by ASTM D7957 [18] would be prohibitively time-consuming and costly, especially when testing is performed by external laboratories. The results of this project suggest that acceptance protocols should prioritize tensile tests (which govern design) and use rational, statistically based sample sizes tailored to lot size and target confidence levels, while relying on prior durability research and pre-qualification programs for properties that do not require re-measurement for every project.

6.2 Key Structural and Constructability Findings

From a construction standpoint, the Harkers Island Bridge demonstrates that a fully FRP-reinforced, prestressed concrete bridge can be constructed within typical NCDOT schedules and methods, but not without adjustments.

Early production showed end-region cracking in CFRP-prestressed piles and FIB girders due to transfer-length/bursting effects at lower concrete strengths and incomplete confinement around bottom strands. These issues were mitigated by delaying the release of prestress and field cutting (allowing the concrete to gain higher strength) and by revising the confinement details so that all bottom strands were enclosed at the girder ends. Furthermore, non-ferrous alternatives for lifting loops remain a challenge: traditional carbon-steel loops conflicted with the project's corrosion-elimination goals. In contrast, stainless-steel loops represent a pragmatic compromise (workable but potentially suboptimal and imposing cutting challenges), thereby motivating future exploration of FRP-based lifting solutions and the development of standardized guidance.

GFRP stirrups and bars performed as intended, yet field crews reported splintering and itching during handling, labeling and identification errors, and manufacturing limits on bent geometries that necessitated splices and affected the schedule. In practice, standardizing bar shapes and coordinating manufacturers' bend limits during design will help reduce risk. Despite these issues, construction was completed 10 months ahead of schedule, and early field observations after opening indicate that the structure is performing as expected. The decision to retain Bridge No. 96 as a fishing pier and pedestrian facility has preserved an important community asset and demonstrates that innovation in structural materials can coexist with attention to local needs and cultural context. It is worth noting that GFRP bar splintering is related to the type of surface treatment, which varies among various GFRP bar manufacturers. Similarly, limitations on bent-bar geometries vary across manufacturers, emphasizing the need for early communication with potential GFRP bar producers.

6.3 Limitations and Future Work

The limitations of the present study should also be acknowledged. First, the material testing program focused on tension and bend behavior of CFRP strands, CFRP spirals, and GFRP bars. It did not include new durability testing (e.g., alkali exposure, creep rupture, or fatigue) for the specific materials used in Harkers Island. Instead, the project relied on the substantial body of existing durability research and on supplier certifications. This is consistent with the view that long-term durability testing is better suited to product-level qualification programs (e.g., AASHTO Product Evaluation & Audit Solutions or FRP Institute plant audits) than to individual bridge projects.

However, as part of future special provisions, NCDOT may also consider incorporating a simple resin-verification test as a practical durability-related quality-control measure for FRP bars. One promising option is the attenuated total reflectance Fourier-transform infrared (ATR-FTIR) spectroscopy test, which can be used to compare the resin signature of bars delivered to the project against that of a pristine reference resin sample provided by the manufacturer [34], [35]. The purpose of this test would not be to directly measure long-term durability, but rather to confirm that the bars were manufactured with the intended resin system, typically vinylester or epoxy, which is expected to provide the durability performance assumed in design. Because ATR-FTIR is relatively fast, versatile, and less burdensome than conventional long-term durability tests, it may represent a practical addition to future QA/QC specifications as a screening tool to verify resin consistency at the project level.

Second, no bent-bar tests were performed on GFRP stirrups used in the bridge. The geometry of the stirrups supplied to the project did not permit fabrication of specimens compliant with ASTM D7914 [21]. Ordering new bars solely for research would not have captured lot-to-lot variability within the project. The assumption of compliance with ASTM D7957 [18] based on meeting the minimum bend radius requirements remains reasonable but has not been verified at the project level. Planned future work on L-shaped bend tests, consistent with emerging Canadian practice [17], is expected to address this gap.

Third, Chapter 5 outlines a comprehensive experimental program on full-scale 54 in. FIB girders to be tested in shear. However, those tests had not yet been completed at the time of writing. The proposed matrix is designed to complement NCHRP 12-121 by focusing on realistic end-region details and support locations, and a consistent a/d ratio of 3.1, representative of beam behavior. Once completed, the results will provide critical data on the shear behavior of large FRP-prestressed girders transversely reinforced with GFRP stirrups. They will allow direct comparison between all-FRP and steel-reinforced configurations. These results are expected to be documented in a separate companion report and in journal publications.

Finally, the statistical evaluation of tension and bend tests, while extensive for a single project, still reflects the behavior of a limited set of products, manufacturers, and exposure conditions. Broader datasets, ideally involving multiple bridge projects and laboratories, will be needed to confirm whether the sampling strategies and acceptance criteria proposed here are universally applicable or should be tailored by product type and manufacturer.

Despite these limitations, the Harkers Island Bridge project has already provided a rich set of lessons on material behavior, constructability, and QA/QC for all-FRP reinforced and prestressed bridges. The findings summarized in this chapter lay the groundwork for the recommendations and implementation plan presented in the next chapter, as well as for continued collaboration among NCDOT, industry partners, and the research community as FRP moves further into mainstream bridge practice.

Chapter 7. RECOMMENDATIONS, IMPLEMENTATION, AND TECHNOLOGY TRANSFER

7.1 QA/QC and Material Testing Recommendations

For future FRP-reinforced bridge projects, the QA/QC at a project level should prioritize:

- Tension tests of CFRP strands (strength and modulus in accordance with ASTM D7205 [20]), as these directly support design assumptions for prestressed piles and girders.
- Tension tests of GFRP bars used in structural components, to confirm compliance with ASTM D7957 [18] strength requirements and design assumptions.
- Bend-strength tests for CFRP spirals (or bars) and bent GFRP bars, performed in accordance with ASTM D7914 [21] or CSA S807 [17], to verify the strength reduction at bends, which is critical for transverse reinforcement.

Special care should be given to the bar geometries specified for testing at bend locations. If ASTM D7914 [21] is used, the shortest allowable clear length between concrete blocks is preferred, as this reduces the likelihood of rotation and eccentricity effects that can distort measured bend strength. Conversely, if the CSA S807 [17] L-shaped configuration is used, bars with sufficient leg length should be ordered (at least 4 ft. with at least $12d_b$ beyond the bend, where d_b is the bar diameter) so that the test can be executed without geometric limitations. In both cases, companion straight samples from the same lot should be ordered and tested in tension as per ASTM D7205 [20], allowing direct evaluation of the strength reduction at the bend location.

Other properties (e.g., fiber content, transverse strength, water absorption) should be established primarily at the product-qualification level, rather than remeasured exhaustively for each project and lot, given the consistency observed in prior studies and the high testing burden. In this regard, the AASHTO PEAS program, in collaboration with the FRP Institute, plays a key role through plant audits to verify material compliance. Future bridge-related projects should preferentially use FRP products qualified by the AASHTO PEAS program.

For solid round FRP bars, the cross-sectional area can be obtained from the measured effective diameter. In contrast, measuring the cross-sectional area of 7-wire CFRP strands using Archimedes' principle is time-consuming and may be unnecessary. Instead, the strand diameter should be checked to confirm it does not exceed the maximum allowable value, which could be problematic in heavily reinforced, optimized sections. A range of suitable measured diameters should be provided, as with solid round GFRP bars. Then, the nominal cross-sectional area shall be used for design and strength calculations.

7.1.1 Number of Replicates Per Lot

Given that variability in tensile strength and modulus for the CFRP strands and GFRP bars used in the project is relatively low, only a limited number of specimens need to be randomly sampled from the products destined for field use. For a 5% margin of error in the estimated mean, the required number of replicate tension tests per lot is 2, 3, 4, or 5 for confidence levels of 90, 95, 99, and 99.7%, respectively.

Based on the preliminary results obtained in this project, the recommended QA/QC protocol to undertake the tensile tests listed in

Table 17 and Table 18 is:

- Randomly select five specimens from each lot, providing the option to achieve a 99.7% confidence level in the material collected if needed.
- Test two specimens per lot in tension in accordance with ASTM D7205 [20], loading at least to the minimum guaranteed tensile strength specified in the Special Provisions, while recording strains at least up to 50% of the expected ultimate (rupture) capacity. Spot-check the diameter of each tested specimen and confirm that it does not exceed the maximum diameter allowed in the Special Provisions and/or applicable ASTM standards.
- Calculate the modulus of elasticity using the nominal area and confirm that the lot average modulus exceeds the minimum value specified in the Special Provisions.
- If non-compliance is observed, test additional specimens from the same lot one at a time until either the lot-average modulus meets the specified requirement or a total of five specimens have been tested. If the stiffness requirement remains unmet after testing five specimens, the lot should be rejected.
- If any of the specimens tested fail before reaching the minimum guaranteed tensile strength, the lot should be rejected once it has been verified that the premature failure did not occur due to a preparation issue (i.e., pipe crushing, anchor slippage, previously damaged specimen).

Table 17. Recommended QC requirements for 0.6 in. CFRP strands

No.	Property	Test Method	Requirement	Specimens per Lot
1	Measured Cross-Sectional Area	ASTM D7205	Measured diameter with the PET wrap (0.55 – 0.68 in.)[a]	2 – 5[d]
2	Guaranteed Tensile Strength		≥ Minimum guaranteed value reported by the manufacturer[b]	
3	Tensile Modulus		≥ 20,000 ksi[c]	
4	Resin type	ATR – FTIR Spectroscopy	Match the results of a pristine resin sample provided by the manufacturer	1

[a] Use the nominal cross-sectional area reported by the manufacturer for strength and stiffness calculations (0.179 in^2).
[b] In lieu of an ASTM CFRP strand standard.
[c] Use the mean tensile modulus for design and serviceability checks (22,400 ksi).
[d] Based on the confidence level selected (90 – 99.7%). See Section 4.3.1.3.

For CFRP bent products, there are currently no ASTM standards specific to CFRP, and the bend-strength data generated in this project have been inconclusive. As an interim measure, it is recommended that no CFRP material be used as stirrups or transverse reinforcement, recognizing that forthcoming research results and future ASTM standards will better inform the required properties, test methods, number of replicates, and acceptance criteria.

Table 18. Recommended QC requirements for GFRP bars

No.	Property	Test Method	Requirement	Specimens per Lot
1	Measured Cross-Sectional Area	ASTM D7205 or ASTM D8505	Within the range listed in ASTM D7957 or ASTM D8505[a]	5
2	Guaranteed Tensile Strength		≥ Minimum guaranteed ultimate tensile force listed in ASTM D7957 or ASTM D8505	
3	Tensile Modulus		≥ 6,500 ksi (ASTM D7957) ≥ 8,700 ksi (ASTM D8505)	
4	Resin type	ATR – FTIR Spectroscopy	Match the results of a pristine resin sample provided by the manufacturer	1
5	Strength of 90° bends	ASTM D7914	≥ 60% of the minimum guaranteed ultimate tensile force listed in ASTM D7957[b]	5

[a] Use the nominal cross-sectional area for strength and stiffness calculations.
[b] Companion straight portions from the same lot, sufficient for a tensile test, are required.

7.1.2 Sampling and Lot Traceability

The experience at Harkers Island underscores the importance of logistics, not just test methods. Sampling and lot traceability provisions are essential for a robust QA/QC program. Future specifications should:

- Require suppliers to provide additional straight bars per lot specifically sized for tension testing (meeting minimum clear length and anchorage requirements).
- Require additional bent specimens per lot that are compatible with the selected bend-strength test so that the bend strength can be routinely verified.
- Mandate durable, legible lot tags that remain attached through shipping and field handling, using consistent units and notation (e.g., bar size, length, lot ID, product type).
- Require a simple traceability framework (e.g., lot IDs recorded on placement drawings or delivery tickets) so that field-installed bars and strands can be linked back to test results.

7.2 Design and Detailing Recommendations

7.2.1 End-Region Detailing for CFRP-Prestressed Members

Experience with CFRP-prestressed piles and FIB girders indicates that end-region behavior is sensitive to confinement and timing. Future designs should:

- Ensure that all bottom strands at the girder ends are fully enclosed by transverse reinforcement within the transfer and bursting region, avoiding unconfined strands near the flange or web edges.
- Consider a tighter spiral pitch near pile ends, extending beyond the anticipated cut line, to reduce splitting when piles are cut in the field.

- Explicitly incorporate minimum concrete strength at detensioning and cutting into design checklists and specifications, recognizing that higher release strengths can reduce cracking risk. This may be especially critical for elements such as battered piles, which require custom templates.

7.2.2 Lifting Loops and Handling Details

Lifting loops emerged as a critical issue. The decision to use stainless-steel lifting strands was a practical solution, but not fully aligned with the goal of eliminating all ferrous reinforcement. Stainless-steel loops also created field challenges (e.g., cutting difficulties) and residual corrosion concerns, even if limited. Future NCDOT projects should:

- Treat stainless-steel lifting loops as an interim solution, with clear detailing and corrosion-protection requirements.
- Encourage development and evaluation of FRP-based lifting systems (e.g., CFRP loops, GFRP bolts, or web-opening details with GFRP bars) as part of new research or pilot projects.
- Include lifting details and acceptable alternatives directly in the contract drawings and specifications, based on what precasters can realistically fabricate.

7.2.3 Transverse Reinforcement and Stirrup Spacing

The planned shear testing of 54 in. FIB girders will explore the effect of GFRP stirrup spacing and manufacturer differences. Until those results and NCHRP 12-121 findings are available, NCDOT should:

- Adopt conservative maximum stirrup spacings for GFRP stirrups in prestressed girders, especially in critical shear regions.
- Recognize that deep sections may exhibit different size effects than shallower beams that dominate existing test data.

Once the experimental program and national guidance are available, these limits can be revisited and, where appropriate, relaxed.

7.2.4 Detailing Simplicity and Standardization

The Harkers Island experience confirms that simpler, more repetitive details reduce risk and delays. Future FRP bridge designs should:

- Favor a limited set of standard bar shapes with consistent bend radii, compatible with manufacturer capabilities.
- Maximize repetition of details (e.g., the same stirrup shape across many spans or bents) to reduce fabrication errors.
- Use link slabs and straightforward geometry where possible, avoiding unique or highly irregular bent shapes that complicate FRP fabrication.

Standard detail sheets derived from the Harkers Island drawings can serve as templates for these practices. If special details are strictly required for a particular project, production capabilities should be discussed further in advance with the manufacturer.

7.3 Construction Practices

7.3.1 Field Handling and Worker Safety

Feedback obtained from the contractor and construction workers highlighted that:

- GFRP bars can cause splintering and itching, affecting worker comfort and productivity, which can negatively impact bidding offers presented by potential contractors. This issue is manufacturer-related but should be considered when developing special provisions.
- FRP components require careful handling to avoid damage from sharp bends, impact, abrasion, or extended exposure to UV rays. Note that alternatives to corrosion-resistant reinforcement, such as epoxy-coated steel bars, have similar handling requirements and require UV protection as well.
- Manufacturers should be encouraged to investigate surface treatments to allow visual inspection. It would be valuable to develop procedures to identify surface damage to the PET wrap covering the CFRP strands, thereby reducing the likelihood of premature failure in precast beds.

Therefore, for future projects, NCDOT should:

- Include explicit PPE requirements in the specifications (e.g., gloves, long sleeves, eye protection) for crews working extensively with GFRP and discourage direct skin contact with exposed fibers.
- Consider different surface treatments for GFRP bars, where appropriate, to reduce splintering and improve handling. Note that each manufacturer uses different surface treatments, and this may not be an issue for all of them.

7.4 Technology Transfer, Publications, and Recognition

This section summarizes how the project outcomes are being shared within NCDOT and with the broader community.

7.4.1 Intended Users and Internal Implementation

The primary internal users of this report and its recommendations are:

- Structures Management Unit: For design guidance, standard FRP details, and end-region reinforcement recommendations.
- Materials and Tests Unit: For QA/QC protocols, replicate counts, and acceptance criteria for CFRP strands, CFRP spirals, and GFRP bars.
- Construction Unit: For field handling, lifting strategies, cracking tolerance, and documentation practices.
- Asset Management Unit: For long-term monitoring and inspection practices for FRP-reinforced structures.

7.4.2 Publications and Ongoing Technical Dissemination

The Harkers Island Bridge and companion research are expected to generate multiple technical outputs, including:

Completed conference papers, such as:

- *P. Acuña, R. Seracino, "Harkers Island Bridge Case Study: North Carolina's First All-FRP-Reinforced and Prestressed Concrete Bridge", Conference Proceedings, 12th International Conference on FRP Composites in Civil Engineering (CICE 2025), January 2026, Lisbon, Portugal.*
- *P. Acuña, T. Brodbeck, R. Seracino, "Experimental Assessment of Carbon and Glass FRP Bent Bar Tensile Rupture Capacity", Conference Proceedings, 12th International Conference on FRP Composites in Civil Engineering (CICE 2025), January 2026, Lisbon, Portugal.*

Planned journal papers, focusing on:

- Harkers Island Bridge case study.
- Statistical evaluation of CFRP strand and spiral properties and implications for QA/QC.
- Bend-strength behavior and test methods for CFRP spirals and GFRP stirrups.
- Shear performance of deep FIB girders with FRP transverse reinforcement

Doctoral dissertation synthesizing the bridge case study, material characterization, bent-bar behavior, and structural testing into a comprehensive reference for all-FRP bridge design and assessment. These publications will help ensure that NCDOT's experience contributes to national and international practice.

7.4.3 Outreach, Awards, and Future Technology Transfer

Throughout the project, knowledge transfer and visibility have been reinforced by:

- Field workshops and site tours, including events organized in collaboration with the FRP Institute, where DOT staff, manufacturers, designers, and academics visited the bridge and discussed lessons learned.
- NCDOT visits to the Constructed Facilities Lab, where staff observed CFRP and GFRP material tests and discussed QA/QC strategies and future standardization.
- Technical presentations in regional and national venues, including invited talks where the Harkers Island Bridge was highlighted as a case study in all-FRP reinforced coastal infrastructure.
- The Harkers Island Bridge and its all-FRP reinforcement strategy have also received significant external recognition, including:
    - *2024 Operations Excellence Award – AASHTO America's Transportation Awards (Operations Excellence category).*
    - *2025 PCI Harry H. Edwards Industry Advancement Award.*
    - *2025 PCI Transportation Award – Best Bridge with a Main Span from 76–200 ft.*
    - *CAGC Pinnacle Award for the Harkers Island Bridge Project (Balfour Beatty / NCDOT).*
    - *IIFC Award for Outstanding FRP Field Applications in the "New FRP Structures" category (CICE 2025).*
    - *Selection of the Harkers Island Bridge Replacement as the featured project at the 2025 Zia Lecture series.*

These recognitions underscore that, beyond meeting local needs, the project is viewed nationally and internationally as a reference example for durable, innovative coastal infrastructure.

7.5 Future Research Needs

Finally, the project highlights several priority areas where further research would directly support broader and more efficient deployment of FRP reinforcement:

Full-scale FIB girder tests in shear

Complete the planned test matrix for 54 in. FIB girders (two with CFRP prestressing and GFRP stirrups, one with conventional steel) and compare ultimate capacities, cracking patterns, and failure modes with

AASHTO and MCFT-based predictions. Use these results to refine shear design provisions and to assess potential size effects for deep, FRP-prestressed members.

Standardization of CFRP strand and spiral testing

Support the development of an ASTM standard dedicated to CFRP strands, including realistic anchor geometries, machine-compliance considerations, and recommended strain ranges for modulus determination. Further evaluate L-shaped bend tests for CFRP spirals and GFRP stirrups to establish robust bend-strength criteria aligned with practical fabrication limits.

Long-term field performance and monitoring

Implement a monitoring program (e.g., periodic inspections, selected instrumentation, or non-destructive evaluation) to track crack widths, deflections, and environmental exposure effects on the Harkers Island Bridge over time. Use these data to validate or refine durability assumptions and environmental reduction factors used in design.

FRP lifting devices

Investigate FRP-based lifting solutions (e.g., CFRP lifting loops, GFRP/steel hybrid details, or web-opening concepts) through analysis and testing, aiming to provide standardized, non-corrosive options for plant and field handling.

Cost, risk, and life-cycle performance assessment

Combine initial construction costs, reduced maintenance expectations, and observed construction challenges into a quantitative life-cycle cost and risk assessment comparing FRP and steel alternatives for representative coastal bridges.

REFERENCES

[1] Z. Van Brunt, R. Seracino, G. Lucier, and M. Pour-Ghaz, "Assessment of Deteriorated Cored Slabs Bridges No.: 150035 and 150039," North Carolina State University, Raleigh, NC, NCDOT Project No.: 2014-35 FHWA/NC/2014-35, 2016.

[2] R. Seracino, G. Lucier, S. Rizkalla, and G. Shapack, "CFRP Strands in Prestressed Cored Slab Units," North Carolina State University, Raleigh, NC, NCDOT Project No.: 2014-09 FHWA/NC/2014-09, 2016.

[3] S.-H. Lin, R. Seracino, B. McCoy, Z. Bourara, and G. Lucier, "Mechanically-Fastened FRP to Retrofit Existing Prestressed Concrete Bridge Beams," North Carolina State University, Raleigh, NC, North Carolina Department of Transportation Research and Development Unit FHWA/NC/2018-16, 2022.

[4] N. F. Grace, F. C. Navarre, R. B. Nacey, W. Bonus, and L. Collavino, "Design-Construction of Bridge Street Bridge — First CFRP Bridge in the United States," *pcij*, vol. 47, no. 5, pp. 20–35, Sep. 2002, doi: 10.15554/pcij.09012002.20.35.

[5] J. Gergely, D. M. Boyajian, D. T. Young, and C. R. Frank, "Analysis and Testing of a Bridge Deck Reinforced with GFRP Rebars," University of North Carolina at Charlotte, Civil Engineering Department, Charlotte, NC, HWY-2005-22 FHWA/NC/2006-35, 2007.

[6] B. Benmokrane, A. H. Ali, H. M. Mohamed, M. Robert, and A. ElSafty, "Durability Performance and Service Life of CFCC Tendons Exposed to Elevated Temperature and Alkaline Environment," *J. Compos. Constr.*, vol. 20, no. 1, p. 04015043, Feb. 2016, doi: 10.1061/(ASCE)CC.1943-5614.0000606.

[7] H. Tahsiri, A. Belarbi, and B. Gencturk, "Thermal effects on transfer length and prestress losses in CFRP prestressed prisms," *Construction and Building Materials*, vol. 416, p. 135160, Feb. 2024, doi: 10.1016/j.conbuildmat.2024.135160.

[8] Transportation Research Board and E. National Academies of Sciences and Medicine, *Design of Concrete Bridge Beams Prestressed with CFRP Systems*. Washington, DC: The National Academies Press, 2019. doi: 10.17226/25582.

[9] M. Robert and B. Benmokrane, "Behavior of GFRP Reinforcing Bars Subjected to Extreme Temperatures," *J. Compos. Constr.*, vol. 14, no. 4, pp. 353–360, Aug. 2010, doi: 10.1061/(ASCE)CC.1943-5614.0000092.

[10] N. F. Grace, M. E. Mohamed, and M. R. Bebawy, "Evaluating fatigue, relaxation, and creep rupture of carbon-fiber-reinforced polymer strands for highway bridge construction," *PCIJ*, vol. 68, no. 3, pp. 36–61, 2023, doi: 10.15554/pcij68.3-01.

[11] Y. J. Kim, J. Wang, W.-T. Jung, J.-Y. Kang, and J.-S. Park, "Creep-Fatigue Interaction for Carbon Fiber-Reinforced Polymer-Prestressed Concrete Bridge Girders," *SJ*, vol. 122, no. 2, Mar. 2025, doi: 10.14359/51743304.

[12] N. F. Grace, M. E. Mohamed, M. Chynoweth, N. Kose, and M. Bebawy, "Effect of Temperature Fluctuation and Severe Environments on Durability of CFRP Strands," *J. Compos. Constr.*, vol. 25, no. 4, p. 04021034, Aug. 2021, doi: 10.1061/(ASCE)CC.1943-5614.0001140.

[13] ACI, "Building Code Requirements for Structural Concrete Reinforced with Glass Fiber-Reinforced Polymer (GFRP) Bars—Code and Commentary," *ACI CODE-440.11-22*, 2022.

[14] AASHTO, "AASHTO LRFD Bridge Design Guide Specifications for GFRP-Reinforced Concrete, Second Edition," *American Association of State Highway and Transportation Officials*, 2018.

[15] AASHTO, “Guide Specifications for the Design of Concrete Bridge Beams Prestressed with Carbon Fiber-Reinforced Polymer (CFRP) Systems, 1st Edition,” *American Association of State Highway and Transportation Officials*, 2018.
[16] Canadian Standards Association (CSA Group), “Design and construction of building structures with fibre-reinforced polymers,” *CSA S806:12*, 2021.
[17] Canadian Standards Association (CSA Group), “Specification for fibre-reinforced polymers,” *CSA S807:19*, 2019.
[18] ASTM, “Standard Specification for Solid Round Glass Fiber Reinforced Polymer Bars for Concrete Reinforcement,” *ASTM D7957/D7957M-22*, 2022, doi: 10.1520/D7957_D7957M-22.
[19] J. W. Schmidt, A. Bennitz, B. Täljsten, P. Goltermann, and H. Pedersen, “Mechanical anchorage of FRP tendons – A literature review,” *Construction and Building Materials*, vol. 32, pp. 110–121, Jul. 2012, doi: 10.1016/j.conbuildmat.2011.11.049.
[20] ASTM, “Standard Test Method for Tensile Properties of Fiber Reinforced Polymer Matrix Composite Bars,” *ASTM D7205/D7205M-06*, 2006, doi: 10.1520/D7205_D7205M-06.
[21] ASTM, “Standard Test Method for Strength of Fiber Reinforced Polymer (FRP) Bent Bars in Bend Locations,” *ASTM D7914/D7914M-21*, 2021, doi: 10.1520/D7914_D7914M-21.
[22] ACI, “Guide Test Methods for Fiber-Reinforced Polymers (FRPs) for Reinforcing or Strengthening Concrete Structures,” *ACI PRC-440.3-12*, 2012.
[23] E. A. Ahmed, A. K. El-Sayed, E. El-Salakawy, and B. Benmokrane, “Bend Strength of FRP Stirrups: Comparison and Evaluation of Testing Methods,” *J. Compos. Constr.*, vol. 14, no. 1, pp. 3–10, Feb. 2010, doi: 10.1061/(ASCE)CC.1943-5614.0000050.
[24] A. K. El-Sayed, E. El-Salakawy, and B. Benmokrane, “Mechanical and Structural Characterization of New Carbon FRP Stirrups for Concrete Members,” *J. Compos. Constr.*, vol. 11, no. 4, pp. 352–362, Aug. 2007, doi: 10.1061/(ASCE)1090-0268(2007)11:4(352).
[25] E. Shehata, R. Morphy, and S. Rizkalla, “Fibre reinforced polymer shear reinforcement for concrete members: behaviour and design guidelines,” *Can. J. Civ. Eng.*, vol. 27, no. 5, pp. 859–872, Oct. 2000, doi: 10.1139/l00-004.
[26] JSCE, “Recommendation for Design and Construction of Concrete Structures Using Continuous Fiber Reinforcing Materials,” *Japanese Society of Civil Engineers, Concrete Engineering Series 23*, 1997.
[27] J. L. Devore, “Probability and Statistics for Engineering and the Sciences,” *Cengage Learning*, no. Ninth, 2016.
[28] ASTM, “Standard Practice for Calculating Sample Size to Estimate, With Specified Precision, the Average for a Characteristic of a Lot or Process,” *ASTM E122−17*, 2022, doi: 10.1520/E0122-17R22.
[29] T. Imjai, R. Garcia, M. Guadagnini, and K. Pilakoutas, “Strength Degradation in Curved Fiber-reinforced Polymer (FRP) Bars Used as Concrete Reinforcement,” *Polymers*, vol. 12, no. 8, p. 1653, Jul. 2020, doi: 10.3390/polym12081653.
[30] A. Khalil, R. A. Hawileh, and M. Attom, “Exploring Strength of Straight and Bent GFRP Bars: Refinements to CSA S807:19 Annex E,” in *SP-360: Proceedings of the 16th International Symposium on Fiber-Reinforced Polymer (FRP) Reinforcement for Concrete Structures (FRPRCS-16)*, American Concrete Institute, 2024, pp. 242–253. doi: 10.14359/51740628.
[31] N. F. Grace, S. K. Rout, K. Ushijima, and M. Bebawy, “Performance of Carbon-Fiber-Reinforced Polymer Stirrups in Prestressed-Decked Bulb T-Beams,” *J. Compos. Constr.*, vol. 19, no. 3, p. 04014061, Jun. 2015, doi: 10.1061/(ASCE)CC.1943-5614.0000524.
[32] A. Al-Kaimakchi and M. Rambo-Roddenberry, “Structural Assessment of AASHTO Type II Prestressed Concrete Girder with GFRP or Stainless-Steel Shear Reinforcement,” *J. Bridge Eng.*, vol. 27, no. 7, p. 04022056, Jul. 2022, doi: 10.1061/(ASCE)BE.1943-5592.0001899.
[33] E. Bentz, *RESPONSE*. [Online]. Available: https://www.hadrianworks.com/download.html

[34] R. C. De Araújo Moura, D. V. Ribeiro, and P. R. L. Lima, "Durability of Concrete Reinforced with GFRP Bars Under Varying Alkalinity and Temperature Conditions," *Buildings*, vol. 15, no. 16, p. 2832, Aug. 2025, doi: 10.3390/buildings15162832.
[35] S. Vemuganti, R. Chennareddy, A. Riad, and M. Taha, "Pultruded GFRP Reinforcing Bars Using Nanomodified Vinyl Ester," *Materials*, vol. 13, no. 24, p. 5710, Dec. 2020, doi: 10.3390/ma13245710.
[36] ACI, "Guide for the Design and Construction of Structural Concrete Reinforced with Fiber-Reinforced Polymer Bars," *ACI PRC-440.1-15*, 2021.
[37] ACI, "Design and Construction of Externally Bonded Fiber Reinforced Polymer (FRP) Systems for Strengthening Concrete Structures," *ACI PRC-440.2-23*, 2023.
[38] ACI, "Prestressing Concrete Structures with FRP Tendons," *ACI PRC-440.4-04*, 2004.
[39] fib, "Model Code for Concrete Structures," *fib Model Code*, 2020.
[40] ACI, "Building Code for Structural Concrete—Code Requirements and Commentary," *ACI CODE-318-25*, 2025.
[41] P. Poudel, A. Belarbi, B. Gencturk, and M. Dawood, "Flexural behavior of full-scale, carbon-fiber-reinforced polymer prestressed concrete beams," *PCIJ*, vol. 67, no. 5, pp. 22–39, 2022, doi: 10.15554/pcij67.5-01.
[42] M. R. Manaa, A. Belarbi, B. Gencturk, and M. Dawood, "Experimental investigation of full-scale post-tensioned composite AASHTO beams prestressed with carbon-fiber-reinforced polymer cables," *PCIJ*, vol. 69, no. 1, pp. 40–57, 2024, doi: 10.15554/pcij69.1-03.
[43] B.-T. Zheng, B. Gencturk, A. Belarbi, and P. Poudel, "Nonlinear Finite-Element Modeling of Concrete Bridge Girders Prestressed with Carbon Fiber–Reinforced Polymers," *J. Bridge Eng.*, vol. 29, no. 8, p. 04024058, Aug. 2024, doi: 10.1061/JBENF2.BEENG-6693.
[44] H. Tahsiri and A. Belarbi, "Evaluation of prestress relaxation loss and harping characteristics of prestressing CFRP systems," *Construction and Building Materials*, vol. 331, p. 127339, May 2022, doi: 10.1016/j.conbuildmat.2022.127339.
[45] F. Forouzannia, B. Gencturk, M. Dawood, and A. Belarbi, "Calibration of Flexural Resistance Factors for Load and Resistance Factor Design of Concrete Bridge Girders Prestressed with Carbon Fiber–Reinforced Polymers," *J. Compos. Constr.*, vol. 20, no. 2, p. 04015050, Apr. 2016, doi: 10.1061/(ASCE)CC.1943-5614.0000613.
[46] Transportation Research Board and E. National Academies of Sciences and Medicine, *Stainless Steel Strands for Prestressed Concrete Bridge Elements*. Washington, DC: The National Academies Press, 2025. doi: 10.17226/29245.
[47] A. Mechaala, D. Stefaniuk, and A. Belarbi, "Comparative performance analysis of straight and harped prestressing seven-wire strands: High-strength stainless steel vs. conventional carbon steel," *Construction and Building Materials*, vol. 439, p. 137421, Aug. 2024, doi: 10.1016/j.conbuildmat.2024.137421.
[48] A. Mechaala, D. Stefaniuk, and A. Belarbi, "Flexural behavior of full-scale AASHTO type I girders prestressed with stainless steel strands," *Engineering Structures*, vol. 333, p. 120160, Jun. 2025, doi: 10.1016/j.engstruct.2025.120160.
[49] D. Stefaniuk, A. Mechaala, and A. Belarbi, "Transfer length of stainless-steel strands in prestressed bridge elements: A combined experimental and numerical modeling approach," *Engineering Structures*, vol. 325, p. 119482, Feb. 2025, doi: 10.1016/j.engstruct.2024.119482.
[50] A. Belarbi, A. Okeil, and A. Nanni, "Shear Design of Prestressed Concrete Girders Using FRP as Auxiliary Reinforcement," in *Building for the Future: Durable, Sustainable, Resilient*, A. Ilki, D. Çavunt, and Y. S. Çavunt, Eds., in Lecture Notes in Civil Engineering, vol. 350. Cham: Springer Nature Switzerland, 2023, pp. 1069–1079. doi: https://doi.org/10.1007/978-3-031-32511-3_109.
[51] N. Grace, M. Bebawy, and M. Kasabasic, "Evaluation and Analysis of Decked Bulb T Beam Bridge," Center for Innovative Material Research (CIMR), Dept. of Civil Engineering, Lawrence Technological University, Lansing, MI, Contract Number: 2010-0293 RC-1620, 2015.

[52] N. Grace, M. Bebawy, M. Mohamed, M. Kasabasic, E. Ababio, and P. Kornyoh, "Evaluation of 0.7 Inch Diameter Carbon Fiber Reinforced Polymer Pretensioning Strands in Prestressed Beams," Center for Innovative Material Research (CIMR) Lawrence Technological University (LTU), Lansing, MI, Contract or Grant No. 2016-0065 Z3 SPR-1707, 2022.
[53] T. R. Board, National Academies of Sciences Engineering, and Medicine, *Use of 0.7-in. Diameter Strands in Precast Pretensioned Girders*. Washington, DC: The National Academies Press, 2022. doi: 10.17226/26677.
[54] ASTM, "Standard Specification for Basalt and Glass Fiber Reinforced Polymer (FRP) Bars for Concrete Reinforcement," *ASTM D8505/D8505M-23*, 2023, doi: 10.1520/D8505_D8505M-23.
[55] ASTM, "Standard Test Method for Bond Strength of Fiber-Reinforced Polymer Matrix Composite Bars to Concrete by Pullout Testing," *ASTM D7913/D7913M-14*, 2020, doi: 10.1520/D7913_D7913M-14R20.
[56] J. D. Tanks, S. R. Sharp, C. Ozyildirim, and D. K. Harris, "Carbon Fiber Reinforced Polymer (CFRP) for Pretension Applications: Material Acceptance Criteria and Advancing Anchorage Designs," Virginia Transportation Research Council, Richmond, VA, RC 00068 VTRC 20-R5, 2019.
[57] K. Mohamed, B. Benmokrane, C. Nazair, and M.-A. Loranger, "Development and Validation of a Testing Procedure for Determining Tensile Strength of Bent GFRP Reinforcing Bars," *J. Compos. Constr.*, vol. 25, no. 2, p. 04020087, Apr. 2021, doi: 10.1061/(ASCE)CC.1943-5614.0001102.
[58] K. Mohamed, C. Nazair, M.-A. Loranger, and B. Benmokrane, "In-Site Quality Control of the Tensile Strength of Glass Fiber-Reinforced Polymer (GFRP) Bent Bars," in *8th International Conference on Advanced Composite Materials in Bridges and Structures*, B. Benmokrane, K. Mohamed, A. Farghaly, and H. Mohamed, Eds., Cham: Springer International Publishing, 2023, pp. 405–412.
[59] T. Cadenazzi, S. Nolan, G. Mazzocchi, Z. Stringer, and A. Nanni, "Bridge Case Study: What a Contractor Needs to Know on an FRP Reinforcement Project," *J. Compos. Constr.*, vol. 24, no. 2, p. 05020001, Apr. 2020, doi: 10.1061/(ASCE)CC.1943-5614.0000998.
[60] A. Mufti *et al.*, "Durability of GFRP Reinforced Concrete in Field Structures," in *SP-230*, American Concrete Institute, 2005. doi: 10.14359/14898.
[61] B. Shafei, B. Phares, and D. Saini, "Field Investigation of Bridge Deck Reinforced with Glass Fiber Reinforced Polymer (GFRP) Rebar," Bridge Engineering Center Iowa State University, St. Paul. Minnesota, Contract (C) or Grant (G) No. (C) 99004 (wo) 24 MN 2020-05, 2020.
[62] C. Foley *et al.*, "In-Situ Monitoring and Testing of IBRC Bridges in Wisconsin," Marquette University Department of Civil & Environmental Engineering, Madison, WI, Contract or Grant No. WisDOT SPR# 0092-05-02 WHRP 10-09, 2010.
[63] S. Nolan, M. Rossini, C. Knight, and A. Nanni, "New directions for reinforced concrete coastal structures," *J Infrastruct Preserv Resil*, vol. 2, no. 1, p. 1, Dec. 2021, doi: 10.1186/s43065-021-00015-4.
[64] A. Mehrabi, S. S. Khedmatgozar Dolati, P. Malla, A. Nanni, and J. Ortiz, "A Framework for Field Inspection of In-service FRP Reinforced/Strengthened Concrete Bridge Elements"," Florida International University & University of Miami, Miami, FL, Office of Bridges and Structures Federal Highway Administration 800014727, 2024.
[65] H. T. Nguyen *et al.*, "Long-term Application of Carbon Fiber Composite Cable Tendon in the Prestressed Concrete Bridge-Shinmiya Bridge in Japan," *MATEC Web Conf.*, vol. 206, p. 02011, 2018, doi: 10.1051/matecconf/201820602011.
[66] N. F. Grace, M. E. Mohamed, M. Kasabasic, M. Chynoweth, K. Ushijima, and M. Bebawy, "Design, Construction, and Monitoring of US Longest Highway Bridge Span Prestressed with CFRP Strands," *J. Bridge Eng.*, vol. 27, no. 7, p. 04022047, Jul. 2022, doi: 10.1061/(ASCE)BE.1943-5592.0001881.

[67] T. Cadenazzi, B. Keles, M. K. Rahman, and A. Nanni, “Life-Cycle Cost and Life-Cycle Assessment of a Monumental Fiber-Reinforced Polymer Reinforced Concrete Structure,” *J. Constr. Eng. Manage.*, vol. 148, no. 9, p. 05022007, Sep. 2022, doi: 10.1061/(ASCE)CO.1943-7862.0002339.
[68] T. Cadenazzi, G. Dotelli, M. Rossini, S. Nolan, and A. Nanni, “Cost and environmental analyses of reinforcement alternatives for a concrete bridge,” *Structure and Infrastructure Engineering*, vol. 16, no. 4, pp. 787–802, Apr. 2020, doi: 10.1080/15732479.2019.1662066.
[69] T. Cadenazzi, G. Dotelli, M. Rossini, S. Nolan, and A. Nanni, “Life-Cycle Cost and Life-Cycle Assessment Analysis at the Design Stage of a Fiber-Reinforced Polymer-Reinforced Concrete Bridge in Florida,” *Advances in Civil Engineering Materials*, vol. 8, no. 2, pp. 128–151, Feb. 2019, doi: 10.1520/ACEM20180113.
[70] T. Cadenazzi, H. Lee, P. Suraneni, S. Nolan, and A. Nanni, “Evaluation of probabilistic and deterministic life-cycle cost analyses for concrete bridges exposed to chlorides,” *Cleaner Engineering and Technology*, vol. 4, p. 100247, Oct. 2021, doi: 10.1016/j.clet.2021.100247.
[71] G. Shapack, Z. Van Brunt, R. Seracino, G. Lucier, S. Rizkalla, and M. Pour-Ghaz, “Improving the Durability of Coastal Bridges with CFRP Prestressed Cored Slabs,” in *SP-322: A Symposium Honoring Khaled Soudki: Towards Sustainable Infrastructure with Fiber Reinforced Polymer Composites*, American Concrete Institute, 2018. doi: 10.14359/51706966.
[72] B. C. McCoy, Z. Bourara, R. Seracino, and G. W. Lucier, “Anchor Bolt Patterns for Mechanically Fastened FRP Plates,” *J. Compos. Constr.*, vol. 23, no. 4, p. 04019024, Aug. 2019, doi: 10.1061/(ASCE)CC.1943-5614.0000951.
[73] B. C. McCoy, Z. Bourara, G. W. Lucier, R. Seracino, M. Liu, and S.-H. Lin, “Prestressed MF-FRP: Experimental Study of Rapid Retrofit Solution for Deteriorated Prestressed C-Channel Beams,” *J. Perform. Constr. Facil.*, vol. 35, no. 1, p. 04020124, Feb. 2021, doi: 10.1061/(ASCE)CF.1943-5509.0001536.
[74] S.-H. Lin, B. C. McCoy, G. W. Lucier, R. Seracino, and N. A. Pierce, “Rapid Prestressed Concrete Retrofit with Prestressed Mechanically-Fastened Fiber-Reinforced Polymer: Field Performance and Observation for a Deteriorated Prestressed Concrete Bridge,” *Transportation Research Record: Journal of the Transportation Research Board*, vol. 2678, no. 4, pp. 804–818, Apr. 2024, doi: 10.1177/03611981231186981.
[75] O. Khalafalla, M. Pour-Ghaz, A. ElSafty, and S. Rizkalla, “Durability of CFRP strands used for prestressing of concrete structural members,” *Construction and Building Materials*, vol. 228, p. 116756, Dec. 2019, doi: 10.1016/j.conbuildmat.2019.116756.
[76] A. Caner and P. Zia, “Behavior and Design of Link Slabs for Jointless Bridge Decks,” *pcij*, vol. 43, no. 3, pp. 68–80, May 1998, doi: 10.15554/pcij.05011998.68.80.
[77] V. Briere, K. A. Harries, J. Kasan, and C. Hager, “Dilation behavior of seven-wire prestressing strand – The Hoyer effect,” *Construction and Building Materials*, vol. 40, pp. 650–658, Mar. 2013, doi: 10.1016/j.conbuildmat.2012.11.064.
[78] ASTM, “Standard Test Methods for Density and Specific Gravity (Relative Density) of Plastics by Displacement,” *ASTM D792-20*, 2020, doi: 10.1520/D0792-20.
[79] ASTM, “Standard Test Method for Water Absorption of Plastics,” *ASTM D570-22*, 2022, doi: 10.1520/D0570-22.

APPENDICES

Appendix A. LITERATURE REVIEW

A.1. Scope

The purpose of this chapter is to place the Harkers Island Bridge project and the associated NCDOT research programs within the broader context of current knowledge on FRP-reinforced and FRP-prestressed concrete. The focus is on topics that directly influence the design, detailing, and material acceptance strategies adopted for this project.

Appendix A is organized around five main themes: (1) Design codes and guidelines, (2) National research programs on corrosion-resistant reinforcement, (3) Material standards and acceptance testing for FRP reinforcement, (4) Field performance and durability, and (5) Prior NCDOT research and the path to Harkers Island. The chapter concludes in Section A.7 with a synthesis of the main findings and a concise statement of the remaining research needs, particularly regarding material variability and acceptance testing, behavior of bent FRP elements, and shear performance of deep FRP-prestressed girders. These needs are then translated into the specific research questions addressed in this report, and provide a direct link to the experimental, analytical, and statistical work presented in Chapter 2 through Chapter 5.

A.2. Design Codes and Guidelines for FRP-Reinforced and FRP-Prestressed Concrete

The design of FRP-reinforced and FRP-prestressed concrete members has evolved over the past three decades from research-based recommendations to more formal guide specifications and, more recently, to mandatory code provisions. This section summarizes the main documents governing the use of FRP reinforcement in bridge and building applications and highlights the limitations that motivate the research presented in this report.

A.2.1 Early Design Recommendations and Guide Documents

Early FRP design documents in the US were developed primarily by ACI as “report” or “guide” documents rather than standard codes. ACI Committee 440 produced a series of documents addressing different aspects of FRP use in concrete structures, including design of GFRP-reinforced members, externally bonded FRP systems, and prestressing with FRP tendons [36], [37], [38].

For internal reinforcement, ACI 440.1R [36] provided recommendations for the design and construction of concrete members reinforced with FRP bars, including flexural and shear design equations, serviceability limits, and durability considerations. These provisions were largely based on experimental research and case studies from North America, Japan, and Europe, and were calibrated to be conservative in the absence of long-term field data. However, as a guide document, ACI 440.1R [36] did not carry mandatory status in building codes or bridge specifications and had to be adopted by individual owners on a project-by-project basis.

Similar guidance was developed in other countries through CSA S806 in Canada [16] and fib Bulletins in Europe [39], providing design equations and detailing recommendations for GFRP reinforcement and, in some cases, CFRP prestressing. Collectively, these documents established the fundamental design philosophy for FRP-reinforced concrete, recognizing the linear-elastic behavior up to rupture, lower modulus relative to steel (for GFRP), and the need to control crack widths and deflections at service, but left many bridge-specific issues to be resolved at the national specification level (mainly through DOTs).

A.2.2 AASHTO Guide Specifications for FRP Bridge Components

AASHTO has developed several guide specifications for the use of FRP in bridge applications. These documents are intended to eventually complement the AASHTO LRFD Bridge Design Specifications (BDS) once they incorporate mandatory language following further refinement and validation.

For GFRP reinforcement, AASHTO published guide specifications for GFRP-reinforced concrete, with design provisions for bridge decks and other concrete components reinforced with GFRP bars [14]. The guide covers material properties, flexural and shear design, serviceability, development and splice lengths, and durability considerations, with resistance and environmental reduction factors calibrated based on available experimental data and limited field experience. The scope is intentionally focused on members where failure is expected to be governed by concrete crushing or bar rupture in flexure.

For CFRP prestressing, AASHTO has published guide specifications for concrete bridge beams prestressed with CFRP systems [15], drawing heavily on the work conducted under NCHRP Project 12-97 [8]. These documents address material characterization (including creep, relaxation, and thermal behavior), prestress losses, flexural strength, serviceability, and fatigue performance of beams prestressed with CFRP strands or tendons. Reliability-based calibration of resistance factors was conducted using experimental databases and analytical models developed for that project, yielding recommended limit states and design factors for CFRP-prestressed members.

Despite their extensive scope, these AASHTO documents are labeled explicitly as guide specifications. They have not yet been incorporated into the main AASHTO LRFD BDS as mandatory provisions, and their adoption differs among state DOTs. Consequently, the use of FRP reinforcement in bridge superstructures occurs primarily in demonstration projects and in specific components, such as decks and short-span beams, where owners are willing to accept the guide provisions.

A.2.3 ACI 440.11 and the Move to Mandatory Code Language

A significant recent milestone in the codification of FRP reinforcement is the publication of ACI 440.11: *Building Code Requirements for Structural Concrete Reinforced with Glass Fiber-Reinforced Polymer (GFRP) Bars* [13]. This document, first issued in 2022, is the first US building code to include mandatory language for the design of concrete members reinforced with GFRP bars.

ACI 440.11 [13] follows the organizational structure of ACI 318 [40] and incorporates many of the design concepts previously presented in ACI 440.1R [36], but with explicit code-style provisions. The code addresses material requirements, flexural and axial design, shear and torsion, development and splice design, and serviceability. It also introduces environmental reduction factors to account for long-term degradation of strength and stiffness in aggressive environments.

Although ACI 440.11 [13] is focused on building-type members rather than bridges, its publication is vital for two reasons. First, it demonstrates that a standardized code framework for GFRP reinforcement is feasible and acceptable to the broader structural engineering community. Second, it provides a reference point for owners and specification committees considering how to incorporate GFRP into bridge codes, including potential alignment between ACI and AASHTO provisions for flexural, shear, and serviceability design.

A.2.4 Limitations and Implications for Bridge Design

The documents summarized above represent significant progress toward a robust design framework for FRP-reinforced and prestressed concrete. However, from the perspective of a state DOT designing large coastal bridges, several limitations remain:

Guide vs. mandatory status:

The FRP-oriented documents developed by AASHTO [14], [15] are still issued as guide specifications and are not fully incorporated into the LRFD BDS. Hence, their adoption is discretionary and may be limited to pilot projects. In contrast, ACI 440.11 [13] is a code-level document but does not directly address bridge-specific issues.

Limited calibration for shear:

Most of the calibration work in ACI and AASHTO FRP documents has focused on the behavior of GFRP-reinforced members. Experimental data on the shear behavior of deep, heavily prestressed girders with FRP reinforcement are relatively scarce. The latter is particularly critical as those are the typical configurations used in modern bridge girders.

Bent-bar, spiral, and anchorage behavior:

Existing provisions for the development and anchorage of FRP bars are based primarily on straight bars and simplified bond models. Strength reduction at bent locations (e.g., stirrups and spirals) and the behavior of confinement reinforcement in anchorage zones are less well characterized than for steel, and test methods and interpretations of bent-bar strength can vary across research programs.

Material variability and statistical basis for design values:

ASTM standards for FRP bars and strands specify test methods, minimum properties, and specimen numbers primarily for product qualification. While this is appropriate for establishing that a material meets a given specification, it does not directly answer how many tests are practical or necessary for routine lot-by-lot acceptance on a bridge project. In parallel, the design values and environmental reduction factors used in current ACI and AASHTO provisions are calibrated against experimental databases that are still expanding; therefore, it is not always transparent to owners how a limited number of acceptance tests on a given project should be linked to those underlying databases and design values.

Bridge-scale field experience:

Field performance data for FRP-reinforced decks and short-span bridges are accumulating, but limited experience remains with large, multi-span bridges where all primary load-carrying components are reinforced or prestressed with FRP. This is particularly true in highly corrosive marine environments, such as those in Harkers Island.

A.3. National Research Programs on Corrosion-Resistant Reinforcement

Several national research programs have directly addressed the use of corrosion-resistant reinforcement and prestressing systems for concrete bridge members. These efforts, conducted primarily under the National Cooperative Highway Research Program (NCHRP) and state DOT-university partnerships, provide much of the technical foundation for current AASHTO guide specifications and for projects such as the Harkers Island Bridge. This section highlights the most relevant programs and their implications.

A.3.1 NCHRP Project 12-97 – Design of Concrete Bridge Beams Prestressed with CFRP Systems

NCHRP Project 12-97, Design of Concrete Bridge Beams Prestressed with CFRP Systems [8], was commissioned to develop a design framework for concrete bridge beams using CFRP tendons as the main prestressing reinforcement. The project began with an extensive review of existing experimental data and

field applications, covering material properties, bond behavior, time-dependent effects, and structural performance of CFRP-prestressed members.

A comprehensive experimental program was conducted on both pre-tensioned and post-tensioned beams prestressed exclusively with CFRP tendons or strands [41], [42]. The specimens were designed to investigate flexural behavior, prestress losses, cracking, deflection, and ultimate strength under static and fatigue loading. Complementary analytical and finite element models were developed to simulate the response of CFRP-prestressed beams over a range of span lengths, reinforcement ratios, and load combinations [43]. Reliability analyses were then performed to calibrate resistance factors and assess the adequacy of the proposed design equations for use within a limit-states framework. The principal outcomes of NCHRP 12-97 [8] include:

- Recommended material property models for CFRP tendons, including creep, relaxation, and thermal effects [7].
- Equations for estimating prestress losses specific to CFRP [44].
- Strength and serviceability design provisions for flexure in CFRP-prestressed beams [15].
- Reliability-calibrated resistance factors suitable for incorporation into AASHTO guide specifications [45].

In the context of the Harkers Island Bridge, NCHRP 12-97 [8] provides the primary reference for flexural design, prestress loss calculations, and resistance factors for CFRP-prestressed beams. However, the project focused primarily on flexural behavior, with limited coverage of shear, auxiliary reinforcement, and end-zone details, which are key aspects of the present research program.

A.3.2 NCHRP Project 12-120 – Stainless Steel Prestressing Strands

Recognizing that FRP is not the only corrosion-resistant option, NCHRP Project 12-120, Design and Detailing of Concrete Bridges with Stainless Steel Prestressing Strands [46], examined the use of stainless-steel strands as an alternative to conventional steel. The objectives were to characterize the mechanical properties and corrosion resistance of stainless-steel strands, evaluate their structural performance in prestressed concrete girders, and develop design and detailing recommendations compatible with AASHTO LRFD BDS.

The research program included tension, fatigue, and relaxation tests on stainless-steel strands, as well as large-scale girder tests to compare the flexural and shear behavior of stainless-steel strands with that of conventional prestressed members [47], [48], [49]. Analytical studies and reliability analyses were used to assess the need for modified resistance factors and detailing provisions. The final report concluded that stainless steel strands offer significantly improved corrosion resistance compared with conventional strands, with mechanical properties generally compatible with existing design assumptions, albeit with somewhat reduced ductility.

While the present report focuses on CFRP rather than stainless steel, NCHRP 12-120 [46] is important because it illustrates the broader national interest in corrosion-resistant prestressing systems, and demonstrates a similar pattern of research: material characterization, large-scale testing, and reliability-based design calibration. Together, NCHRP 12-97 [8] and 12-120 [46] show that both FRP and stainless steel are long-term alternatives to conventional steel prestressing in aggressive environments.

A.3.3 NCHRP Project 12-121 – FRP Auxiliary Reinforcement for Concrete Bridge Girders

NCHRP Project 12-121, Design of Prestressed Concrete Bridge Girders Using FRP Auxiliary Reinforcement, was initiated as a natural extension of 12-97 [8]. Whereas 12-97 [8] concentrated on CFRP strands as the primary prestressing system, 12-121 focuses on the auxiliary reinforcement required

to complete a practical bridge girder design. The project addresses the use of FRP bars and other FRP products for shear reinforcement (stirrups), end-zone reinforcement, transverse and skin reinforcement, horizontal shear transfer, and confinement in concrete bridge beams prestressed with CFRP.

The experimental program for 12-121 includes large-scale tests of CFRP-prestressed beams with FRP auxiliary reinforcement over a range of shear-span-to-depth ratios, cross-section geometries, and loading configurations. Some tests are configured to isolate end-region behavior by moving supports inward, allowing concentrated study of anchorage, bursting, and transfer length effects without interference from global flexural or shear behavior. Analytical models and reliability analyses are being developed in parallel to inform proposed design provisions for shear and auxiliary reinforcement in CFRP-prestressed bridge beams.

At the time of writing, NCHRP 12-121 is still in progress, with completion anticipated in early 2026. As a result, only preliminary information is available from project statements and interim presentations [50]. Nevertheless, the outcomes of this work are highly relevant to the Harkers Island research program. The large-scale shear tests and end-region studies being conducted under NCHRP 12-121 address many of the same questions that arise in the design of deep FIB girders with FRP transverse reinforcement, and the eventual design recommendations from that project are expected to complement and inform the findings presented in this report.

A.3.4 Other National and State-Level Contributions

In addition to NCHRP projects, several state DOT-university collaborations have contributed important data on FRP-prestressed systems and corrosion-resistant reinforcement. A series of projects led by Lawrence Technological University for the Michigan DOT investigated the performance of decked bulb-T bridges incorporating GFRP and CFRP reinforcement [51]. These studies evaluated structural behavior, constructability, and long-term performance and demonstrated the feasibility of using FRP materials in precast superstructure systems.

More recently, Grace et al. [52] examined the use of 0.7 in. diameter CFRP strands for prestressing applications, building on the traditional 0.6 in. size. Larger-diameter CFRP strands provide greater cross-sectional area and strength, potentially reducing the number of strands required and improving fabrication efficiency. The test programs included material characterization and member-level performance evaluation to assess whether existing design provisions and detailing practices remain appropriate for larger strands.

Parallel to the FRP work, NCHRP Report 994 [53] explored the use of 0.7 in. steel prestressing strands in precast, pre-tensioned girders, highlighting a broader trend toward larger-diameter strands in both steel and FRP systems. Although the Harkers Island Bridge uses 0.6 in. CFRP strands, these studies are relevant for future NCDOT projects that may consider alternative strand diameters to optimize reinforcement layouts.

Taken together, the national and state-level research programs summarized in this section provide a substantial technical foundation for the design of CFRP-prestressed members and for the use of FRP and stainless steel as corrosion-resistant alternatives to conventional prestressing steel. However, they also reveal several areas requiring additional data and guidance, particularly regarding the behavior of deep girders in shear, auxiliary FRP reinforcement, and the integration of material variability and acceptance testing into design recommendations. These gaps are addressed, in part, by the experimental and analytical work presented in the later chapters of this report.

A.4. Material Standards and Acceptance Testing for FRP Reinforcement

The successful use of FRP reinforcement in bridge construction depends not only on design provisions but also on clear material standards and robust yet practical acceptance-testing protocols. For steel reinforcement and prestressing strand, this framework is well established: ASTM product specifications and test methods align closely with AASHTO design provisions and are routinely incorporated into DOT special provisions. For FRP, the situation is still evolving. Current standards provide relatively complete guidance for GFRP bars, while CFRP prestressing strands and bent FRP elements remain less codified, leaving state agencies to bridge the remaining gaps through project-specific specifications and research.

A.4.1 Standards for GFRP Bars and Associated Test Methods

For GFRP bars, the primary product specifications are ASTM D7957 [18] (covering straight and factory-bent shapes) and ASTM D8505 [54] (which also includes basalt FRP bars but covers only straight cut lengths). These standards define geometric tolerances, mechanical properties, and, in the case of ASTM D7957 [18], minimum bend diameters for solid round GFRP bars used as concrete reinforcement. Both standards require an external surface enhancement suitable for bonding to concrete (i.e., no smooth bars).

ASTM D7205 [20] supports mechanical characterization of these bars by establishing procedures for determining the quasi-static tensile strength and modulus of FRP composite bars, including specimen preparation, gripping, gauge length, and strain measurement. Bond behavior is typically evaluated using ASTM D7913 [55], which prescribes a pull-out test configuration to quantify bond strength between FRP bars and concrete. These materials and test standards are directly referenced in the ACI CODE 440.11 [13]. Together, these documents provide a coherent framework for specifying, designing, and accepting GFRP reinforcement in bridge decks and substructure components.

A.4.2 CFRP Prestressing Strands and Bent CFRP Elements

In contrast to GFRP bars, there is currently no dedicated ASTM product specification for CFRP products. Design and acceptance of these products in bridge projects have largely followed recommendations from national research programs and DOT-specific guidelines, mainly by following the same requirements for GFRP bars, which may not necessarily apply. These documents emphasize the need to characterize tensile strength and modulus, long-term creep and relaxation, thermal compatibility, bond behavior, and anchorage performance of CFRP strands used in pretensioned or post-tensioned applications.

Several agencies have proposed QA/QC test matrices for CFRP strands that adapt existing steel-oriented standards and supplement them with composite-specific procedures. For example, research sponsored by the Virginia Department of Transportation (VDOT) outlined a suite of acceptance and quality-control tests focused on tensile strength, modulus, area verification, relaxation, and selected durability indicators that state DOTs could implement without developing entirely new test infrastructure [56]. These efforts, together with ongoing work in the ASTM D30.10 Committee on Composite Materials, are gradually converging toward a CFRP-oriented product specification and test framework; however, owners still rely heavily on project-specific provisions.

Acceptance testing for bent CFRP elements (stirrups, spirals, hoops) is even less standardized. The current test method (ASTM D7914 [21]) specifies a tension test for FRP bars with bends, in which the bar is anchored in concrete blocks and loaded until rupture at or near the bend. While widely referenced, this configuration is sensitive to small misalignments and eccentricities, which can introduce unintended bending moments and lead to high coefficients of variation in measured strength. Alternative test set-ups with improved alignment [57], [58] have been adopted in the Canadian standard CSA S807 [17], which reports significantly lower scatter for bent-bar strength.

Recent research, including work summarized later in this report, has highlighted that bend radius is the dominant parameter influencing strength at FRP bends, with surface treatments and other secondary variables playing a minor role (e.g., concrete strength, fiber type, embedding length) [23], [24], [29]. Current design provisions for GFRP bends in ACI 440.11 [13] reference minimum r/d ratios from ASTM D7957 [18], which also requires the strength of a bent portion to be at least 60% of the minimum guaranteed ultimate tensile force of a companion straight portion. However, analogous provisions for CFRP spirals or stirrups have not yet been formalized, leaving state agencies to extrapolate from GFRP guidance, rely on manufacturers' recommendations, or omit this parameter from project specifications.

A.4.3 QA/QC Frameworks, Lot Definition, and Testing Demand

Beyond individual standards, there is an active debate about how to translate material test results into project-level QA/QC programs that are both rigorous and practical. In several recent FRP bridge projects, there has been a tendency to treat the complete set of tests referenced in ASTM material standards as a de facto checklist for project-level acceptance. When all these requirements are imposed at the lot level without clearly distinguishing between product-qualification testing and project-specific quality control, the resulting test count can become unrealistically large.

A central issue in this discussion is the definition of a "lot" for FRP products. Traditional definitions, such as all material produced with the same constituents and processing parameters, are not always consistent with how FRP is manufactured, inventoried, or shipped. Some documents define lots by linear footage, whereas others define them by production runs or shipment groupings. The choice has direct consequences for the number of samples that must be tested and, therefore, for schedule, cost, and the feasibility of implementing extensive acceptance programs in routine practice. Case studies, such as the Halls River Bridge in Florida [59], have shown that if lot definitions and test requirements are not carefully calibrated, material testing can become a critical-path activity during construction.

In this context, AASHTO's Product Evaluation and Audit Solutions (PEAS) program serves as a key mechanism for pre-qualifying structural products at the national level and reducing duplication of effort among individual state DOTs. PEAS provides a common framework for product evaluation and plant audits, and its Composite Concrete Reinforcements (CCR) committee specifically addresses FRP reinforcement used in concrete members. When a product line is evaluated and listed under PEAS, participating DOTs can rely on that pre-qualification, together with BABA compliance, rather than repeating complete product-qualification testing on every project. Complementary industry-led efforts, such as the FRP Institute's manufacturer certification and audit program, play a similar role by standardizing test protocols, conducting periodic plant audits, and maintaining qualified-product lists. Together, these efforts point toward a joint model in which most durability and detailed characterization tests (e.g., creep, fatigue, environmental conditioning) are performed at the product-qualification and plant-audit levels, rather than being re-created for every bridge project.

Within this emerging framework, our view is that tension tests and bent-bar (or bend-strength) tests are currently the most informative candidates for project-level QA/QC, because they directly control the design tensile strength of straight and bent FRP elements and indirectly reflect overall material quality. Other tests, such as water absorption, density-based area measurements, fiber content, or microstructural characterization, remain important, but are often better suited to centralized product-qualification programs (e.g., PEAS listings, FRP Institute audits) than to routine project-level acceptance, given their complexity and cost. As FRP standards evolve, it will be essential to clarify which properties should be verified at the product line level and which should be checked periodically on a project basis to confirm the consistency of supplied materials.

A.4.4 Relevance to the Harkers Island Project

The Harkers Island Bridge project provides a concrete example of these broader challenges. NCDOT's initial special provisions for CFRP strands and spirals were based mainly on steel-oriented procedures and early FRP projects, resulting in a very high number of required tests per lot. As the project progressed, the acceptance program was refined in consultation with NCDOT, the FRP manufacturers, and the NC State research team to focus on the most critical properties for structural performance and design verification.

For CFRP strands, more than 300 tension tests were conducted on production samples to verify tensile strength and stiffness and to build a statistically robust database of material properties. For CFRP spirals used in prestressed piles, 19 square spirals with the same geometry as those installed in the field were tested in accordance with the ASTM D7914 [21] configuration, with one specimen drawn from each lot. Additional tests on larger-radius spirals were conducted as part of a complementary effort to investigate the effects of r/d ratio and surface treatment on bend strength.

The resulting datasets revealed two valuable trends:

- Tension tests on CFRP strands exhibited relatively low scatter and behavior consistent with normal statistical distributions, suggesting that moderate sample sizes per lot may be sufficient for reliable quality control.
- Bent-bar tests on CFRP spirals, in contrast, showed much higher coefficients of variation, influenced by both bend geometry and test-set-up sensitivity, making it challenging to define acceptance criteria or sample sizes using conventional approaches.

These observations motivated the more detailed statistical analyses presented later in this report, which aim to identify reasonable sample sizes and acceptance criteria that balance safety, reliability, and practicality. In this sense, the Harkers Island project not only relied on existing FRP material standards but also contributed data and insights that can inform the ongoing development of CFRP-specific specifications and QA/QC guidelines.

A.5. Field Performance and Durability of FRP-Reinforced Bridges

Most of the code and guideline developments in Section A.2 have been driven by accelerated testing and member-scale experiments. However, for agencies considering large-scale implementation of FRP reinforcement, the actual field performance of in-service bridges is equally important. This section briefly reviews reported behavior of FRP-reinforced decks and partial bridge applications, followed by selected case studies of bridges that incorporate CFRP prestressing or broader all-FRP systems. The emphasis is on serviceability, durability, and observed deterioration mechanisms, rather than on design details already covered in previous sections.

A.5.1 FRP-Reinforced Decks and Partial Applications

The earliest and most widespread use of internal FRP reinforcement in highway bridges has been in reinforced concrete decks. Several state and provincial DOTs in the US and Canada (e.g., Minnesota, Wisconsin, Florida, Texas, Quebec, Alberta, Nova Scotia) have constructed GFRP-reinforced bridge decks or deck slabs and monitored their performance over periods ranging from 5 to more than 15 years.

Field investigations of these decks typically focus on:

- Serviceability: crack widths, deflections under live load, and vibration response.
- Durability: evidence of degradation of GFRP, condition of the FRP-concrete interface, and performance under de-icing salts and freeze-thaw cycles.
- Wearing surface performance: behavior of asphalt or polymer overlays placed over FRP-reinforced slabs.

A multi-bridge field durability study of GFRP-reinforced concrete structures in Canada (including several bridge decks) found, after 5–8 years of exposure to deicing salts, wet–dry cycles, and freeze–thaw, no observable degradation of the GFRP bars or of the GFRP-concrete interface when examined using optical and electron microscopy and spectroscopy [60]. The bond between GFRP and concrete remained intact, and there was no significant change in the glass transition temperature of the resin, suggesting that the matrix and fiber–matrix interface were not adversely affected by the in-service environment.

Similar conclusions have been drawn from US-based projects in which GFRP bars replaced epoxy-coated steel in decks. For example, a Minnesota DOT demonstration bridge with GFRP-reinforced deck panels was instrumented to monitor strains, deflections, and temperatures [61]; subsequent evaluation reported that the GFRP deck satisfied serviceability requirements and confirmed the potential of GFRP bars to mitigate corrosion-related deck deterioration. A synthesis of Wisconsin "Innovative Bridge Research and Construction" (IBRC) projects likewise noted that FRP-reinforced decks and hybrid FRP deck systems performed satisfactorily in service, while recommending continued monitoring to better quantify long-term stiffness and crack control [62].

In parallel with internal reinforcement, FRP has also been deployed as stay-in-place deck forms, external strengthening systems, and corrosion-resistant diaphragms and barriers. These applications are increasingly common in Florida, where FDOT has used FRP composites in decks, substructures, and protective elements for coastal bridges [63]. Reported experience indicates that:

- Corrosion of steel reinforcement in FRP-reinforced decks is eliminated where GFRP fully replaces steel.
- Most in-service issues have been associated with wearing surfaces, joints, or construction workmanship, rather than with FRP degradation.
- Service behavior (crack widths, deflections) is generally acceptable when the design follows existing FRP guidelines. However, higher reinforcement ratios are often required to control crack widths due to the lower modulus of GFRP.

Because the number of FRP decks has grown substantially, several groups have developed standardized inspection frameworks for in-service FRP-reinforced or FRP-strengthened concrete bridge elements. For example, Mehrabi et al. [64] proposed a field inspection protocol for FRP-strengthened and FRP-reinforced decks that emphasizes visual inspection, non-destructive testing, and targeted sampling where needed. More recent work has expanded these concepts into a broader framework for field inspection of FRP-reinforced structural concrete, reinforcing the view that FRP components in existing bridges have generally performed well, while also recognizing that inspection practices must be adapted to a proper inspection guide.

Overall, the accumulated evidence from decks and partial applications suggests that, when properly detailed and constructed, GFRP-reinforced concrete decks can provide durable, corrosion-free performance for at least the first decade of service, with serviceability governed by conventional crack-width and deflection limits rather than by material deterioration.

A.5.2 All-FRP or FRP-Prestressed Bridges and Instrumented Case Studies

Field performance data for bridges that incorporate CFRP prestressing or rely on FRP as the primary reinforcement in primary load-carrying members are more limited, but several noteworthy case studies have been reported.

One of the earliest and most frequently cited examples is the Shinmiya Bridge in Japan, completed in 1988 [65], where Carbon Fiber Composite Cable (CFCC) tendons were used as the primary prestressing reinforcement in the main girders of a coastal highway bridge. Long-term monitoring and subsequent analytical investigations have shown that the CFCC tendons have maintained their integrity over multiple decades of service, with no evidence of corrosion. Besides, measured deflections and prestress losses have remained consistent with predictions from elastic creep and shrinkage models. These results are often cited as proof of concept for the long-term durability of CFRP prestressing in marine environments.

In North America, several bridges with CFRP-prestressed girders or decked bulb-T systems have been constructed and tested in the field. Work by Grace et al. [51], [66] on decked bulb-T beam bridges prestressed with CFRP tendons included the construction of full-scale bridge models, static and fatigue testing, and subsequent field implementation and evaluation for a Michigan DOT project. Experimental and analytical results showed that the CFRP-prestressed systems met serviceability criteria for deflection and cracking and provided flexural capacities comparable to or greater than those of comparable steel-prestressed systems. More recent Michigan DOT research on 0.7 in. diameter CFRP strands [52] confirmed that these larger-diameter tendons can achieve reliable anchorage and prestress levels, further supporting their use in bridge girders.

Florida and other states have also implemented FRP-reinforced and CFRP-prestressed elements in coastal bridges, often in combination with life-cycle cost analyses and resilience metrics [59], [67], [68], [69], [70]. Nolan et al.'s [63] synthesis of FRP applications in Florida notes that internal FRP reinforcement has been successfully used in substructures and decks to target 100-year design lifespans, with early field observations indicating stable behavior and reduced maintenance needs relative to steel-reinforced counterparts.

These case studies consistently show that CFRP prestressing and extensive internal FRP reinforcement perform satisfactorily in the field, but they remain relatively few in number. Most documented FRP-prestressed bridges are of modest span and scale compared with the Harkers Island Bridge, and only a subset is located in highly aggressive coastal environments.

A.6. Prior NCDOT Research on FRP and Coastal Bridges

Over the past decade, NCDOT has sponsored a series of research projects at NC State University to understand the deterioration of existing steel-prestressed coastal bridges and to evaluate FRP-based alternatives for both new construction and rehabilitation. These projects, together with complementary durability studies on CFRP strands, provided much of the technical foundation and institutional confidence needed to pursue the Harkers Island Bridge as an all-FRP-reinforced structure.

A.6.1 Deterioration of Coastal Prestressed Cored-Slab Bridges

Prestressed concrete cored slabs have been widely used in North Carolina since 1969 for simple spans ranging from 40 to 70 ft. Field experience, however, showed that in coastal regions these systems can exhibit extensive corrosion of internal steel reinforcement after less than 40 years in service. To better quantify this problem and develop rational assessment guidelines, NCDOT sponsored Project 2014-35, documented in the report titled "Assessment of Deteriorated Cored Slabs" [1].

The study focused on two coastal bridges in Carteret County (Bridge No's. 150035 and 150039), for which field inspections had documented widespread spalling, delamination, rust staining, and highly variable visual conditions. The research program included:

- Field investigation: detailed mapping of visible deterioration, sounding for delamination, and concrete surface resistivity measurements.
- Laboratory testing: removal of 12 cored slabs for non-destructive evaluation, extraction of concrete cores and prestressing strand samples, half-cell potential measurements, and flexural tests to failure.
- Post-test forensics: documentation of the actual condition of strands and stirrups after demolition, including cases where delaminated patches masked severe underlying corrosion.

The results showed that:

- Extensive corrosion of bottom prestressing strands and stirrups can occur beneath relatively modest surface deterioration, leading to substantial loss of flexural capacity.
- Patch repairs are highly variable in effectiveness; some patches remain sound, whereas others delaminate and accelerate corrosion by trapping moisture.
- Traditional inspection records often lack the depth and consistency (e.g., qualitative depth of spalls, condition behind delamination) needed for reliable load rating.

Van Brunt et al. [1] proposed practical recommendations for field inspection (e.g., qualitative depth categories for spalls, explicit documentation of changes over time) and highlighted the need for more durable alternatives to steel-prestressed cored slabs in coastal environments. This work provided direct evidence of the limitations of traditional systems and motivated NCDOT's interest in corrosion-resistant reinforcement, including FRP.

A.6.2 CFRP-Prestressed Cored Slabs with GFRP Stirrups

Building on the deterioration study, NCDOT Project 2014-09, titled "CFRP Strands in Prestressed Cored Slab Units" [2], investigated FRP-prestressed cored slabs as direct replacements for the deteriorated steel systems. The goals were to (i) assess whether CFRP-prestressed, GFRP-reinforced cored slabs could match or exceed the flexural and shear capacity of conventional steel-prestressed slabs, and (ii) develop practical details compatible with existing precast production methods. The research program included:

- Material characterization: tension tests on CFRP strands and GFRP bars to validate manufacturer properties and compare stress–strain behavior with steel.
- Bond and development length: beam-end tests on CFRP strands to evaluate bond strength and to calibrate development length predictions relative to ACI 440.4R [38] expressions.
- Full-scale member tests: two 45 ft. CFRP-prestressed cored slabs were tested in flexure, and two 15 ft. slabs were tested in shear.

The cored slabs were designed to match the geometry and load-carrying capacity of standard steel-prestressed NCDOT slabs, enabling production on existing beds using familiar procedures. Experimental results showed that:

- CFRP-prestressed slabs achieved flexural and shear capacities comparable to or greater than those of steel control specimens.
- Failures were governed by concrete crushing or shear mechanisms rather than premature rupture of CFRP strands or GFRP stirrups, indicating that well-detailed FRP reinforcement can provide adequate strength.

- Serviceability behavior (deflections and cracking) was acceptable, with stiffness adequately predicted when FRP material properties and prestress levels were correctly incorporated.

This project demonstrated that fully FRP-prestressed cored slabs are a viable replacement system for coastal bridges [71] and validated many of the material and bond assumptions later employed in the Harkers Island design.

A.6.3 Mechanically Fastened FRP Retrofit for Deteriorated Prestressed Beams

While full replacement with FRP-prestressed members is the ideal option for new projects, NCDOT also needed solutions for existing deteriorated bridges that could not be replaced immediately. NCDOT Project 2018-16, titled "Mechanically-Fastened FRP to Retrofit Existing Prestressed Concrete Bridge Beams" [3], developed a prestressed mechanically fastened FRP (MF-FRP) system for rapid flexural strengthening of deteriorated C-channel and cored-slab beams. Key elements of this work included:

- Development of an MF-FRP system using prestressed FRP strips mechanically anchored to the soffit of the beam, avoiding the surface preparation and curing demands of bonded systems.
- Small-scale tests on fasteners, strip anchorage details, and installation procedures to optimize constructability and performance [72].
- Full-scale tests on deteriorated beams repaired with MF-FRP, showing that the retrofit can restore lost prestress and significantly increase inventory and operating load ratings [73].
- Long-term testing under sustained load and fatigue to assess the expected service life of the retrofit [74].

A layered-sectional analysis (LSA) model was developed and shown to accurately reproduce the full flexural response of repaired beams, providing a tool for design and load rating of MF-FRP retrofits. This project complements the Harkers Island work in two ways. First, it reinforces the broader NCDOT strategy of using FRP not only in new construction but also as a rapid retrofit solution for aging infrastructure. Second, the MF-FRP research further familiarized NCDOT and NC State with FRP material behavior, prestressing, and field implementation issues relevant to an all-FRP bridge.

A.6.4 Durability of CFRP Strands for Prestressing

In parallel with these NCDOT-sponsored projects, NC State researchers conducted a comprehensive durability study of CFRP strands used for the prestressing of concrete members, as reported by Khalafalla et al. [75]. Although not an NCDOT project per se, this work directly supports NCDOT's confidence in CFRP strands.

The study investigated the synergistic effects of environmental exposure and sustained loading on seven-wire CFRP strands with a geometry similar to steel prestressing strands. Specimens were subjected to:

- Sustained stress equal to 65% of the guaranteed tensile strength.
- Immersion in alkaline solution at 55 °C.
- Exposure durations up to 7,000 hours.

Mechanical tests before and after conditioning showed that:

- Tensile strength reductions were limited (on the order of a few percent) even under combined sustained load and aggressive alkaline exposure.
- Elastic modulus decreased only slightly, indicating that stiffness is largely preserved.
- Bond and shear strength also remained within acceptable ranges, suggesting that the primary degradation mechanisms are modest under the tested conditions.

The authors concluded that properly manufactured CFRP strands exhibit durable behavior under conditions intended to simulate typical bridge exposures, and that explicitly accounting for combined environmental and sustained loading effects can lead to more rational, potentially less conservative, design assumptions.

A.6.5 Synthesis and Relevance to the Harkers Island Bridge

These projects define a coherent progression in NCDOT's approach to corrosion-resistant bridge systems:

1. Problem definition (deteriorated cored-slabs): Van Brunt et al. [1] documented the extent and consequences of corrosion in existing coastal cored-slab bridges.
2. FRP as a replacement system (CFRP-prestressed cored slabs): Shapack et al. [2] showed that cored slabs prestressed with CFRP strands and reinforced with GFRP stirrups can provide structural performance comparable to traditional systems, while eliminating internal corrosion.
3. FRP as a retrofit (MF-FRP strengthening): Lin et al. [3] extended FRP applications to rapid strengthening of existing deteriorated prestressed beams, offering NCDOT a practical tool to extend service life while replacements are planned.
4. Long-term durability (CFRP strands): Khalafalla et al. [75] provided experimental evidence that CFRP strands maintain a high proportion of their strength and stiffness under simultaneous environmental and sustained loading, supporting their use as primary prestressing reinforcement in aggressive environments.

The Harkers Island Bridge can be viewed as the logical next step in this sequence. Instead of applying FRP in individual components or as a retrofit, NCDOT committed to using CFRP and GFRP as the primary internal reinforcement throughout the main load-carrying elements of a large coastal bridge.

A.7. Summary and Identified Research Needs

The literature and prior research reviewed in this chapter show that the technical basis for using FRP reinforcement in bridge structures has advanced significantly over the past three decades. Guide specifications, code documents, national research programs, and prior NCDOT projects have demonstrated that FRP-based systems can achieve satisfactory structural performance and provide substantial durability benefits in aggressive environments. At the same time, several important gaps remain, particularly in areas directly relevant to a large, all-FRP-reinforced bridge such as the Harkers Island Bridge project.

A.7.1 Research Questions Addressed in This Report

In response to the needs identified above, the Harkers Island Bridge research project was structured around the following central questions:

1. How should FRP material properties be tested and statistically evaluated for design and acceptance?
   - What are the representative tensile and bend strengths for the CFRP strands, CFRP spirals, and GFRP bars used in the project?
   - How many tests are needed per lot to estimate these properties with acceptable confidence?
   - How can test results be translated into design values and acceptance criteria that are both rational and practical for future projects?

2. How do bent FRP elements (CFRP spirals and GFRP stirrups) behave at bend locations, and what strength reduction factors are appropriate?
    - How do bend radius, surface treatment, and test configuration influence strength at bends?
    - Are current minimum bend radius recommendations adequate or overly conservative for the geometries used in piles and girders?
    - How should design provisions be formulated to reflect the observed behavior while maintaining clear, implementable rules for practice?
3. How do deep, FRP-prestressed bridge girders behave in shear, and how well do existing models capture this behavior?
    - What are the shear capacities and failure modes of full-scale FIB girders with CFRP strands and FRP transverse reinforcement representative of the Harkers Island design?
    - How do these results compare with predictions from current AASHTO and ACI provisions and from ongoing research such as NCHRP 12-121?
    - What adjustments, if any, are needed to shear design and detailing for FRP bridge girders?
4. What integrated recommendations can be made for future FRP bridge projects?
    - Based on the combined material, statistical, and structural findings, what guidance can be offered to NCDOT regarding specification of FRP products, QA/QC testing programs, and acceptance criteria?
    - How should FRP reinforcement be detailed in piles, girders, substructures, and decks to ensure constructability, durability, and reliable performance?
    - How can the experience gained from Harkers Island be generalized to inform future all-FRP or hybrid FRP–steel bridge projects in North Carolina and beyond?

Appendix B. HARKERS ISLAND BRIDGE DESCRIPTION

B.1. Project Background

Harkers Island is a small coastal community in Carteret County, North Carolina, located a few miles east of Morehead City and adjacent to the Cape Lookout National Seashore. The island has a permanent population of approximately 1,200 residents and relies heavily on boat building, commercial and recreational fishing, tourism, and access to the Cape Lookout barrier islands. Thereby, a reliable roadway access across the town of Straits is essential for daily mobility, economic activity, and hurricane evacuation.

The bridge site is characterized by shallow tidal waters, direct exposure to salt-laden winds, frequent wetting and drying, and occasional extreme storm events. These conditions are particularly aggressive for conventional steel-reinforced and prestressed concrete structures. NCDOT classifies this region as highly corrosive, and its standard practice for concrete bridges in such areas has been to increase concrete cover, use epoxy-coated reinforcing steel, and incorporate corrosion-inhibiting admixtures such as calcium nitrite, silica fume, and fly ash. Experience with the existing Harkers Island bridges, however, demonstrated that even enhanced conventional systems require major repair or replacement within a few decades of service, motivating the search for more durable reinforcement solutions.

B.1.1 Existing Bridges and Need for Replacement

Prior to the current project, Harkers Island was served by North Carolina Highway 70 through two sequential bridges: the Earl C. Davis Memorial Bridge (Bridge No. 73) and Carteret County Bridge No. 96 (see Figure A - 1). Together, these structures provided the only roadway link between the mainland and the island. The original crossing, completed in 1941, consisted of two timber bridges aligned north–south and touching down on a small intermediate island. In the late 1960s and early 1970s, these timber structures were replaced by prestressed concrete bridges with conventional steel prestressing strands and internal steel reinforcement. Bridge No. 73 included a steel swing span to accommodate navigation in the channel, while Bridge No. 96 provided the remaining length of the crossing.

After roughly five decades of exposure to the marine environment, both bridges exhibited extensive deterioration. Routine inspections documented corrosion of prestressing strands and internal reinforcement, cracking and spalling of concrete, and a steady increase in maintenance needs. By 2013, the condition of Bridge No. 96 had deteriorated to the point that an emergency full superstructure replacement was required due to severe corrosion of the original steel prestressing strands in the cored-slab units. Subsequent inspections in 2015 classified Bridge No. 73 as structurally deficient and Bridge No. 96 as functionally obsolete, reflecting both physical condition and geometric and operational limitations.

In addition to the structural deterioration, the swing span of Bridge No. 73 created reliability and safety issues. Mechanical problems and corrosion of moving components occasionally prevented the span from opening or closing reliably for vessel traffic, disrupting marine operations and causing delays for roadway users. The narrow roadway width and inadequate shoulders on the existing bridges further constrained emergency response and evacuation capacity.

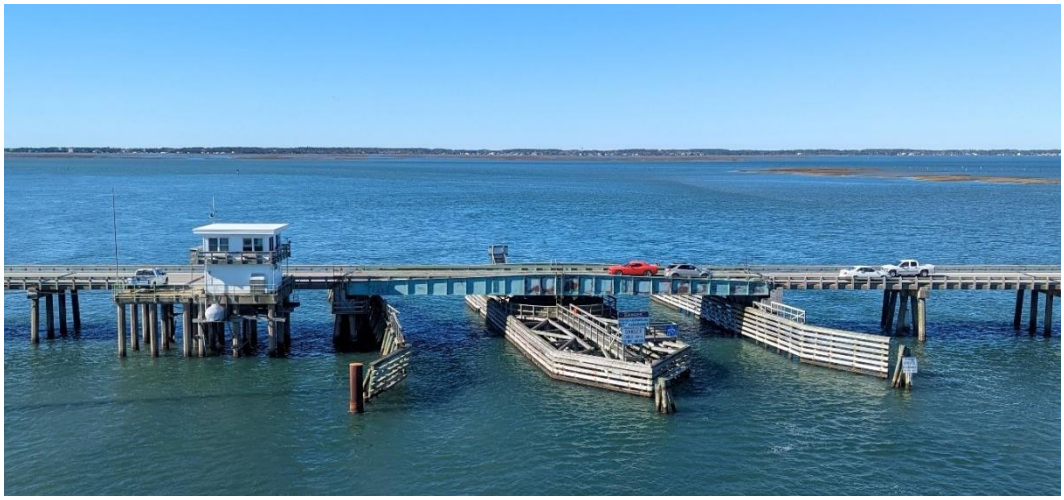

(a) Bridge No. 73 (Earl C. Davis Memorial Bridge) – Demolished

(b) Bridge No. 96 – Remains as pedestrian access and fishing pier

Figure A - 1. Prior bridges connecting Harkers Island

Given the combination of advanced deterioration, functional limitations, and the critical role of the crossing, NCDOT determined that full replacement of the existing bridges represented the most effective long-term solution. The new structure would need to meet current geometric and operational standards, eliminate the movable span, and significantly improve durability relative to conventional steel-reinforced designs under the local exposure conditions.

B.1.2 Selection of Harkers Island as the first NC's All-FRP-Reinforced Bridge

When preliminary design for the Harkers Island Bridge replacement began around 2017, NCDOT had just completed a project on CFRP-prestressed cored slabs [2] and had accumulated nearly a decade of experience with GFRP-reinforced bridge decks [5] and FRP repair systems [3]. Internal discussions among the Structures Management, Construction, Materials & Tests, and Geotechnical units identified Harkers Island as an ideal candidate for large-scale implementation of FRP reinforcement because:

- The existing bridges had clearly demonstrated the vulnerability of steel reinforcement under the local exposure conditions.
- The replacement structure would be relatively long and heavily reinforced, providing an opportunity to evaluate FRP across a wide range of elements.
- Economies of scale could help offset the higher unit cost of FRP materials, making the overall project cost competitive with a conventional solution when life-cycle performance is considered.

NCDOT leadership ultimately endorsed a strategy to design the entire structural system (piles, caps, columns, girders, and deck) with FRP reinforcement wherever feasible, using steel reinforcement only in a few localized components, such as the parapet rail, where FRP-reinforced alternatives could not be implemented due to the lack of crash-test information. To support this innovative project, the Federal Highway Administration (FHWA) awarded NCDOT a $1 million Accelerated Innovation Deployment (AID) Demonstration grant to help offset the incremental material costs associated with FRP.

B.1.3 Role of the Harkers Island Bridge in NCDOT's FRP Roadmap

Within this broader program, the Harkers Island Bridge serves several strategic roles for NCDOT:

1. Prototype for Fully FRP-Reinforced Bridges:
   It is NCDOT's first bridge in which all major structural components are reinforced or prestressed exclusively with FRP, making it a full-scale demonstration of the technology in a highly corrosive coastal environment.
2. Platform for Material Acceptance and Quality Control:
   The project includes expanded acceptance testing of FRP bars and strands. NCSU conducted all quality-control testing on randomly sampled materials to verify manufacturer certifications and assess variability in properties relevant to design.
3. Case Study for Design and Construction Practices:
   Lessons learned from the design process, detailing decisions, fabrication of FRP-reinforced components, and field construction activities, including the use of a temporary work trestle and construction under in-water work restrictions, will inform future NCDOT guidance on FRP bridge projects.
4. Benchmark for Future Research and Monitoring:
   The bridge provides a unique opportunity to correlate laboratory tests, analytical models, and code provisions with the performance of an in-service structure over time. The companion research program documented in this report is intended to establish that benchmark and to recommend procedures for future monitoring and evaluation.

Hence, the Harkers Island Bridge replacement project is both a critical infrastructure investment for a coastal community and a key milestone in NCDOT's long-term strategy to deploy FRP reinforcement as a durable, cost-effective solution for bridges in aggressive environments.

B.2. New Bridge Layout and Structural System

This section expands on the summary presented in Section 1.4.2 by describing the overall geometry and structural configuration of the new Harkers Island Bridge. The focus is on how the spans, girders, and substructure are arranged, setting the stage for the material- and FRP-specific discussions in later chapters.

B.2.1 Overall Geometry and Alignment

The new Harkers Island Bridge follows an alignment that deliberately avoids the small intermediate island used by the original timber and concrete bridges. Instead, the replacement structure is shifted slightly to the east, crossing the water directly (see Figure 5). This relocation allowed construction to proceed largely independent of the existing bridges, minimizing traffic disruptions during the project, as shown in Figure A - 2.

The bridge consists of 28 simply supported spans with a total length of 3,200 ft. The deck width is 34 ft. 7 in. and accommodates two 12 ft. travel lanes and 4 ft. shoulders on each side. A single 125 ft.-long navigation span provides a vertical clearance of 45 ft. above the water surface, ensuring unobstructed passage for commercial and recreational vessels. By raising the profile near the navigation channel and eliminating the swing span used in the previous bridge, the new layout improves sight distance, traffic flow, and operational reliability while preserving marine access through the town of Straits.

Figure A - 2. Construction site layout

B.2.2 Superstructure Configuration

The superstructure consists of precast, prestressed Florida I-beam (FIB) girders supporting a cast-in-place lightweight sand concrete deck. Three FIB depths are used to span the varying distances along the crossing:

- 56 FIB girders with a depth of 54 in. (5,580 linear ft.),
- 44 FIB girders with a depth of 72 in. (5,707 linear ft.), and
- 15 FIB girders with a depth of 78 in. (1,815 linear ft.).

The spans away from the navigation channel are arranged with a four-girder cross-section (see Figure A - 3) and span lengths of 100–130 ft., depending on location. In contrast, the three spans surrounding the navigation channel employ a five-girder cross-section with the deepest FIB girders (78 in.) to accommodate the longer span and higher demands in this region.

The deck is 8½ in. thick and cast-in-place over the FIB girders using a lightweight sand-concrete mix. The use of a relatively thin, lightweight deck reduces dead load and helps maintain serviceability criteria, which is particularly important when the internal reinforcement consists of FRP rather than steel. Link slabs [76] are used at selected locations to reduce the number of deck joints and to simplify detailing of FRP reinforcement across span breaks. All FIB girders are supported on steel-laminated elastomeric bearing pads with stainless steel sole plates and anchor bolts, consistent with NCDOT standard practice for coastal bridges.

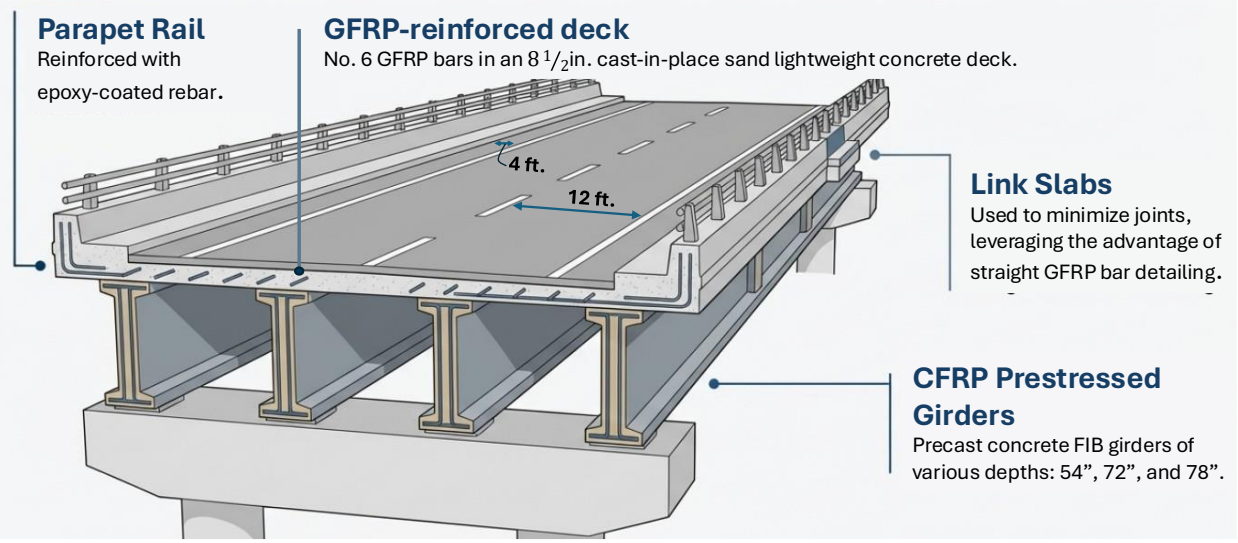

Figure A - 3. Typical superstructure cross-section sketch

B.2.3 Substructure and Foundations

The substructure system combines pile bents and multi-column bents supported by precast, prestressed concrete piles, reflecting both geotechnical conditions and navigational requirements. Most interior supports consist of cast-in-place pile caps supported directly on groups of 24 in. square precast, prestressed concrete piles (Figure A - 4a). This configuration is used at 19 bents, where the spans are shorter, and the required elevation can be achieved without intermediate columns.

In regions where the superstructure must rise to provide navigation clearance, the bridge uses three-column bents (Figure A - 4b). At these locations, cast-in-place caps are supported on three circular columns with diameters ranging from 3.5 to 4.0 ft., resting on larger pile groups. The number of piles in each footing increases with span length and demand:

- Near the approaches, a single row of five piles supports each bent.
- In the transition to the navigation span, caps with ten piles are used.
- At the navigation span itself, 15-pile groups arranged in three rows support each side of the opening.

Several bents incorporate inclined piles with a 1.5:12 batter to enhance lateral load resistance and improve performance under vessel collision and extreme lateral loads (Figure A - 5a). End bents and roadway approaches are protected against scour and erosion by precast, prestressed concrete sheet-pile walls reinforced with conventional steel prestressing strands (Figure A - 5b). These elements are located above the tidal zone and are not exposed to direct saltwater immersion, which is why steel prestressing was retained in this specific application.

(a) Pile caps directly on piles *(b) Three-column bents*

Figure A - 4. Substructure system

(a) Batter piles *(b) Steel-prestressed scour protection*

Figure A - 5. Batter piles and sheet-pile walls

B.2.4 Roadway Cross Section and Functional Features

The roadway cross-section of the Harkers Island Bridge is consistent with current NCDOT standards for a rural two-lane facility in this corridor. The deck accommodates: (i) two 12 ft. lanes, (ii) 4 ft. shoulders on each side, and (iii) standard concrete barrier rails at the deck edges. The Grade 60 epoxy-coated rebar used in the barrier rails can be seen in Figure A - 6.

Compared with the previous bridges, the new cross-section provides improved shoulders and clear width, which benefits both routine operations and emergency response. The barrier geometry and reinforcement layout were carefully coordinated so that the main structural deck and supporting members could be reinforced entirely with straight GFRP bars, while the barrier itself retained epoxy-coated steel reinforcement consistent with existing crash-tested details. The driving surface, once the bridge construction was completed, is shown in Figure A - 7.

Figure A - 6. Epoxy-coated bars reinforcing the parapet rail

Figure A - 7. New Harkers Island Bridge cross-section

B.3. FRP Passive and Prestressing Reinforcement

The Harkers Island Bridge was conceived from the outset as an internally FRP-reinforced structure for all primary load-carrying components. Two types of reinforcement were mainly used: (i) GFRP bars as passive reinforcement, and (ii) CFRP strands and spirals for longitudinal prestressing and transverse reinforcement in piles, respectively. This strategy enabled NCDOT to eliminate internal steel reinforcement in the main structural elements while maintaining details familiar to designers, precasters, and contractors.

B.3.1 Selection and Roles of FRP Materials

GFRP bars as passive reinforcement:

Five bar diameters were specified in accordance with ASTM D7957 [18]. No. 5 bars are used as the primary stirrups in the FIB girders and as transverse reinforcement in pile caps, while No. 6 bars are used extensively in the lightweight concrete deck. Smaller and larger diameters were used as needed for secondary reinforcement, column reinforcement, and miscellaneous details. Owens Corning produced the GFRP bars used in this project. Overall, the superstructure required approximately 715,000 ft. of GFRP reinforcement, with an additional 200,000 ft. in the substructure. GFRP-reinforced elements are shown in Figure A - 8.

(a) Bent columns *(b) Pile caps*

Figure A - 8. GFRP reinforcement cages

CFRP strands as prestressing reinforcement:

A single 0.6 in. diameter seven-wire strand, manufactured by Tokyo Rope USA and commercially sold as Carbon Fiber Composite Cable (CFCC), was used throughout the project for longitudinal prestressing in both FIB girders and square piles. Approximately 650,000 ft. of CFRP prestressing strands were used in the girders and 325,000 ft. in the piles. A companion 0.28 in. single-wire CFRP strand (uni-strand CFCC) was used as transverse spirals in the piles, providing confinement to the prestressing strands and the concrete core.

Limiting the number of FRP products and diameters served two purposes. From a design perspective, it simplifies the development of standard details and reduces the number of distinct design checks required. From a construction standpoint, it limited the number of suppliers and validation tests, making it feasible to implement a robust quality-control program for both straight and bent FRP elements.

B.3.2 Precast, Prestressed Components

All precast, prestressed concrete elements that form the primary load path (FIB girders and 24 in. square piles) use CFRP for longitudinal prestressing and GFRP for all internal transverse and shear reinforcement, except for the piles, which are transversely reinforced with a continuous uni-strand CFCC spiral. Typical reinforcement arrangements for girders and piles in their prestressing beds are shown in Figure A - 9. Their reinforcement details are summarized below:

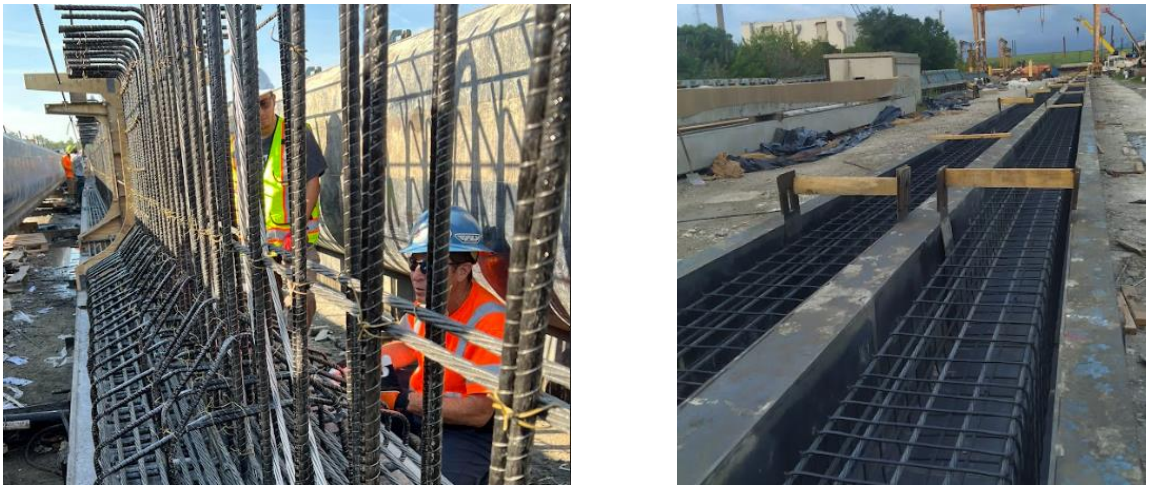

(a) FIB girders *(b) Square piles*

Figure A - 9. Prestressing beds

FIB girders:

Each of the three FIB girders (54, 72, and 78 in.) is prestressed with a standardized pattern of 0.6 in. CFRP strands, ranging from 44 strands in the shallower girders to 64 strands in the deepest section. Two strands are placed in the web to enhance shear and negative moment capacity while preserving a layout similar to conventional steel-prestressed girders (Figure A - 10). Transverse reinforcement in the girders consists of GFRP stirrups, selected by the precast contractor from alternatives that included both CFRP and GFRP options. The final choice of No. 5 GFRP stirrups provided adequate shear capacity while maintaining a uniform detailing scheme across all spans.

Prestressed piles:

The 24-in. square piles are prestressed with 16 CFRP strands and confined by a continuous CFRP square spiral. This configuration mirrors conventional steel-prestressed piles in layout but replaces both the longitudinal strand and the transverse spiral with noncorroding CFRP. The relatively high concrete strength specified for these elements (10 ksi), combined with the transverse confinement, was intended to ensure adequate drivability and long-term performance in the highly corrosive marine environment. Figure A - 11 shows piles at the precast yard.

Figure A - 10. 54 in. CFRP-prestressed FIB girders

Figure A - 11. 24 in. CFRP-prestressed square piles

B.3.3 Cast-in-Place Substructure and Deck

All cast-in-place structural components (pile caps, columns, bent caps, and the bridge deck) are reinforced exclusively with GFRP bars, spirals, and stirrups. The reinforcement detailing replicates familiar steel reinforcement layouts wherever possible.

Pile caps, columns, and bent caps:

GFRP cages in the substructure follow conventional bar spacing and development practices, with larger-diameter GFRP bars used for primary flexural reinforcement and smaller bars or spirals for confinement and shear (see Figure A - 12). In several locations, inclined (battered) piles are anchored into GFRP-reinforced pile caps to resist vessel collision and lateral loads.

(a) Pile cap reinforcement cage

(b) Bent column

Figure A - 12. Substructure GFRP reinforcement

Deck reinforcement:

The 8½ in. thick lightweight concrete deck is reinforced with GFRP bars in both directions (Figure A - 13), with No. 6 bars serving as the primary longitudinal reinforcement. The chosen bar spacing and cover were selected to control crack widths under service loads while remaining compatible with the deck thickness and construction methods used on other NCDOT bridges.

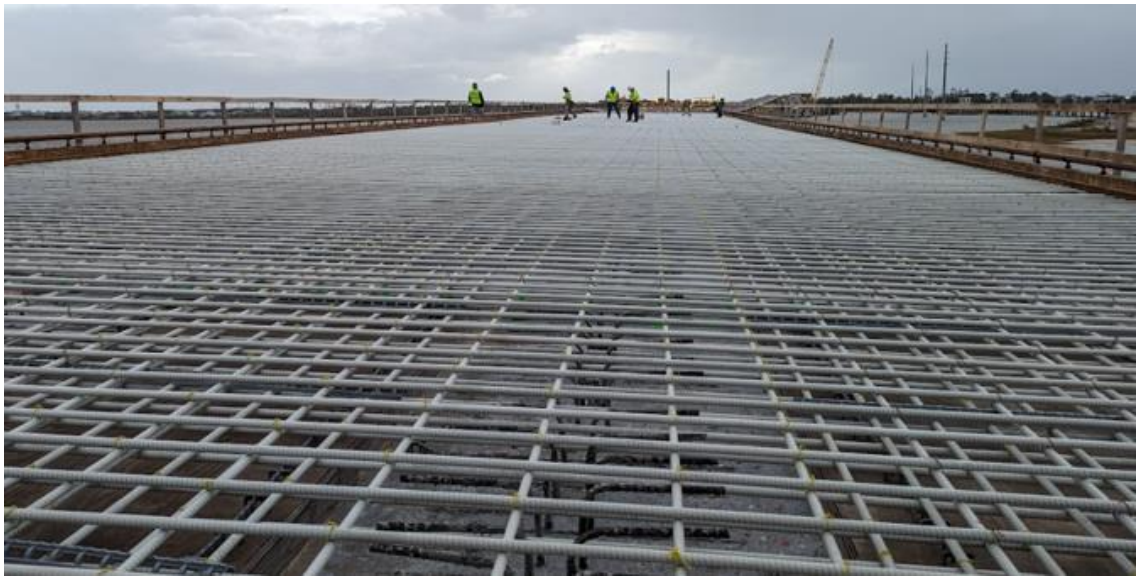

Figure A - 13. Deck GFRP reinforcement

B.3.4 Minimization of Steel and Detailing Simplifications

Although the project's goal was to eliminate internal steel, two families of elements still rely on conventional steel reinforcement: (i) prestressed concrete sheet-pile walls used for scour protection at the approaches, and (ii) the deck barrier rail, which is reinforced with epoxy-coated Grade 60 steel to satisfy crash-testing requirements. These components are either not in constant contact with saltwater (sheet piles) or are governed by existing safety hardware specifications that currently do not permit FRP alternatives.

Within the FRP-reinforced components, detailing decisions were made to keep reinforcement shapes and fabrication as simple as possible. For example:

- FRP elements requiring bends (e.g., stirrups, spirals, column hoops) were pre-formed during manufacturing, since neither GFRP nor CFRP can be bent in the field.
- Link slabs [76] were employed instead of continuous-for-live-load diaphragms with multi-bend bars, avoiding complex GFRP bending geometries that would have been challenging to fabricate and install.
- Transverse reinforcement details were standardized across girder types to streamline shop drawings, fabrication, and quality control.

These choices reflect a broader strategy: use FRP to address durability concerns, but avoid unnecessary complexity in the reinforcing layouts so that the system is buildable and scalable beyond this single project.

B.3.5 Design Philosophy and Target Performance

The FRP reinforcement strategy was developed with a long service life and minimal maintenance as primary objectives. NCDOT targeted a design life of at least 75 years for the replacement structure, recognizing that eliminating internal steel corrosion is key to achieving this goal in a coastal environment. The resulting system demonstrates that a large coastal bridge can be detailed and constructed using FRP as the primary internal reinforcement, while remaining compatible with NCDOT standards and with established precast and cast-in-place construction practices.

The following principles therefore guided the selection and distribution of CFRP and GFRP reinforcement:

- Assign CFRP strands to roles where stiffness and prestressing are critical (piles and girders).
- Use GFRP bars for all passive reinforcement in cast-in-place elements and as transverse reinforcement in girders to provide crack control and shear capacity.
- Retain conventional steel only where current crash-test or scour-protection standards necessitate it.

B.4. Project Delivery, Timeline, and Stakeholders

B.4.1 Project Delivery Approach and Overall Schedule

NCDOT elected to use a design-bid-build delivery method, preparing the contract documents and serving as the Engineer of Record for the bridge superstructure and substructure. The roadway design and environmental documentation were completed through NCDOT's standard project development process, with input from local stakeholders and federal agencies.

The project was advertised and let through NCDOT's standard bidding process in the summer of 2021. Multiple bids were received, and Balfour Beatty was selected as the prime contractor. Construction operations began in September 2021, following issuance of the notice to proceed.

Despite a six-month annual moratorium on in-water work, which prohibited any in-water activities between April 1 and September 30 to protect sensitive marine habitats, the project was successfully completed in December 2023, only 27 months after the start of construction and 10 months ahead of the contractual completion date. This outcome is particularly notable given the learning curve associated with full-scale FRP implementation and the logistical challenges of working in shallow coastal waters.

B.4.2 Construction Timeline and Major Milestones

It is helpful to summarize here the key phases and milestones that shaped the project's overall delivery. Additional construction-related observations are discussed in later chapters where they relate directly to material performance, quality control, or research activities. Also, a supplementary construction photo documentation is provided in Appendix C.

<u>Preconstruction and mobilization (mid-2021):</u>

After the contract award, Balfour Beatty mobilized to the site and established a limited laydown area of approximately 2 acres near the north abutment. The constrained site required just-in-time deliveries for most materials, which, from a life-cycle assessment (LCA) perspective, limited the potential advantages of FRP's lower weight (e.g., smaller cranes to handle reinforcement bundles and cages on-site or more material delivered per truck).

Temporary work trestle and initial in-water work (late 2021):

Because shallow water depths and environmental restrictions made barge operations impractical, the contractor constructed a temporary trestle parallel to the new bridge alignment (Figure A - 14). The trestle was designed to support all major construction activities, including pile driving, pier construction, girder erection, and deck placement, within the October–March in-water work window.

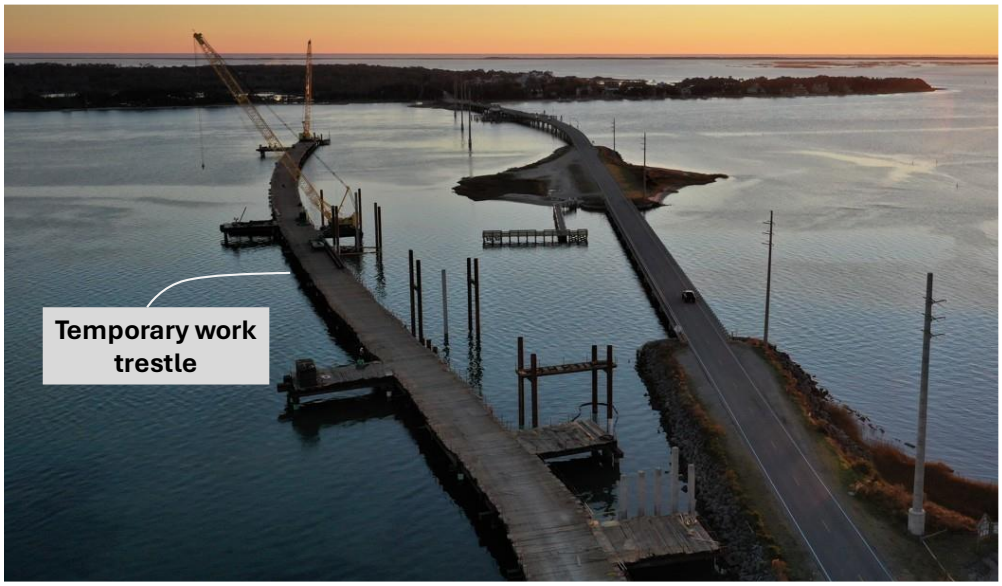

Figure A - 14. Temporary work trestle

Foundation and substructure construction (2021–2022):

During the first in-water work window, the contractor focused on driving CFRP-prestressed concrete piles and constructing pile caps and columns wherever access from the trestle was available. The sequencing was largely governed by the environmental moratorium: as much in-water work as possible was completed between October and March, so that above-water activities could continue during the restricted months. A series of piles and pile caps is presented in Figure A - 15.

Figure A - 15. CFRP prestressed concrete piles and early pile cap construction

Fabrication and erection of FIB girders (2022):

In parallel with substructure work, Coastal Precast Systems (CPS) fabricated the FIB girders using CFRP strands and GFRP stirrups at their facility, with NCDOT and NCSU involved in quality control and material testing. The 54 in. girders were shipped to the site by truck, whereas the 72 and 78 in. girders were delivered by barges via the Atlantic Intracoastal Waterway and erected from the work trestle as spans became available, as shown in Figure A - 16.

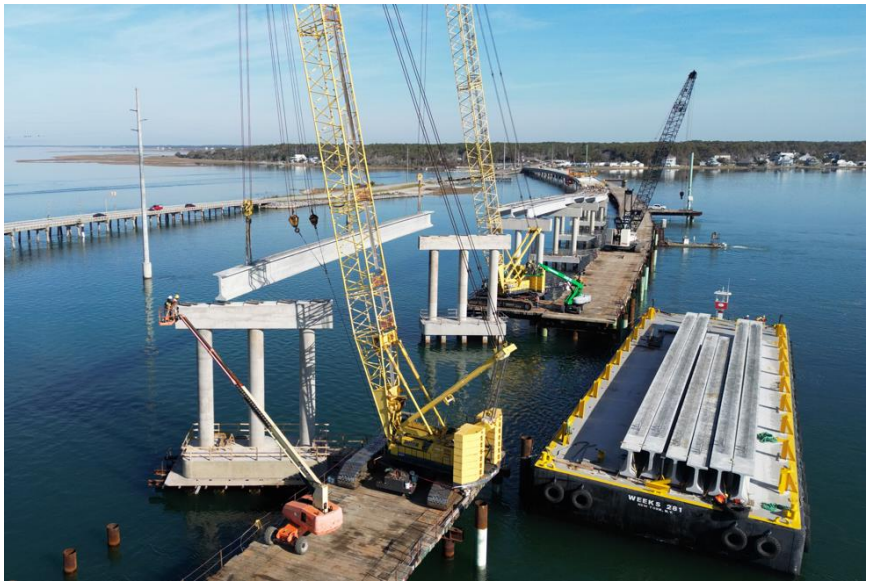

Figure A - 16. Erection of FIB girders using cranes on the work trestle

Deck construction and finishing works (2022–2023):

Once girder lines were in place, the lightweight GFRP-reinforced cast-in-place deck (Figure A - 17) was constructed in stages, followed by barriers, railings, and approach tie-ins. This above-water work could proceed during the April–September periods when in-water operations were restricted, helping to maintain continuous progress and avoid idle time.

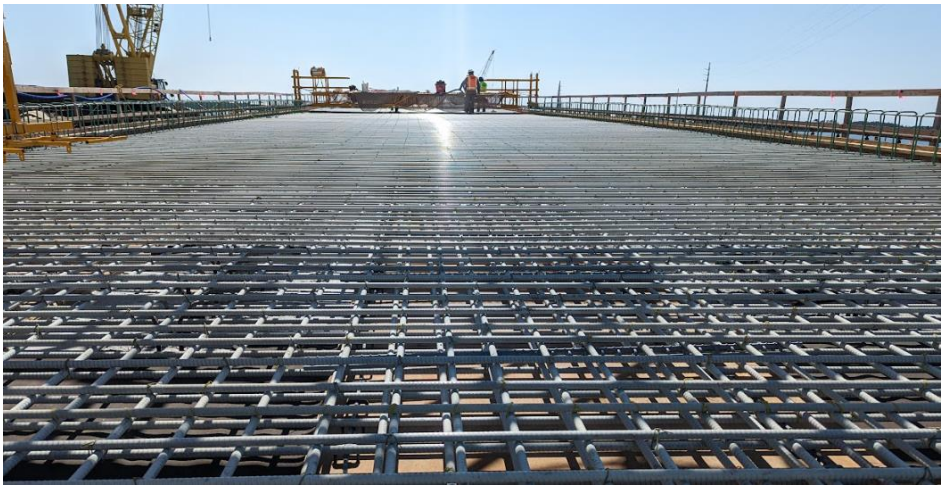

Figure A - 17. Deck portion right before concrete pouring

Traffic switch and project completion (late 2023-mid 2024):

Final activities included shifting traffic from the existing structures to the new alignment, completing approach roadway construction, and carrying out the demolition of Bridge No. 73. The new bridge opened to traffic in December 2023, marking the successful completion of North Carolina's first all-FRP-reinforced bridge. Notably, bridge No. 96 was left entirely in place and repurposed as a dedicated fishing pier and pedestrian facility, preserving direct access to the intermediary island. This decision responded directly to resident input, which emphasized both the practical value of this access and the cultural significance of the existing bridge as a community gathering space. An aerial view of the completed bridge is depicted in Figure A - 18.

Figure A - 18. Completed Harkers Island Bridge

B.4.3 Key Stakeholders and Roles

The successful completion of the Harkers Island Bridge required sustained coordination among multiple organizations. The principal stakeholders and their roles are summarized below:

North Carolina Department of Transportation (NCDOT): Owner and designer

- Led project development, environmental documentation, and final bridge design.
- Issued project specifications and special provisions governing FRP materials and QC.
- Provided on-site inspection, construction oversight, and long-term monitoring responsibilities.

Balfour Beatty US Civils: Prime contractor

- Responsible for overall construction means and methods, including trestle design, pile driving operations, substructure and superstructure construction, and demolition of existing bridges.
- Managed subcontractors, coordinated material deliveries within the constrained laydown area, and optimized construction sequencing around the in-water work moratorium.

Coastal Precast Systems (CPS): Precast supplier

- Fabricated all precast elements: CFRP-prestressed piles and FIB girders.
- Worked closely with NCDOT and NCSU to coordinate sampling, testing, and adjustments to reinforcement details as cracking behavior and constructability issues were observed in early girders.

Tokyo Rope USA (CFRP) and Owens Corning (GFRP): FRP material suppliers

- Produced CFRP strands and GFRP bars in accordance with project-specific special provisions.
- Supported plant audits, material certification, and development of specimen preparation procedures for testing.

NC State University research team: Independent research and QA/QC support

- Conducted material characterization tests (e.g., tension tests and bent-bar tests) on CFRP and GFRP samples obtained from production lots.
- Participated in monthly construction progress meetings at the contractor's field office in Havelock, NC, and carried out regular site visits to observe construction, document issues, and collect data.
- Developed analytical tools, full-scale testing programs, and recommendations intended to inform NCDOT's future FRP projects.

B.5. Practical Challenges and Lessons Learned in FRP Implementation

While the earlier sections describe the overall structural system and construction sequence of the Harkers Island Bridge, the project also encountered several practical challenges in the large-scale implementation of FRP reinforcement. Many of these issues are not captured directly in design drawings or specifications but have significant implications for constructability, schedule, and future projects. This section highlights selected challenges faced during fabrication and construction, along with observations from the contractor and precast supplier.

B.5.1 Coordination of FRP Procurement and Manufacturing Limitations

Unlike traditional steel reinforcement, FRP bars and spirals cannot be bent in the field. All bends must be performed at the manufacturing plant, strictly in accordance with length and shape specifications. Consequently, the project required more detailed early coordination among the designer, NCDOT, the FRP manufacturers, and the precaster than is typical with steel-reinforced bridges. Two aspects were particularly consequential:

Manufactured bends:

Several bar shapes specified in the design could not be fabricated exactly as intended due to manufacturing limitations (e.g., maximum straight length beyond a bend or restrictions on tight reentrant corners). This required adding splices and lap lengths in areas not planned initially and involved ongoing discussions to balance structural requirements, bend geometry limitations, and production efficiency. However, such restrictions are manufacturer-dependent and may not exist on a case-by-case basis. These limitations should be discussed once the supplier is known.

Lead times and fabrication risk:

Because every bent FRP bar shape must be pre-manufactured, any late design change or fabrication error can result in significant lead time. The contractor and the precaster identified this as a key risk: if a batch of complex-geometry bars did not fit, the impact on the refabrication schedule could be substantial. This experience highlights the value of standardizing bar shapes and using repetitive details wherever possible, so that material from other lots or spans can be reallocated if issues arise.

These constraints suggest that, for future FRP bridge projects, the design phase should explicitly address manufacturing limits on bend geometry and length, and incorporate sufficient standardization to enable practical contingency strategies.

B.5.2 Prestressing Operations

The use of CFRP prestressing strands in piles and FIB girders also required adaptations in typical precast yard practices.

Prestressing and strand handling:

CFRP strands are linearly elastic up to rupture and do not yield like steel. Although the specified jack stresses are within the elastic range, the perceived brittleness of CFRP made workers understandably cautious during stressing and formwork operations. To avoid tying transverse reinforcement directly around fully tensioned CFRP strands, the precaster implemented procedures such as:

- Using conventional steel strands outside the concrete cross-section to temporarily support GFRP stirrups during cage assembly, so that the stirrups could be tied without relying on the CFRP strands as hanging points (see Figure A - 19a) Notably, this was only applicable to the FIB girders, where some stirrups were protruding.
- Sequencing stressing and cage assembly to minimize the time workers spent near fully tensioned CFRP tendons.

Use of splice connector and jacking hardware:

Conventional multistrand jacks and chucks are designed for steel strands. To maintain compatibility with existing equipment, the precaster used splice connectors to transition from CFRP strands inside the member to short steel strands at the end of the formwork, where the jacks and wedges could be applied. The splice regions were staggered due to the thickness of the splice connectors (see Figure A - 19b). This procedure adds another layer of detailing and quality control that is not present in steel-only systems.

B.5.3 Lifting loops and handling of FRP-prestressed girders:

One notorious constructability challenge on the project was the seemingly simple task of lifting and handling the FRP-prestressed girders. For traditional steel-prestressed girders, the standard practice is to create lifting loops by extending a few prestressing strands or by using steel lifting bars or embedded devices near the ends. These loops are easy to detail, familiar to precasters and contractors, and can be cut in the field with a torch after installation.

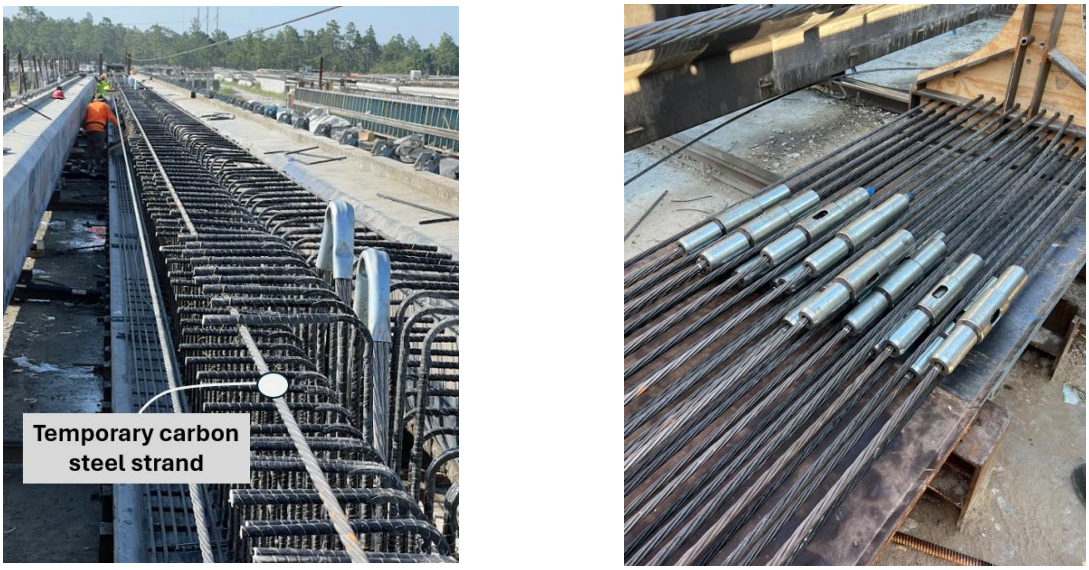

(a) Temporary steel strands *(b) Staggered strand connectors*

Figure A - 19. FRP prestressing operations

For Harkers Island, however, NCDOT's objective of eliminating internal sources of corrosion wherever feasible made the use of traditional carbon-steel lifting loops undesirable. Although the quantity of steel in a set of lifting loops is small and localized near the girder ends, those strands would remain permanently embedded in a highly corrosive environment. In contrast, the parapet rail reinforcement, which is epoxy-coated steel, was considered acceptable because it is not part of the primary load path and can be replaced if needed. This constraint triggered an extended discussion, where several alternatives were considered:

- *Lifting baskets and soffit recesses*

  Based on prior experience, the contractor proposed using steel "lifting baskets" or cradles that support the girder from below, bearing in shallow recesses or notches formed in the bottom flange. Synthetic straps could then be wrapped around the bottom of the girder to lift and rotate it, with the recesses later filled with non-shrink grout once the girder was in place. Although this approach avoids leaving steel embedded in the girder, it introduces additional formwork complexity, requires careful detailing of recesses to avoid stress concentrations, and adds steps to both casting and finishing.

- *Internal FRP-based lifting details*

  Another concept explored in the early stages was to use openings in the web and pass a bar, or similar device, through the section to serve as a lifting point. From a research perspective, this option is attractive because it can be optimized to minimize stress concentrations and maintain a fully non-corroding internal system. However, it would require dedicated analytical and experimental work to validate the structural effects of the web opening and the bar, as well as detailed guidance on the location of the opening relative to prestressing, shear reinforcement, and the transfer length. Given the time and scope constraints of the Harkers Island project, this concept was deferred as a potential future research project rather than implemented in the field.

- *GFRP bolts and embedded lifting anchors*

  A third idea considered was the use of GFRP bolts or headed anchors installed near the top flange to serve as lifting points for stripping the girders from the forms and handling them in the yard. This approach would keep the lifting components non-corrosive and external to the primary prestressing system, but raised questions about the local anchorage capacity of the bolts, potential flange cracking, and the practicality of removal or abandonment after erection. As with the web-opening concept, these questions pointed toward a substantial research effort beyond the scope of the current project.

Faced with these unresolved issues and the need to maintain the production schedule, NCDOT ultimately chose a stainless-steel lifting solution as a pragmatic compromise (Figure A - 20c). For each girder, three bundles of stainless-steel strands were detailed as lifting loops, with two bundles engaged at each end during handling and erection (a total of four lifting bundles per girder). Stainless steel is a non-carbon steel with much higher corrosion resistance than black steel, while still compatible with existing prestressing and lifting hardware.

This solution was not without concerns. Some team members were initially uneasy about the perceived brittleness of stainless steel relative to conventional prestressing steel, particularly under dynamic handling loads. Still, in practice, the lifting operations proceeded without incidents. The approach provided a workable, non-black-steel option that satisfied both the schedule and NCDOT's durability objectives for the project.

However, the use of stainless-steel lifting loops introduced new field-level complications. In particular, the stainless-steel strands could not be cut using conventional oxy-fuel torches after the girders were erected on site. The contractor had to rely on alternative cutting tools, which added time and effort during the finishing stages. In post-project feedback, field personnel expressed a clear preference for lifting solutions that either avoid permanent metallic loops altogether or use materials and hardware that can be removed or trimmed using standard tools.

Further, discussions with the CFRP strand supplier indicated that CFRP strands can be bent and used as lifting loops, provided bend radii and stresses during handling remain within allowable limits. From a durability standpoint, CFRP loops would be fully compatible with the rest of the prestressing system and eliminate the need for any steel-based lifting components. However, this concept raises critical questions about the performance of bent CFRP strands under repeated lifting cycles, the appropriate reduction factors for strength at bends, and the long-term implications of such details on member performance. These topics are closely related to the broader issues of bend strength and detailing addressed in later chapters and represent promising avenues for future experimental and analytical work.

In summary, the lifting-loop problem illustrates how seemingly secondary details can become critical within an all-FRP design philosophy. The Harkers Island experience shows that durable, non-black-steel lifting solutions are achievable (here via stainless-steel loops) but also highlights the need for continued research on FRP-based lifting details, standardized guidance on their design, and practical field procedures for their installation and removal.

B.5.4 End-region cracking

End-region behavior proved to be one of the most sensitive and instructive aspects of working with CFRP-prestressed elements on the Harkers Island project. Both the piles and the FIB girders exhibited cracking patterns near the ends during de-tensioning, highlighting how details commonly used with steel cannot always be directly extrapolated to CFRP systems.

CFRP-prestressed piles: Hoyer effect, early-age strength, and spiral pitch

For the CFRP-prestressed square piles, some cracking was observed at the ends shortly after prestress transfer. These cracks were attributed primarily to the combination of Hoyer-effect–induced tensile stresses [77] and relatively low early-age concrete strength. As prestress is released, the strand attempts to shorten, producing radial and longitudinal tensile stresses in the surrounding concrete near the ends. When this occurs at lower concrete strengths, the concrete is less able to resist tensile stresses, making end regions more susceptible to cracking and splitting.

Once this behavior was identified, the contractor modified production procedures by delaying pile-end cutting after driving. At the precast plant, de-tensioning was also postponed until a higher compressive strength was achieved (at least 6 ksi, rather than 5 ksi). In practice, this meant ordering piles further in advance so the concrete could continue curing before the ends were cut. This change was effective: end-region cracking in piles became much less frequent, but at the cost of longer production cycles and increased inventory on the casting beds.

In addition to timing, the confinement detailing at the pile ends is a significant contributor. As is common practice, the CFRP spiral pitch was reduced near the pile ends to increase confinement for drivability and to resist damage during de-tensioning. However, once piles are driven and subsequently cut in the field to achieve the final grade, the new pile head often falls in a region where the spiral pitch transitions back to a wider spacing. At that location, the confinement is reduced relative to the original head region assumed in design.

The Harkers Island experience suggests that, for CFRP-prestressed piles, spiral pitch patterns may need to be reconsidered so that tighter confinement extends farther from the pile ends, covering the range of locations where field cuts are likely to occur. Otherwise, the combination of high local prestress, lower confinement, and field cutting can create conditions favorable to end-region cracking, even when the original head region performs well. Alternatively, schedule coordination to accommodate longer wait times before cutting the ends appears to be a good temporary solution. In most cases, the extent of cracking in the field was limited to the pile cap embedment depth (Figure A - 20a), so additional repairs were not required.

FIB girders: unconfined strands, transfer length, and splitting cracks

End-region cracking was also observed in the CFRP-prestressed FIB girders. In this case, the implications were even more significant because several girders had to be rejected under NCDOT's acceptance criteria. The initial girder designs followed details that are common in steel-prestressed practice, including:

- Longitudinal strands concentrated in the bottom flange, with two strands into the web.
- A confinement bar around the bottom flange that did not fully enclose all the bottom strands.

These transverse reinforcement patterns, influenced by conventional steel detailing, where certain strands are routinely left outside the lowest transverse bars without major issues, proved problematic in the CFRP application, as early production girders exhibited transverse tensile cracks at the bottom flange near the ends during or shortly after prestress release (Figure A - 20b), and longitudinal and splitting cracks along the bottom flange and into the web region. Also, it was evident that some strands had slipped slightly into the section, indicating local bond and confinement issues. Additionally, longitudinal cracking in the web was observed, associated with the two CFRP strands placed in the web region.

These observations are consistent with a condition in which prestress transfer occurs over a relatively short distance, leading to high bond stresses and concentrated tensile stresses in the end region. While CFRP strands can exhibit shorter apparent transfer lengths than steel, the total confinement and transverse reinforcement in the initial details were not proportioned with that behavior in mind. Several bottom strands were located outside the effective confinement provided by the bottom bar, so the concrete immediately surrounding those strands was more vulnerable to splitting. The response was twofold:

Procedural adjustment:

As with the piles, the precaster began waiting longer before releasing the prestress, allowing the concrete in the girder to gain additional strength. This helped, but it did not fully resolve the issue because the underlying confinement detail remained unchanged.

(a) Pile cracking (b) Bursting (c) Stainless steel lifting loops

Figure A - 20. Challenges encountered

Design modification:

After the first set of girders, NCDOT and the design team modified the girder details to ensure that the flange confinement reinforcement encloses all bottom strands. These changes reduced the incidence of end-region cracking and provided a more robust load path for transferring prestress to concrete.

Taken together, the pile and girder end-region issues highlight the need for:

- Explicit consideration of concrete strength at transfer and the timing of cutting and handling operations.
- Confinement layouts (spiral pitch in piles, transverse reinforcement, and confinement bars in girders) that reflect where prestress transfer actually occurs and where field cuts are likely to be made.
- A cautious approach to directly tailor steel-based details into CFRP applications without additional analysis or testing.

B.5.5 Handling and Installation of GFRP Bars in the Field

From the contractor's perspective, the behavior of GFRP bars during handling and installation was, in many respects, similar to that of conventional reinforcing steel: bars could be carried, tied, and assembled into cages using standard tools and procedures, and their lighter weight was viewed as an advantage for manual handling and trucking. However, when lifting larger reinforcement cages, their lower stiffness (compared to steel) may require additional consideration, as they are more flexible. Additionally, one aspect emerged as a persistent challenge:

Surface splinters and workers' comfort:

The GFRP bars used on the project had an exposed composite surface with pronounced deformations. During handling and tying, installers experienced significant itching and splintering from loose glass fibers. Even with gloves and protective clothing, this discomfort reduced crew productivity and was recognized by subcontractors as a factor they would incorporate into their bid prices.

In post-project reflections, the contractor emphasized that if FRP is to become a routine material, surface coatings or outer veils that encapsulate the fibers and reduce splintering should be strongly considered during specification. From a construction standpoint, GFRP bars are treated almost the same as traditional rebar in terms of layout and tying. Still, the surface finish has a disproportionate impact on day-to-day installation. Nonetheless, this is also manufacturer-dependent, as surface preparation by other FRP producers may not yield these inconveniences. Note that epoxy-coated black steel bars require additional care in the field to prevent coating damage, and they also require UV protection for long-term exposure.

B.5.6 Contractor Perspective and Cost Considerations

Discussions with the prime contractor highlighted several broader lessons:

Specifications and constructability should evolve together: The contractor viewed NCDOT's FRP specifications as generally clear regarding storage, handling, and protection requirements, but noted that manufacturing limitations (e.g., maximum bent-bar lengths) were not always evident at the design stage. Better integration between design assumptions and manufacturing capabilities, especially for bent bars, would reduce late-stage splices and refabrication.

Standardization of bar shapes is highly valuable: From a scheduling and risk perspective, a more repetitive bar schedule (fewer unique shapes, reused across multiple bents or spans) would make it easier to reassign material from later phases if an early lot has issues, rather than waiting on uniquely fabricated replacements.

Worker experience and cost: The contractor expressed willingness to bid on future FRP-reinforced projects and acknowledged the advantages of lighter material and potential durability benefits. At the same time, they noted that reinforcing installers are likely to be priced in the discomfort associated with GFRP splinters until surface finishes improve. In their view, once the "itching" problem is solved, the decision to use FRP will increasingly be driven by relative material costs rather than constructability. It should be noted that surface treatments are primarily driven by concrete bond enhancement, but the user's comfort may also need to be considered.

Relative material prices: The contractor also highlighted that, at the time of the project, unit prices per pound or per linear foot for FRP products were higher than for black or epoxy-coated steel reinforcement. Although these numbers are time-, project- and market-specific, they reinforce the importance of pairing technical performance with realistic cost analyses when evaluating FRP for future bridges. Certainly, LCA assessment would benefit FRP solutions.

These lessons underscore that large-scale FRP implementation is not solely a design or materials problem; it also requires aligning specifications, manufacturing capabilities, and construction practices. Many of the issues encountered on Harkers Island, such as the need for standardized bar shapes, explicit consideration of bend-fabrication limits, and attention to worker comfort, are likely to recur in future FRP bridge projects. The recommendations developed in subsequent chapters build on these practical observations, aiming to facilitate subsequent implementations for both designers and contractors.

Appendix C. CONSTRUCTION PHOTO DOCUMENTATION

C.1. Purpose, Scope, and Field Documentation

This appendix presents a photographic record of the construction of the new Harkers Island Bridge and related field activities. Its primary purpose is to visually document the sequence of work, from the deterioration of existing bridges to the opening of the new bridge, by showing the following stages: temporary trestle, pile and substructure construction, FIB girder erection, and deck and barrier placement. The emphasis is on representative images with concise captions rather than detailed technical discussion, which is already provided in Figure A - 21.

The photographs compiled here were collected during 24 field visits between late 2021 and early 2024. These include:

- 16 construction site visits while the bridge was under construction.
- 4 visits to precast facilities (CPS in Chesapeake, VA, and Wilmington, NC).
- 1 visit associated with an FRP Institute seminar and bridge tour in November 2022.
- 1 visit for the opening ceremony in December 2023.
- 2 post-completion visits in March and October 2024, to document the salvaged piles from Bridge No. 73 and observe traffic and community use on the new bridge, respectively.

Throughout construction, NCDOT and Balfour Beatty held a monthly construction progress meeting on the third Wednesday of each month at the contractor's field office in Havelock, NC. Whenever possible, members of the NCSU research team attended these meetings in person and then traveled to Harkers Island the same day for a site walk-through. These combined meetings and visits, beginning in October 2021 and continuing through late 2023, provided a structured opportunity to (i) stay informed about construction progress and emerging issues, (ii) observe key FRP-related details in the field, and (iii) build a comprehensive visual record of the project.

The research team also carried out several visits to precast plants, where CFRP-prestressed piles and FIB girders were fabricated. These visits enabled direct observation of stressing, casting, detensioning, and handling procedures, as well as documentation of constructability challenges, including end-region cracking, stirrup-tying strategies, and the use of stainless-steel lifting hooks. Many of the photos in Sections C.4 and C.6 were taken during these plant visits.

From late 2021 through the bridge opening in December 2023, the research team maintained close coordination with Balfour Beatty personnel, NCDOT inspectors, CPS staff, and FRP manufacturers. All parties were consistently welcoming and supportive of the research effort, facilitating safe access to the site, sharing information on construction sequencing and field issues, and allowing extensive photo and video documentation. This collaboration was essential for identifying constructability challenges, such as pile end cracking, girder end cracking, bent-bar fabrication limits, GFRP bar labeling and handling issues, and deck reinforcement placement, as well as for capturing them visually for future reference.

Finally, following completion of the new bridge and demolition of Bridge No. 73, the research team conducted post-completion visits to (i) identify and select salvaged piles from the old structure for subsequent laboratory testing with FRP strengthening alternatives, and (ii) document the new bridge in service. These visits, which are summarized in Section C.8, also captured the repurposing of Bridge No.

96 as a fishing pier and pedestrian facility, showing how the project not only delivered a durable new structure but also preserved an important community gathering space.

Figures in this appendix are organized to follow the approximate construction sequence: existing conditions, temporary works, piles and substructure, girders, deck and barriers, approaches, opening, and post-completion observations. Together, they provide a visual companion to the narrative presented in Appendix B, and help illustrate many of the constructability and implementation issues discussed throughout this report.

C.2. Existing Bridges and Site Conditions

Before the construction of the new Harkers Island bridge, access to the island was provided by two aging structures: the Earl C. Davis Memorial swing-span bridge (Bridge No. 73) and Bridge No. 96. Both bridges were low to the water and exposed to a harsh marine environment (Figure A - 21). After several decades in service, extensive deterioration was evident throughout the substructure and superstructure. Chloride-induced corrosion of reinforcing and prestressing steel had led to cracking, delamination, and spalling at pile caps and beam ends, as well as to localized loss of cover, exposing corroded bars and strands (Figure A - 22). The underside views show widespread staining and patch repairs along the soffit and piles. These conditions motivated NCDOT's decision to replace the existing crossing with a new structure using corrosion-resistant FRP reinforcement.

(a) Traffic interrupted by the swing-span

(b) Swing-span on Bridge No. 73

(c) Bridge No. 96

Figure A - 21. Existing Bridges in Harkers Island

Figure A - 22. Corrosion of existing structural elements

C.3. Temporary Works and Site Logistics

To construct the new Harkers Island bridge while keeping traffic and marine navigation in service, the contractor installed a low-level temporary construction trestle parallel to the new alignment (Figure A - 23). The work trestle provided access for cranes, concrete trucks, and material deliveries along most of the bridge length, without relying solely on barges. This arrangement reduced construction time and limited the number of in-water operations required during pile driving, girder erection, and deck placement.

The trestle effectively served as a mobile construction platform, with cranes and finishing equipment moving from one bent to the next as substructure and superstructure work progressed. A continuous navigation opening was maintained by interrupting the trestle near the swing-span channel, thereby allowing boats to continue to pass. Overall, the temporary trestle was a key element of construction logistics, enabling safe and efficient access to all spans and minimizing disruptions to local traffic.

(a) Trestle progresses from the mainland side

(b) Trestle progresses from the island side

(c) Trestle parallel to the new alignment

Figure A - 23. Temporary trestle

C.4. Pile Fabrication and Installation

C.4.1 Fabrication of CFRP-Prestressed Piles

During several plant visits, the research team observed the whole production sequence, from strand layout and form assembly to concrete casting and curing (Figure A - 24, Figure A - 25 and Figure A - 26). Concrete was mechanically vibrated, and forms were covered immediately after casting to promote proper curing (Figure A - 27).

Figure A - 24. Piles at prestressing beds

Figure A - 25. Concrete pouring for piles

Figure A - 26. Production tags and concrete cylinders

Figure A - 27. Concrete curing with thermal blankets

C.4.2 Detensioning, Lifting, and Storage

After curing, piles were detensioned in accordance with CPS procedures and NCDOT requirements. Concrete cylinders were tested to verify that the target strength had been achieved before strand release. Detensioning was carried out simultaneously at both ends, followed by detaching the steel and CFRP strands that had been linked by custom couplers manufactured by Tokyo Rope USA (Figure A - 28).

Immediately after detensioning, the piles were lifted from the forms using embedded, temporary lifting hardware (Figure A - 29) and transported to on-site storage areas. Minor surface repairs were performed as needed at this stage (Figure A - 30).

Figure A - 28. Detensioning of piles

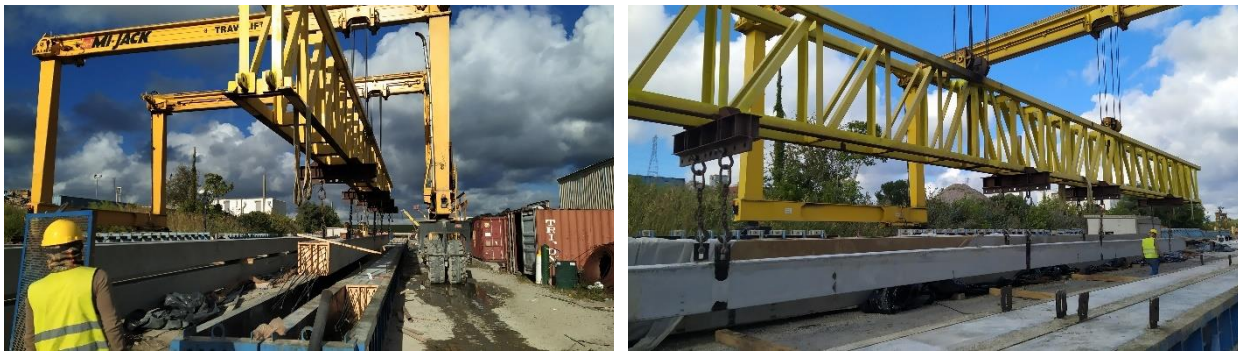

Figure A - 29. Lifting of piles out of their formwork at the precast yard

Figure A - 30. Pile crack repairs

C.4.3 Field Installation and Driving

Once delivered to the project site, piles were driven from the temporary trestle (Figure A - 31). Pile driving progressed, bent by bent, with lengths adjusted to match geotechnical requirements (Figure A - 32). After driving, piles were cut off at the elevation of the pile caps (Figure A - 33). During these operations, transverse and longitudinal splitting cracks were occasionally observed near the cut ends (Figure A - 34). In most cases, these cracks remained embedded within the pile caps, but they provided valuable insight into the interaction between CFRP prestressing, end-region confinement, and construction procedures.

Figure A - 31. Pile delivery and handling

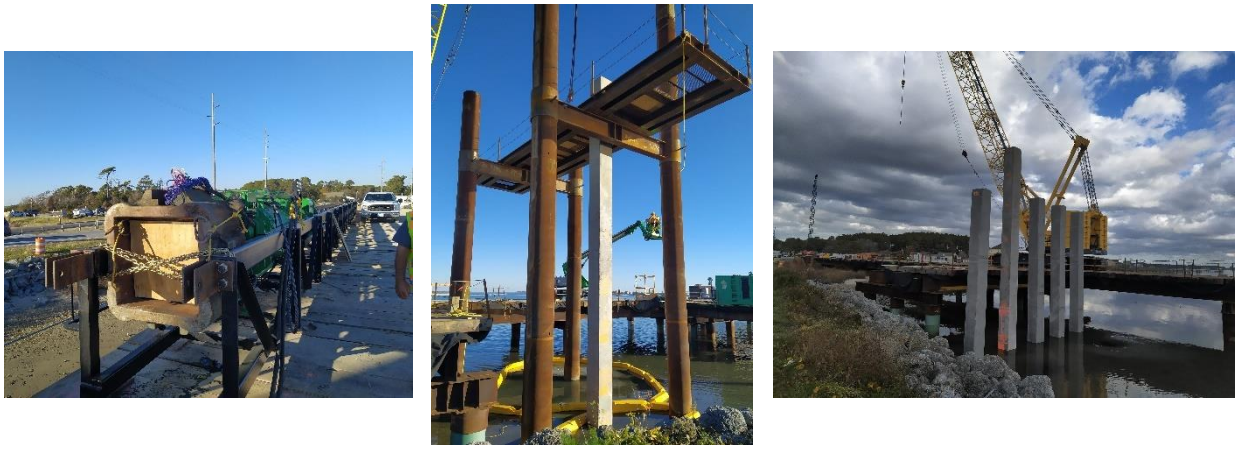

Figure A - 32. Pile driving

Figure A - 33. Batter piles and groups of piles

Figure A - 34. Pile cracking at cut-off ends

C.5. Substructure Construction: Pile Caps and Bents

C.5.1 GFRP Reinforcement Cages

Pile cap reinforcement cages were fabricated on site using GFRP longitudinal bars (Figure A - 35). In several cases, bar shapes had to be revised to accommodate manufacturing limitations on bent GFRP bars, yielding valuable insights for future design and specification improvements. Special procedures, such as coated wire and UV protection, had to be enforced (Figure A - 36). Typical GFRP reinforcement cages before placement are shown in Figure A - 37.

(a) Bent GFRP bars *(b) Straight GFRP bars* *(c) GFRP bar bends*

Figure A - 35. GFRP bars used to build reinforcement cages on site

(a) Identifier tags *(b) Tying wire* *(c) Protection blankets against UV rays*

Figure A - 36. GFRP material handling

(a) Pile cap reinforcement cage *(b) Column bent reinforcement cage*

Figure A - 37. Typical GFRP reinforcement cages

C.5.2 Pile Caps

Once the GFRP cages were completed, temporary formwork was installed around the driven CFRP piles, and the cages were lifted into place. The cages were carefully lowered to fit around the piles, ensuring proper embedment of the CFRP piles within the cap (Figure A - 38).

Concrete for each pile cap was placed in a single pour, with attention to vibration near the congested regions around the piles and under future bearing seats. After curing and formwork removal, the pile caps presented a clean, low-profile footprint (Figure A - 39).

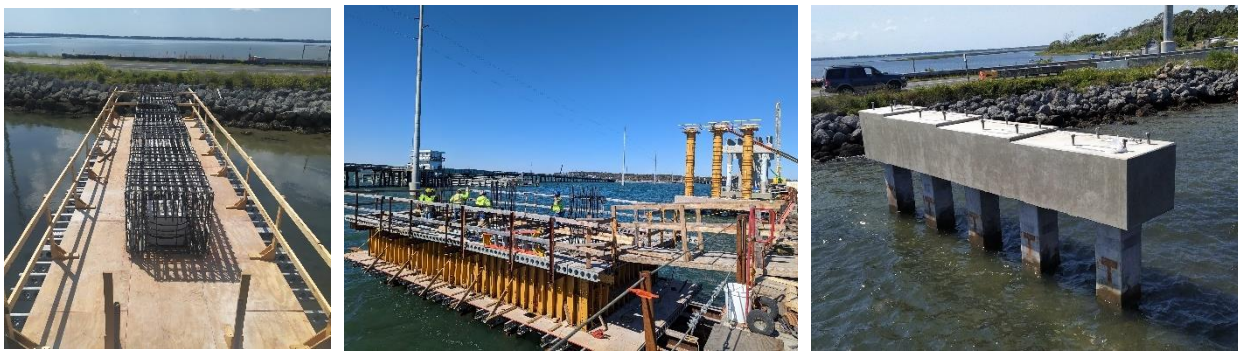

Figure A - 38. Sequence for concrete pouring of pile caps

Figure A - 39. Types of pile caps

C.5.3 Pier Columns and Bent Caps

To achieve the required vertical clearance around the navigation span, pier columns and bent caps had to be cast on top of some pile caps. The geometry of the bents varies along with the alignment to follow the vertical profile and accommodate navigation clearances, but the reinforcement concept remains consistent. Three different bents at multiple stages of construction are shown in Figure A - 40.

Figure A - 40. Pier columns

C.5.4 Retaining Walls and Approach Protection

In contrast to the fully FRP-reinforced primary elements of the bridge, the approach embankments are protected by a series of precast, steel-reinforced retaining wall units. These walls provide scour and erosion protection to the main bridge, stabilizing the roadway fill against wave action, currents, and tidal fluctuations (Figure A - 41 and Figure A - 42).

Figure A - 41. Retaining walls on the mainland side

Figure A - 42. Retaining walls on the island side

C.6. Superstructure Construction

C.6.1 Fabrication of FIB Girders

The girders were produced by Coastal Precast Systems (CPS). In the yard, long prestressing beds were used to cast multiple girders at once. CFRP strands were stressed, GFRP stirrups and reinforcing bars were installed (Figure A - 43), and concrete was cast. After curing and detensioning, the individual girders were separated, lifted from the beds, and staged for inspection and shipment (Figure A - 44).

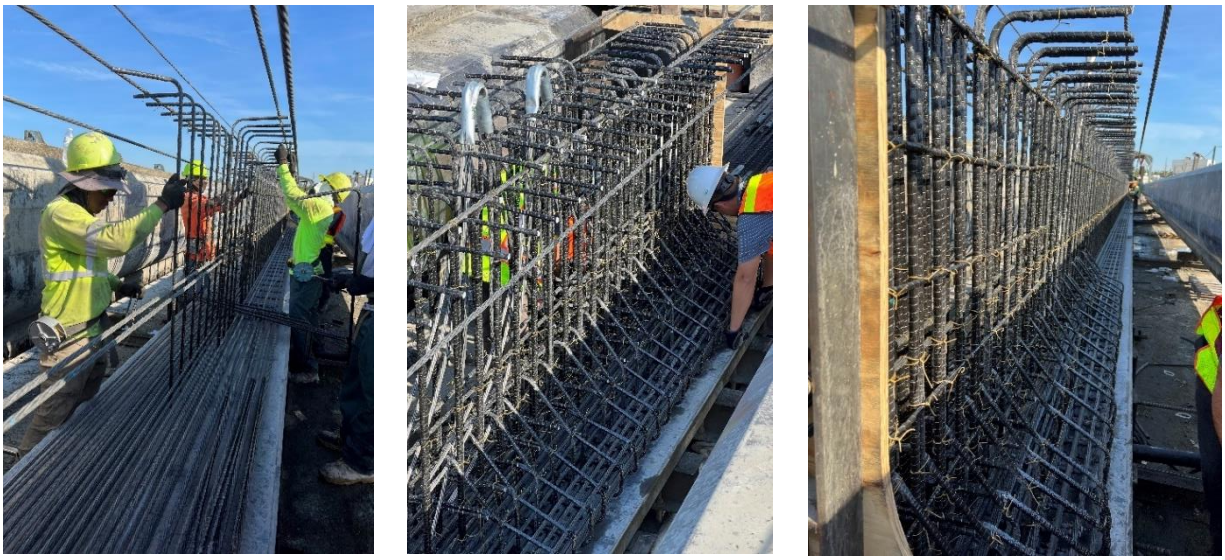

Figure A - 43. FIB girders in the prestressing beds

(a) Longitudinal cracks and concrete spalling near the ends

(b) Transverse cracks and strand slippage near the ends

Figure A - 44. Cracking and spalling at the end of FIB girders

C.6.2 Girder Erection

Girders were transported to Harkers Island by truck or by barge, depending on their length and depth. Erection was carried out using cranes positioned on the temporary trestle. Each girder was lifted from its staging area, rotated into alignment, and carefully set onto stainless-steel sole plates atop laminated elastomeric bearings anchored to the pile caps and bent caps (Figure A - 45). The navigation span and transition spans required the deepest (78 in.) FIB girders and more complex lifting operations, but the general procedure remained consistent throughout the project, with local stainless-steel components limited to anchor plates and bearing-seat hardware. An overview of girder lines is shown in Figure A - 46.

Figure A - 45. Girders in place

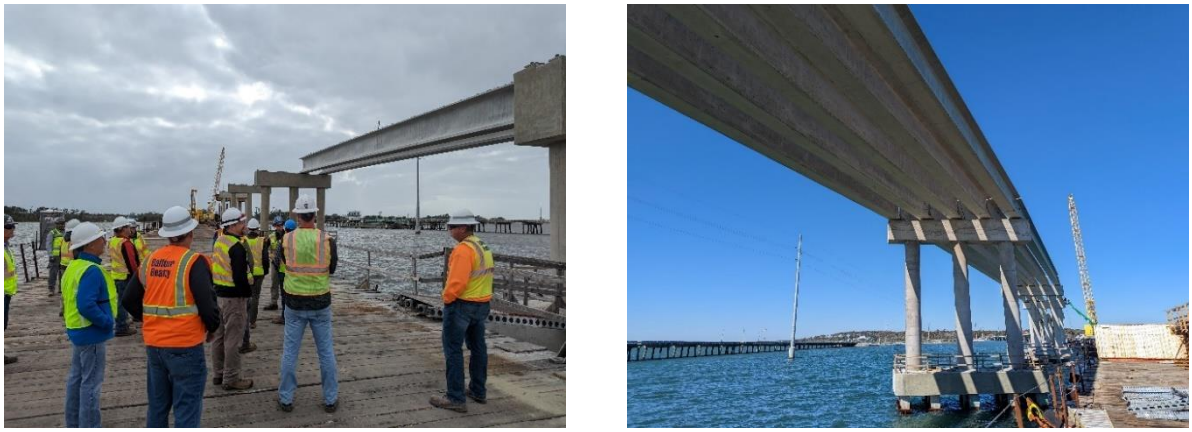

Figure A - 46. FIB girders spanning across bents

C.6.3 Deck Reinforcement and Concrete Placement

Once the girder lines were in place and braced, the GFRP-reinforced deck was constructed span by span. Temporary formwork was installed between girders, followed by placement of GFRP bar mats in the longitudinal and transverse directions (Figure A - 47). Since all deck reinforcement was GFRP, careful attention was given to bar support and cover. Plastic chairs and spacers were used to maintain the specified depth, and minor field adjustments were often required to address chair failures or local bar displacement. The deck was cast in sequential pours, which can be observed in Figure A - 48 and Figure A - 49.

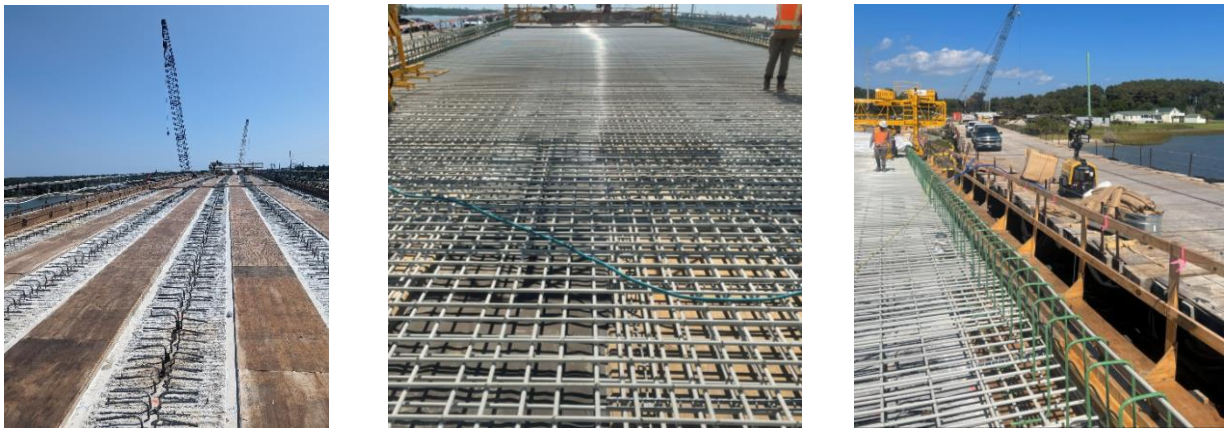

Figure A - 47. Deck reinforcement

Figure A - 48. Deck before and after curing

Figure A - 49. Epoxy-coated reinforcement for rail parapet and deck poured

C.7. Opening Ceremony

The new Harkers Island Bridge was officially opened to the public on December 12, 2023, during a ribbon-cutting ceremony held on the deck of the bridge (Figure A - 50). The event brought together NCDOT leadership, state and local government representatives, Balfour Beatty and CPS personnel, FRP industry partners, and a large number of Harkers Island residents.

For the research team, the ceremony marked the culmination of more than two years of continuous field visits and documentation. For the community, it marked the end of frequent lane closures and load postings. Also, the beginning of a reliable and safe connection to the mainland.

Figure A - 50. Opening ceremony and ribbon cutting

From a project standpoint, the ceremony celebrated the completion of approximately 27 months of uninterrupted construction, roughly ten months ahead of the original schedule, despite the recurring in-water work moratorium. The bridge now stands as both a critical transportation link and a first-of-its-kind all-FRP-reinforced structure for NCDOT (Figure A - 51).

Figure A - 51. Residents enjoying the bridge at the opening ceremony

C.8. Post-Completion Visits (2024)

C.8.1 Salvaged Piles from Bridge No. 73

Although construction of the new Harkers Island Bridge was completed in December 2023, field documentation continued into 2024 as the demolition of Bridge No. 73 progressed. The research team conducted a post-completion visit to identify, select, and relocate salvaged piles for future experimental testing.

On March 1, 2024, the team visited the Otway Sand Mine in Carteret County, where Balfour Beatty was stockpiling the cored slabs and prestressed octagonal piles removed from Bridge No. 73 (Figure A - 52 and Figure A - 53). The primary goal was to:

Document the condition of the piles after decades in service in a harsh marine environment.

Classify piles by length and condition for potential reuse in laboratory testing.

Select a subset of piles suitable for full-scale testing with FRP strengthening schemes.

Later that month, a coordinated relocation operation was carried out: three trucks, each carrying three piles, transported the selected elements from Otway to the NCDOT Division 4 Maintenance Yard in Smithfield, NC, where they are being temporarily stored before transfer to the CFL at NCSU (Figure A - 54).

Figure A - 52. Demolished cored slabs from Bridge No. 73

Figure A - 53. Demolished octagonal piles from Bridge No. 73

Figure A - 54. Recovered piles stored at NCDOT's Smithfield yard

C.8.2 Observations of the New Bridge in Service

In addition to technical site work, the research team also visited the bridge after all construction and demolition activities were completed to observe how the new crossing functions in day-to-day use. During a post-completion visit in October 2024, the research team drove across the new bridge and documented:

- The visual integration of the bridge into the surrounding landscape and community.
- Most importantly, the new role of Bridge No. 96, which was left entirely in place and repurposed as a fishing pier and pedestrian facility.

On this visit, Bridge No. 96 was heavily used by residents and visitors as a gathering space, with people fishing, walking, and socializing along the former roadway alignment (Figure A - 55). This reuse preserves not only physical access to the intermediary island, but also the cultural and social value of the old crossing for the community (Figure A - 56).

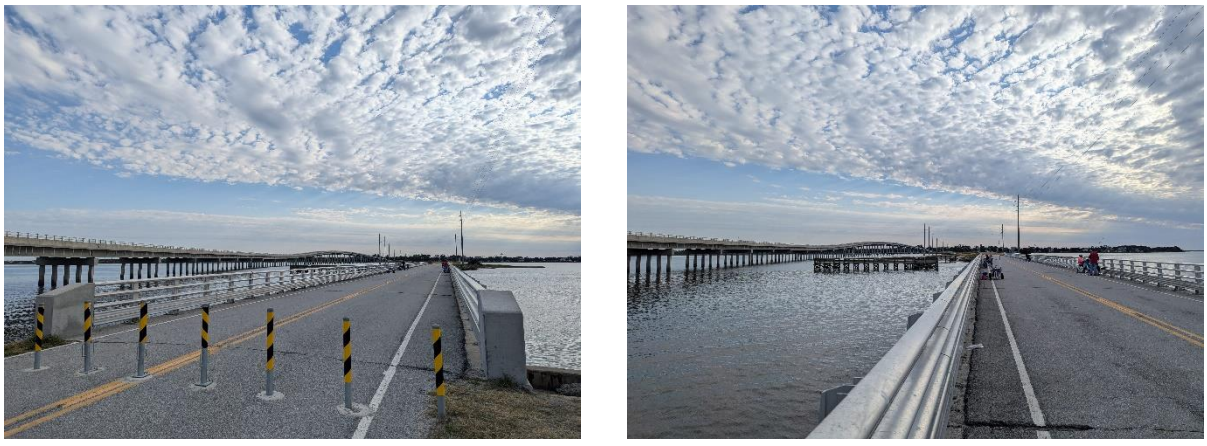

Figure A - 55. Former bridge No. 96 repurposed as a fishing pier

Figure A - 56. Surroundings of the new Harkers Island Bridge

Appendix D. SUPPLEMENTARY AREA AND WATER ABSORPTION TESTS ON 0.6 in. CFRP STRANDS

D.1. Scope and Objectives

This appendix summarizes supplementary tests conducted on the 0.6 in. seven-wire CFRP strands used in the Harkers Island Bridge to determine their measured cross-sectional area and water absorption properties. It should be noted that measuring the cross-sectional area is part of a typical tension test per ASTM D7205 [20], as it is required to compute the modulus of elasticity and tensile strength. Further details related to tension tests were presented in Chapter 2.

These tests were carried out on a subset of 27 strand lots to (1) understand how the PET surface wrap influences measured properties, and (2) evaluate whether these parameters are suitable candidates for routine project-level QA/QC. The results confirm that both measured area and water absorption are highly sensitive to the removal of the PET wrap (see Figure 6b), and that the test procedures are labor-intensive and difficult to scale to every lot. For these reasons, area and water-absorption data were excluded from the statistical analysis in Chapter 4, and tensile modulus was selected as the primary material parameter for project-level QC. Typical samples for measured cross-sectional area and water absorption tests are presented in Figure A - 57a and Figure A - 57b, respectively.

D.2. Test Methods and Specimen Preparation

D.2.1 Cross-Sectional Area by Displacement (ASTM D792)

Since the 0.6 in. CFRP strands are not solid round bars but bundles of seven intertwined wires, the cross-sectional area cannot be determined from an effective diameter as is commonly done for GFRP bars. Instead, the strand area was estimated using the displacement method in ASTM D792 [78] (density and specific gravity of plastics by displacement), as recommended by ASTM D7205 [20].

(a) Samples required for measuring the cross-sectional area per ASTM D792

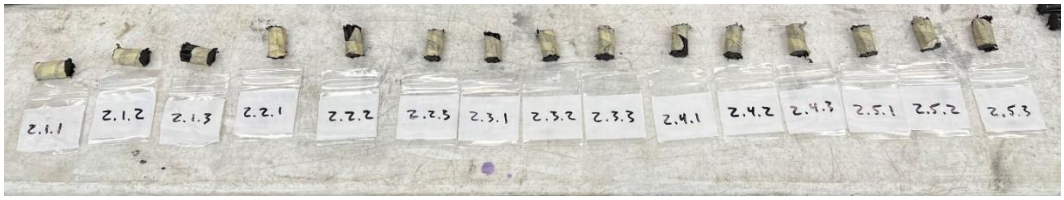

(b) Samples required for measuring water absorption per ASTM D570

Figure A - 57. Strand specimens for area and water-absorption tests

For each determination, five specimens per strand were cut to 4 in. The specimens were weighed in air and then in water to determine volume by buoyancy, from which the cross-sectional area could be inferred. To compare the influence of the PET wrap, tests were performed on strands with the PET wrap (as received) and on strands in which the PET wrap was carefully removed. In total, 27 lots were tested for area: (i) 22 lots with PET wrap, and (ii) 5 lots without PET wrap. For 5 of these lots, the area was measured both with and without the PET wrap, allowing direct comparison.

Specimen preparation required additional care once the PET wrap was removed. Cutting short segments caused the seven wires to untangle and separate, which complicated handling and weighing. Light taping was required to maintain wire integrity during handling. Figure A - 58 shows the test process for measuring the cross-sectional area from volume displacement, using Archimedes' principle, in accordance with ASTM D792 [78].

(a) Cut specimens

(b) Taped and measured specimens

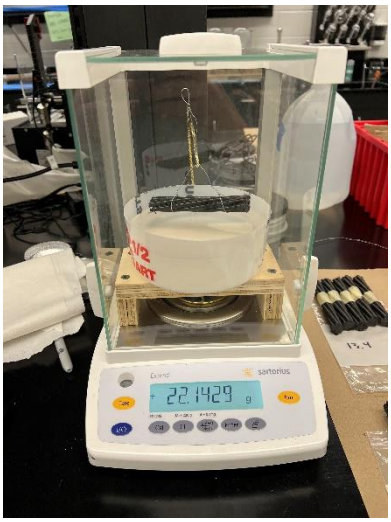

(c) Specimen weighed in air

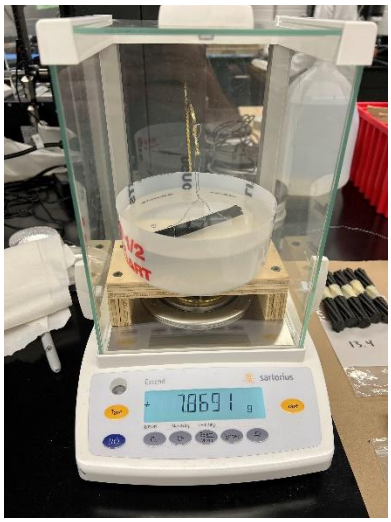

(d) Specimen weighed in water

Figure A - 58. Testing process per ASTM D792

D.2.2 Water Absorption Tests

Water absorption of the 0.6 in. CFRP strands was evaluated in accordance with ASTM D570 [79], as referenced by ASTM D7957 [18] and the special provisions used for the project. Short one-inch-long specimens were cut from selected strands. Once more, two conditions were investigated: with and without a PET wrap. Specimen conditioning and testing followed the procedure adopted from ASTM D570 [79]:

Dry conditioning:

- Specimens were placed in an oven at 122 ± 5.4 °F for 24 h.
- Immediately after removal from the oven, let it cool and weigh on a precision balance to the nearest 0.001 g to determine the initial dry mass.

Immersion and post-immersion weighing:

- Specimens were fully immersed in distilled water for 24 h, + 0.5 h.
- After immersion, specimens were removed from the water, quickly surface-dried with a dry cloth, and weighed immediately to capture the wet mass.
- Water absorption was then calculated as the percentage increase in mass between the dry and wet conditions.

In total, 11 lots were tested for water absorption: 6 with the PET wrap in place and 5 with the PET wrap removed. For three lots, both conditions (with and without PET wrap) were evaluated, allowing direct comparison. In practice, the measured absorption proved highly sensitive to: (i) the duration between removal from water and weighing, and (ii) the extent and consistency of surface drying. Even slight variations in these steps produced noticeable scatter in the measured absorption, which is an important practical consideration when using ASTM D570 [79] as a routine project-level QA/QC tool for CFRP strands.

(a) Cut specimens

(b) Specimens placed in an oven

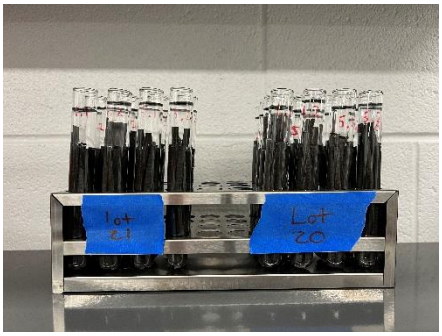

(c) Specimens submerged in water

Figure A - 59. Specimen preparation per ASTM D570

D.3. Summary of Results

D.3.1 Influence of PET Wrap on Measured Area

When the PET wrap was not removed, the measured area for 0.6 in. CFRP strands was close to that of a conventional 0.6 in. steel prestressing strand (≈ 0.217 in.²). This is expected because the displacement method accounts for the volume of the PET wrap and the carbon wires. In contrast, Tokyo Rope reports an effective area of 0.179 in.² in their technical datasheets, corresponding to the load-bearing carbon cross-section only.

After carefully removing the PET wrap and testing only the seven carbon wires per ASTM D792 [78], the measured areas clustered around 0.17 in.^{2}, slightly lower than the datasheet value but generally within a -5% band that is reasonable for this type of test. For lots tested both with and without PET wrap, the effective CFRP area (no PET wrap) was consistently about 78% of the area measured with the PET wrap intact. These results underscore two key points:

- Design and strength calculations must be based on the carbon (effective) area, not the gross area including PET wrap, because the wrap does not contribute meaningfully to axial strength or stiffness.
- Consistently reproducing the manufacturer's effective area requires removing the PET wrap, cutting multiple short specimens, and performing careful displacement test procedures that are labor-intensive and difficult to scale to every lot in a large project.

The most representative descriptive parameters for the measured cross-sectional areas, both with and without PET wrap, are shown in Table A - 1. The low COVs indicate that the results are consistent across both cases. Despite the large number of specimens tested, this only corresponds to 155 strands from 27 different lots, which is significantly lower than the 326 strands from 73 different lots tested as part of the material testing program presented in Chapter 2. After discussing the nuances of measured cross-sectional areas and their implications for calculating the tensile modulus with the NCDOT Steering and Implementation Committee, it was decided to consistently use the manufacturer-reported nominal area rather than measuring the effective area for each strand, which would require five specimens per strand (30 specimens per lot).

Table A - 1. Descriptive parameters for measured cross-sectional areas

Dataset	n	$\bar{x}$	Min	Max	Median	Range	s	COV
With PET	597	0.2193	0.2087	0.2446	0.2182	0.0359	0.00626	2.9%
Without PET	60	0.1690	0.1663	0.1779	0.1690	0.0116	0.00175	1.0%

Moreover, Figure A - 60 shows the data dispersion for the 0.6 in. CFRP strands where the cross-sectional area was measured with the PET wrap in place. The manufacturer-reported area (0.179 in.^{2}) is substantially below the mean measured area with PET wrap. Conversely, Figure A - 61 shows the comparison between the 60 strands for which the area was measured with and without a PET wrap. As noted previously, the mean area without the PET wrap is closer to the manufacturer-reported value. However, the results obtained in this work suggest that area measurements for seven-wire CFRP strands may require revision to standardize the values used. This is particularly critical for the ASTM D30.10 Committee, which is developing a new standard specifically for CFRP bars and strands.

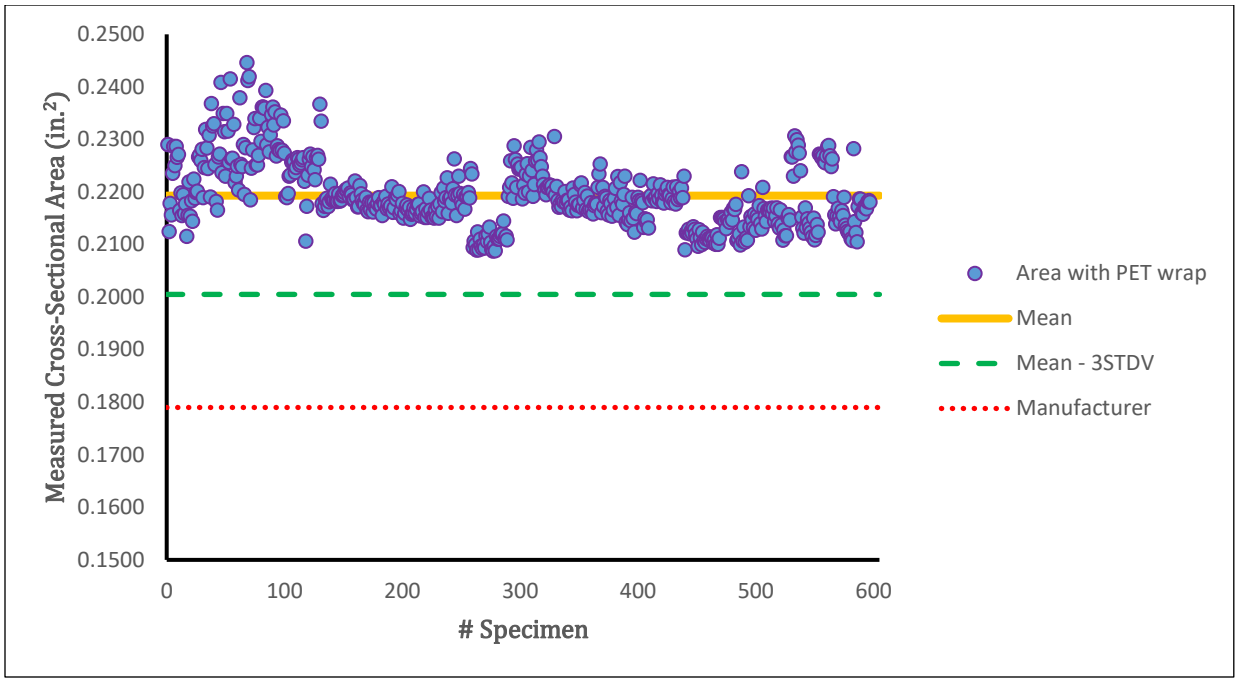

Figure A - 60. Data dispersion for measured cross-sectional areas with PET wrap

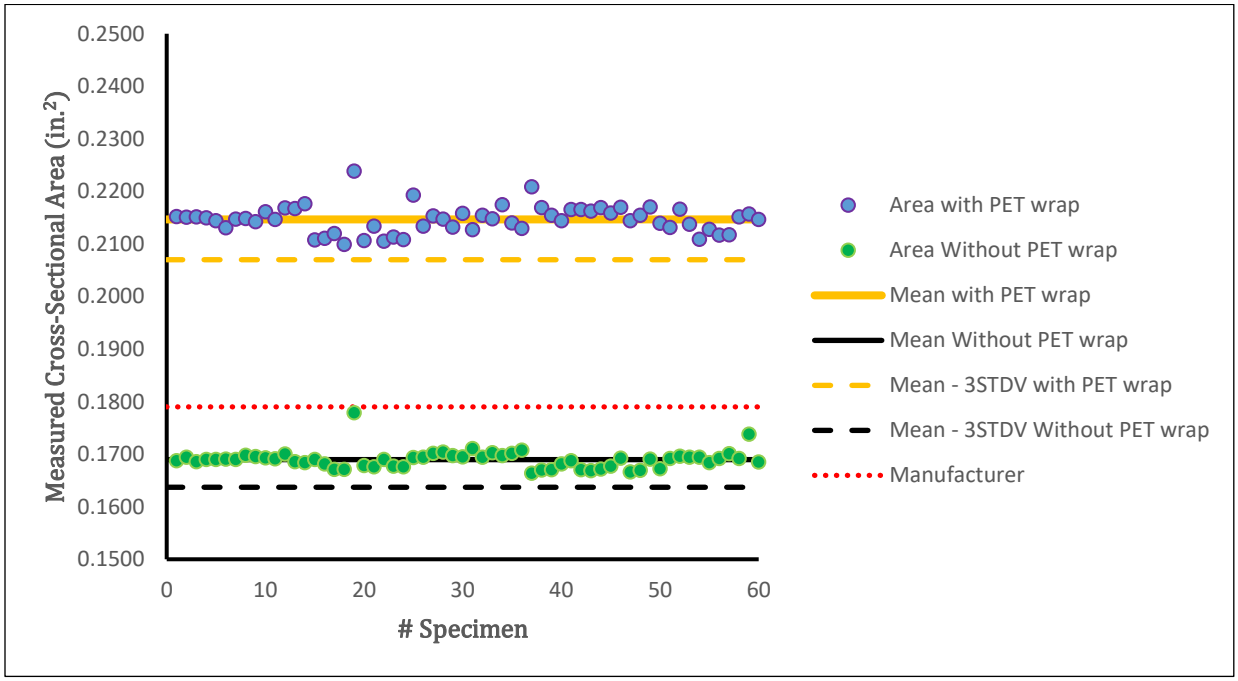

Figure A - 61. Data dispersion for measured cross-sectional areas with and without PET wrap

D.3.2 Influence of PET Wrap on Water Absorption

Water absorption for the 0.6 in. CFRP strands was measured in accordance with ASTM D570 [79]. The results were then compared with the 0.25% maximum water absorption value specified in ASTM D7957 [18] for GFRP bars, which was also included in the special provisions for CFRP, mainly due to the lack of a CFRP-oriented ASTM standard.

The test results show a clear and consistent pattern: when the PET wrap was left in place, the measured water absorption was typically in the 0.30–0.40% range (i.e., above the 0.25% benchmark from ASTM D7957 [18]). On the other hand, when the PET wrap was removed, and only the CFRP wires were tested, all lots yielded average water absorption values below 0.25%. This behavior is expected, given that in the ASTM D570 [79] procedure, mass gain is dominated by the portion of the system directly exposed to water. When the PET wrap is present, it acts as the primary wetting surface and drives the measured absorption, even though it does not contribute to the structural strength or stiffness of the strand. Once the PET wrap is removed, the measured absorption reflects the behavior of the structural CFRP core, the material relevant to mechanical performance and long-term durability.

The latter, once again, highlights the need to further refine the requirements for CFRP products. Based on the results obtained herein, applying the ASTM D7957 [18] 0.25% limit directly to CFRP strands, when measured according to ASTM D570 [79], can be misleading because the PET wrap dominates the measured absorption while not contributing to structural capacity. In addition, the test is labor-intensive, requires precise balances and tight timing control, and is therefore poorly suited for routine lot-by-lot QA/QC on a project such as Harkers Island.

A more appropriate approach is to treat water absorption as a product-level qualification property, verified periodically through independent audits or manufacturer certification programs (e.g., AASHTO PEAS program or FRP Institute audits), rather than a recurring project-level QC requirement for every lot of CFRP strands. Similarly, after discussing these preliminary results with the NCDOT Steering and Implementation Committee, it was decided to focus on mechanical properties determined by tension tests (e.g., modulus of elasticity) to validate the delivered lots for the project. The dispersion of water absorption values is presented in Figure A - 62 and Figure A - 63, for strands with and without PET wrap, respectively.

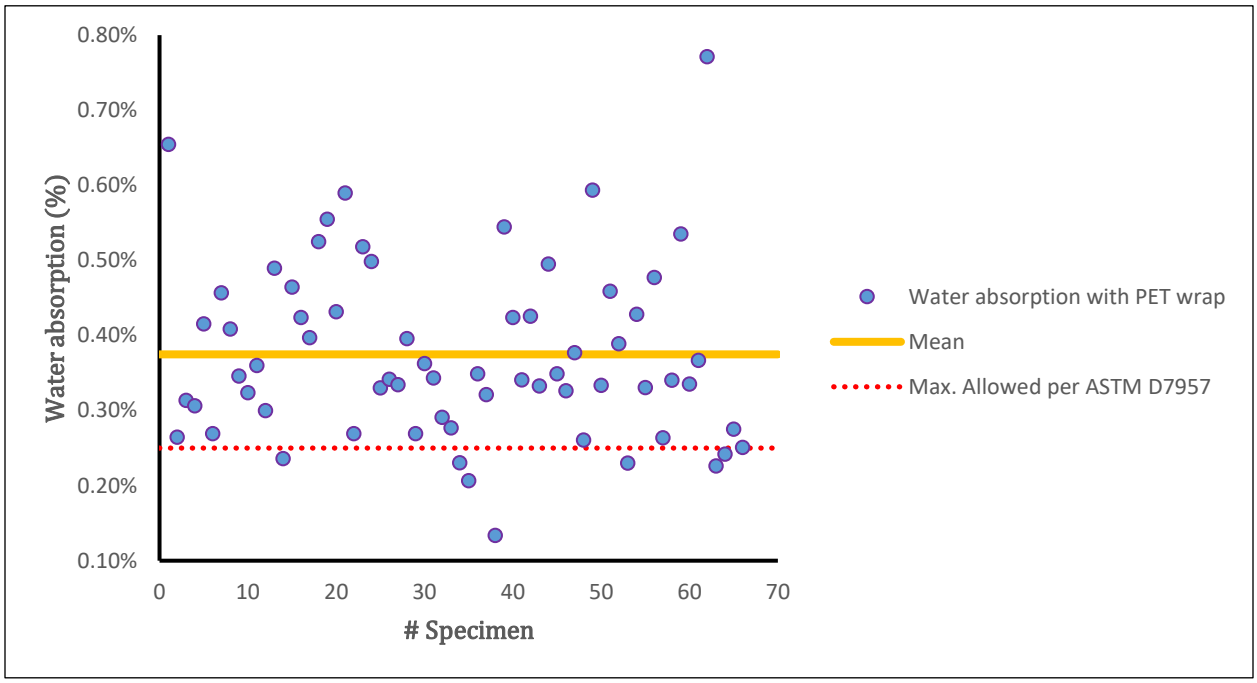

Figure A - 62. Data dispersion for water absorption with PET wrap

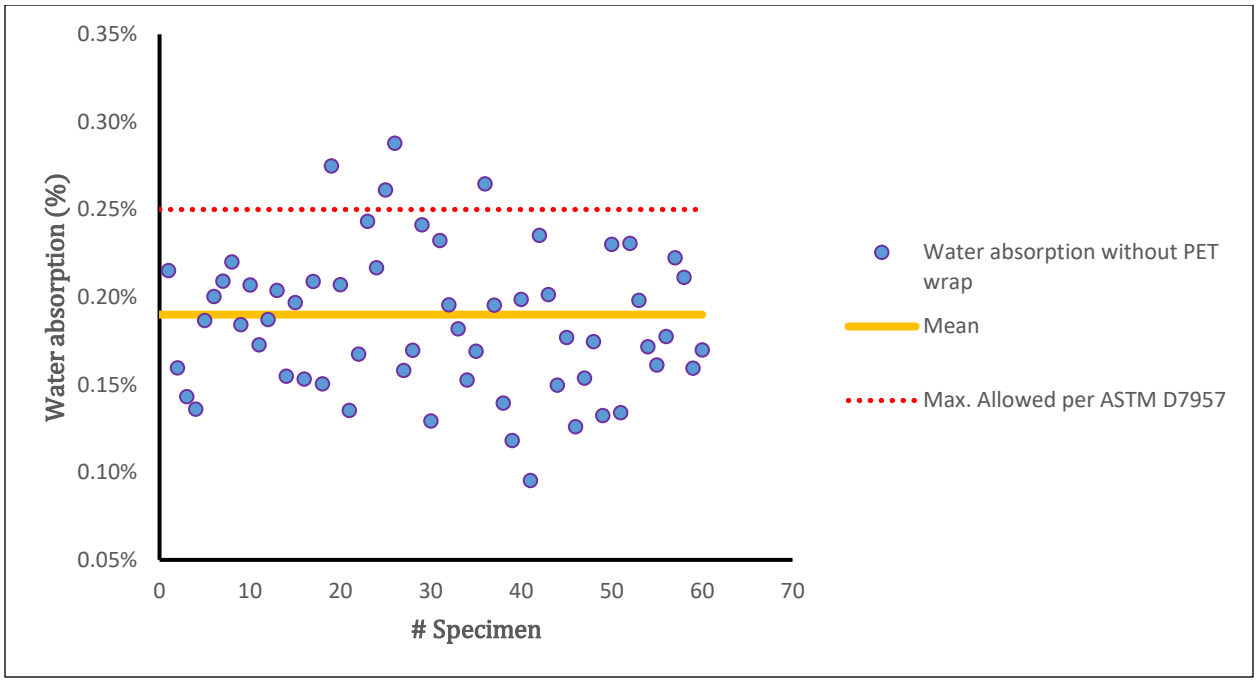

Figure A - 63. Data dispersion for water absorption without a PET wrap

D.4. Implications for QA/QC and Statistical Evaluation

D.4.1 Practical Constraints for Project-Level Area and Water-Absorption Testing

Applying ASTM D792 [78] to every lot in a project like Harkers Island would require six strands per lot delivered for tension testing, at least five short specimens per strand to meet the standard's recommended sample size, and thus roughly 30 specimens per lot for area alone, each requiring careful cutting, PET wrap removal (if effective area is desired), taping of the seven wires, conditioning, and weighing on a high-precision balance.

The research team initially pursued this approach for the first 18 lots. After reviewing the time, effort, and material consumption with the NCDOT Steering and Implementation Committee, it was agreed that the measured areas were consistent and aligned reasonably with manufacturer data once the PET wrap was removed. Extending this procedure to all remaining lots would impose a disproportionate burden on testing and costs without a commensurate gain in information.

A similar conclusion was reached for water-absorption testing. Results were sensitive to handling details (drying time, surface moisture, weighing timing). The number of lots tested (11) was sufficient to demonstrate the dominant influence of the PET wrap and the need for CFRP-appropriate benchmark values. Consequently, area and water-absorption tests were not adopted as routine, per-lot acceptance tests for the remainder of the project.

D.4.2 Observations for Future CFRP Standards

The findings of this appendix suggest several points for future CFRP-specific standards and specifications:

- Effective design properties for CFRP strands should be based solely on the carbon cross-section, not on the gross area including PET wraps. To be consistent with GFRP products, the CFRP manufacturer(s) should provide this information as “nominal area” in data sheets as part of product-qualification level QA.
- If project-level area checks are desired, it may be preferable to measure area with the PET wrap intact and apply an empirically calibrated factor (≈0.78 in this study) to estimate effective area. Alternatively, to be consistent with GFRP products, the CFRP manufacturer(s) should provide the actual diameter (including any surface treatment) that is consistent with maximum diameter limits imposed by ASTM or manufacturer data sheets. If maximum diameter limits are met, then the nominal area should be used for subsequent calculations.
- Water-absorption limits adopted from GFRP bar standards must be re-examined and explicitly defined for CFRP products, especially intertwined strands.

Overall, these supplementary tests provided valuable insight into the behavior of CFRP strands but confirmed that cross-sectional areas and water absorption are better handled at the product-qualification level than as routine, per-lot QC requirements on a large bridge project.

Appendix E. RATIONALE FOR USING TENSILE MODULUS IN SAMPLE SIZE DETERMINATION

E.1. Background

Chapter 4 presented a statistical approach to estimate adequate sample sizes for material acceptance based on 0.6 in. CFRP strands tested in tension according to ASTM D7205 [32]. Also, the three key parameters that can be obtained from the aforementioned tension test were summarized in Section 4.3.1 as follows: (i) measured cross-sectional area, (ii) guaranteed tensile strength, and (iii) tensile modulus.

Although sample sizes can be estimated from the results for each parameter, this work primarily focuses on the tensile modulus, which has been identified as the most sensitive and the most inconsistent among the three outcomes in ASTM D7205 [32]. This appendix provides further explanation on why the other two parameters obtained from ASTM D7205 [32] were not initially used to estimate the sample size.

E.1.1 Measured cross-sectional area

Selecting the area for an FRP product is complex due to numerous factors. FRP products typically have surface treatments that protect the fibers and resin, thereby significantly increasing the total surface area of the product. While proper surface treatment can enhance durability or bonding, it does not improve strength because these external treatments do not add stiffness.

Therefore, product datasheets often list area values that are much lower than the measured cross-sectional area. This happens because some manufacturers report the area after all surface treatments have been removed from the calculation. By doing so, they only include the area that effectively contributes to strength. This adjusted area is typically referred to as the “effective area” or “nominal area” and represents the area that engineers should use when designing and analyzing FRP-reinforced elements.

Although this may seem reasonable, misunderstandings about the appropriate area value could lead to inaccurate calculations. For example, using a smaller area results in higher uniaxial stress, and vice versa, which can significantly affect the material’s modulus of elasticity, since uniaxial stresses are used to determine the slope (stiffness) of the stress-strain curve.

For GFRP bars, the nominal areas for No. 2 through No. 10 bars are specified in ASTM D7957 [18], which standardizes the nominal dimensions. Based on that nominal value, the standard also specifies minimum and maximum limits for fabrication tolerances. Here, manufacturers should aim to meet strength and stiffness requirements based on the nominal area, regardless of whether the measured cross-sectional area falls within the nominal area’s minimum or maximum range.

Currently, there is no ASTM standard addressing CFRP bars or strands, resulting in a lack of standardization of area values used in carbon-based products. However, despite some nuances in area values, evidence indicates that they are highly consistent within the same lot and product (see Appendix D). Therefore, the authors believe that any material non-compliance is unlikely to stem from the area, as the variation around this parameter is essentially negligible. An upcoming ASTM standard for CFRP should include a range of areas to assess compliance, as currently done for GFRP bars.

Finally, the process for determining the area of a non-circular shape (e.g., a 7-wire strand) is time-consuming and relies on Archimedes’ principle (see Appendix D.2.1). This method requires submerging a fixed length in water to measure the displaced volume. Conducting this analysis across multiple sections

of the same specimen and several replicates per lot quickly consumes resources for a test that does not necessarily determine the material's compliance or behavior.

Instead, QA/QC efforts during a large-scale applied project should focus on more meaningful parameters related to strength and stiffness, which are ultimately the critical variables involved in design, determining the size and reinforcement patterns of structural components. The latter aligns with a primary objective of this research: to facilitate a safe and efficient QA/QC protocol.

E.1.2 Guaranteed tensile strength

The strength of a material is undoubtedly one of the most, if not the most, essential characteristics to determine. Every manufacturer will almost certainly perform its own characterization process to determine the strength of its materials. After proper characterization, the guaranteed strength generally refers to the value specified on the product datasheet. It is important to note that, in most cases, the average ultimate strength of a given material (rupture capacity) will be higher than the guaranteed value. This is because ultimate strength will inevitably vary among specimens, even within the same lot. Therefore, manufacturers usually include a safety margin based on their experimental data. A common rule of thumb is to use the mean minus three standard deviations, which provides a 99.7% confidence level (Section 4.2).

Nevertheless, alternative criteria could be used. For instance, Tokyo Rope adjusted the guaranteed tensile strength of 0.6 in. CFRP strands using the TR-T dataset (presented in 4.2.1) by selecting the lowest rupture force observed in their experimental program as the guaranteed strength. This is an even more conservative approach, but it remains practical in this case, given the relatively low standard deviation observed across multiple tests (see Table 9).

Since the guaranteed strength is already based on a conservative estimate derived from experimental data, the likelihood that a specimen is non-compliant is very low (as confirmed by the QA/QC conducted for Harkers Island). Furthermore, it should be remembered that the maximum tensile stress that can be applied to a CFRP strand used for prestressing is $0.7f_{pu}$, where f_{pu} is the guaranteed tensile strength (which is already less than the average ultimate strength). Additionally, code-based designs must incorporate additional factors related to the types of loading, thereby further increasing safety margins.

E.2. Conclusion

In summary, although both the measured cross-sectional area and guaranteed tensile strength are important parameters, they do not fully capture the key factors that validate an FRP material when performing a QA/QC analysis to determine its compliance and reliability. This is especially true for large-scale projects with many lots, where the most efficient method for assessing material compliance is likely preferred. Such efficiency involves minimizing the number of tests while providing the most meaningful results, ensuring certainty and confidence in the materials used.

For the measured cross-sectional area, the results are sufficiently consistent that using it as a reference parameter to determine a sample size would imply that no validation tests are needed, given the low dispersion of the existing data. Therefore, it is not a good candidate for this research objective. It is essential to note that the area values of an FRP product should still be periodically monitored by external control agencies responsible for approving manufacturers and their specific products as valid alternatives for use in structural applications. However, these controls should be conducted as systematic audits of production plants and manufacturers' in-house data. They should not necessarily be required for every project and for every lot.

Even if the special provisions require measurement of the cross-sectional area, a quick spot check of the diameter should suffice to confirm that it does not exceed the maximum allowed diameter. This is crucial because exceeding it could cause spacing issues within the concrete when large amounts of reinforcement are used in optimized sections. Additionally, FRP manufacturers should clearly distinguish, if applicable, between the measured cross-sectional area (the physical space the product occupies) and the effective (or nominal) area used for design purposes. Furthermore, manufacturers should strive to meet the strength and stiffness requirements specified in their datasheets based on the nominal area listed. It is unrealistic to expect that the exact area of an FRP bar, measured in accordance with ASTM D792 [78], must always be used, especially when prior removal of surface coatings is necessary to determine the effective area.

On the other hand, although material strength is relevant, using it as the sole parameter to estimate an adequate sample size is not optimal. This is because the project's special provisions will likely require confirmation that the analyzed product exceeds the minimum guaranteed strength, which is already the lower bound of the strength based on internal experimental data. Given that most, if not all, specimens are expected to exceed this value, the guaranteed strength will also suggest that no further validation is needed.

It is worth noting that testing specimens to failure could be an option. However, special provisions cannot provide a comparable value, as most manufacturers do not report the actual rupture (ultimate) strength. Therefore, testing every specimen to failure for sampling purposes would be a waste of time in most cases. External control agencies should be responsible for periodically reviewing manufacturer data, but testing specimens until failure should not be a mandatory requirement within a project, especially given the safety concerns associated with testing materials that exhibit a brittle failure mode, such as FRP.

Alternatively, using the tensile modulus obtained from a tension test is a much better choice. This modulus effectively links area and strength since both the forces developed during the test and the nominal area are involved in its calculation. Furthermore, the modulus of elasticity indicates the material's stiffness, which indirectly demonstrates an adequate fiber distribution within the section if the material is compliant. The tensile modulus is also widely used in design and analysis. Additionally, manufacturers consistently report this value, facilitating comparison and the preparation of special provisions. Therefore, the elastic modulus is a key parameter that reflects other properties (such as area, strength, and fiber mass content), making it ideal for improving efficiency. Accordingly, the tensile modulus has been used to estimate sample size requirements in this work.

Moreover, since both strength and tensile modulus can be obtained from the same tension test (ASTM D7205 [20]), the specimen can be left in the testing machine until it exceeds the guaranteed value. This would assure all stakeholders and enable the collection of a sufficiently broad range of strains. However, the number of replicates required should be based solely on the tensile modulus results.

For completeness, it is also important to briefly address the other physical and mechanical test requirements listed in Table 1. Performing every test for each lot would be impractical, and some durability-related parameters, such as creep, fatigue, or alkali resistance, have already been thoroughly studied [6], [7], [8], [9], [10], [11], [12]. Notably, this level of scrutiny is not usually applied to other materials, such as steel, despite its well-known tendency to corrode. Therefore, FRP should no longer be viewed solely as a research material; instead, practices that make it a more mainstream option should be adopted, particularly in areas prone to rapid corrosion-induced deterioration. In conclusion, a tension test, particularly the tensile modulus, offers a reasonable estimate of material compliance and will be the primary parameter used. While several other factors could be explored further, they are beyond the scope of this work.

Appendix F. PREPARATION OF FRP TENSION TESTS

F.1. Purpose and Scope

This appendix summarizes the practical steps and lessons learned while preparing CFRP strand and GFRP bar specimens for tension testing in accordance with ASTM D7205 [20]. The intent is to provide project-tested best practices so that NCDOT does not need to repeat the same trial-and-error process. The main objectives for a successful tension test are:

- Preparing reliable steel pipe/grout anchors.
- Achieving rupture in the free gauge length, not in or near the anchors.
- Avoiding premature failure modes (e.g., pipe rupture, bar slippage).

F.2. CFRP Strand Specimens

F.2.1 General Concept and Materials

For the 0.6 in. seven-wire CFRP strands, direct gripping was not feasible due to the low transverse strength and braided geometry of the strands. Instead, each specimen was prepared with steel pipe end anchors filled with expansive grout, which could be gripped within a universal tensile machine (UTM). A set of specimens before and after being tested are shown in Figure A - 64. A typical specimen was 52 in. long, with 18 in. steel pipes at each end.

F.2.2 Recommended Preparation Procedure

The steps below reflect the procedure that consistently produced rupture in the free gauge length:

1. Cut and prepare steel pipes (Figure A - 65)
   - Cut steel pipes to the desired anchor length (≈18 in. in this project).
   - Deburr and lightly grind the pipe ends to remove sharp edges or irregularities.
   - If needed, clean the pipe interior to remove oil, rust, and dirt; contamination can compromise the bond with the grout.
2. Cut and clean CFRP strands (Figure A - 66)
   - Cut strands to the desired total length, allowing for both anchors and the target gauge length.
   - If needed, lightly clean the strand within the pipe region to promote bond (e.g., remove loose dust or surface contaminants, without damaging the fibers).
3. Install pipes and temporary caps (Figure A - 67)
   - Slide a pipe segment onto each end of the strand, ensuring sufficient embedment on both sides of the future gauge length.
   - Use plastic end caps (3D-printed or equivalent) sealed with silicone to close the bottom of each pipe before grouting.
   - Allow the silicone to cure (≈12 hours), so caps remain watertight during grout placement.

(a) Specimens ready to test

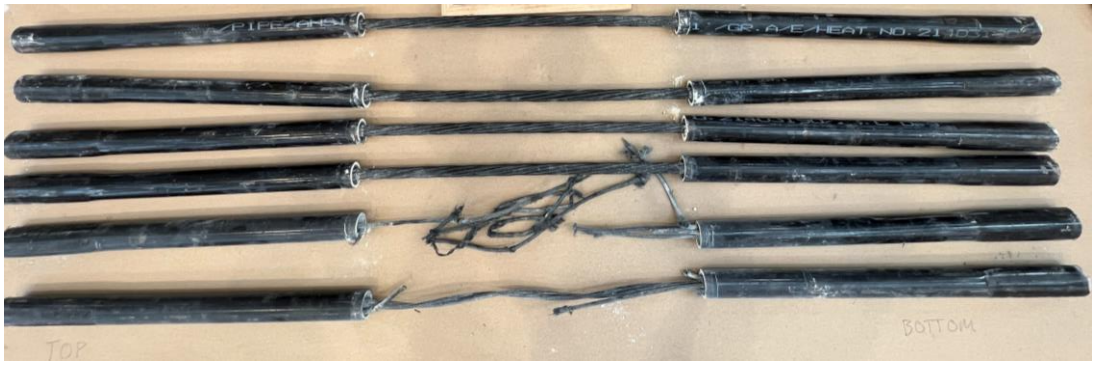

(b) Specimens after being tested (two specimens tested up to rupture)

Figure A - 64. CFRP strand tension test specimens

4. Vertical alignment and first anchor pour (Figure 9)
   - Place the specimen vertically in an alignment jig so the strand is centered within the pipe (no visible contact between the strand and the pipe wall).
   - Mix a commercial expansive cementitious grout (commonly marketed for controlled demolition) with clean, cold water following the manufacturer's recommendations.
   - Using a funnel, fill the annular space inside the lower pipe from the top, gently tapping the pipe to help air escape.
   - Install the top cap and leave the specimen undisturbed for at least 24 hours.
5. Second anchor pour
   - Flip the specimen in the jig and repeat the grouting process for the second pipe end.
   - Again, allow at least 24 hours of undisturbed curing.
6. Curing before testing
   - After both ends have been poured, cure the specimens in the laboratory for at least 7 days before testing.
   - In this project, longer curing times (e.g., 10–14 days) reduced the incidence of unintended failure modes and is recommended when the schedule permits.
7. Final preparation before testing
   - Mark the intended gauge length and the mid-length location for the extensometer.
   - Verify that the strand is centered in each pipe by visual inspection at the pipe ends.
   - Lightly clean the pipe exterior to ensure good contact with the grips.

Figure A - 65. Steel pipes cut and deburred

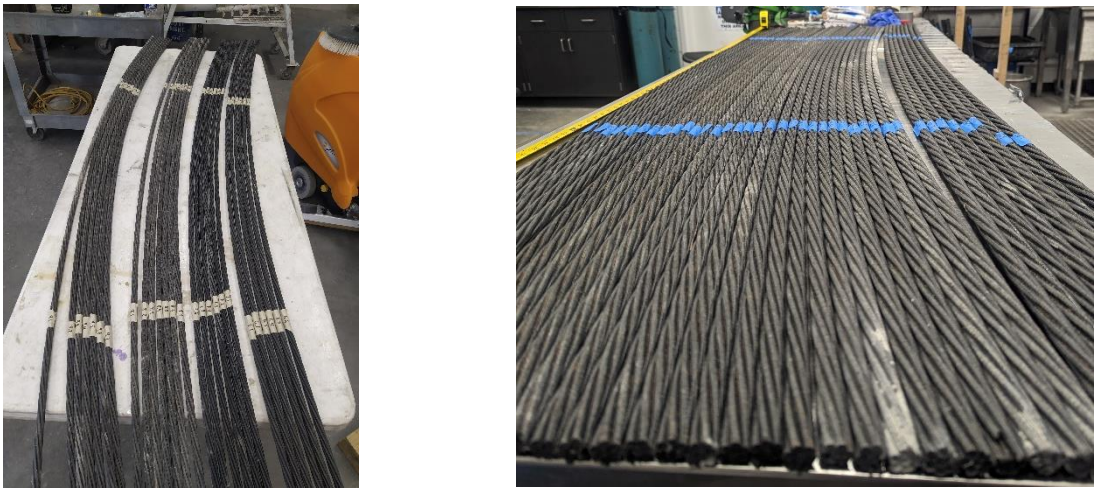

Figure A - 66. CFRP strands identified before cutting

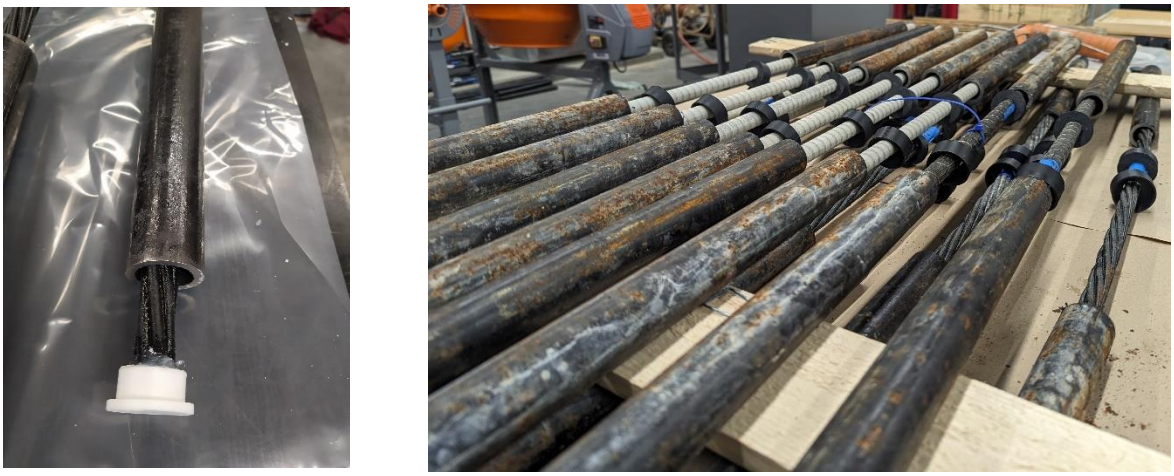

Figure A - 67. Steel pipe and plastic cap installation

F.2.3 Early Failure Modes

Several early tests did not fail within the free gauge length. These unsuccessful specimens were critical to refining the procedure and served as useful reference cases.

Pipe rupture at the grips (Figure A - 68)

In early tests, excessive grip pressure caused local crushing and rupture of the steel pipe at the grip edges. When this occurred, the fractured pipe ring would suddenly release, and the remaining strand section could be violently expelled, sometimes impacting the upper grip region.

This failure mode is unsafe and invalid for acceptance testing. It was mitigated by limiting grip pressure to a value sufficient to prevent slip but low enough to avoid plastic deformation of the pipe. For 0.6 in. CFRP strands, the UTM used for this project required a grip pressure of 3,500 psi per grip. Other laboratories may need to calibrate their own values.

Figure A - 68. Pipe rupture as a premature failure mode

Slip due to non-expansive grout (Figure A - 69)

Initial trials using non-expansive epoxy grout resulted in slip between the strand and grout before reaching the target load. Once slip initiated, the load-displacement response changed abruptly, and the specimen could no longer be used to determine tensile properties. Switching to an expansive demolition-type grout effectively eliminated this failure mode by improving confinement and bond in the anchor region.

(a) Properly bonded strand *(b) Poor bonding leading to slippage*

Figure A - 69. Strand slippage as a premature failure mode

King wire residual strength (Figure A - 70)

In a small number of tests, the strand failed in a brittle manner with most fibers rupturing suddenly, but the central “king wire” remained intact, carrying a residual load of approximately 5 kips. This behavior is consistent with the 7-wire strand construction and was observed only after the CFRP strand had clearly ruptured in the gauge length. Although not strictly an early failure mode, it is included here.

Figure A - 70. King wire remaining after CFRP strand failure

F.3. GFRP Bar Specimens

F.3.1 General Approach

GFRP bar specimens were prepared using the same anchorage concept as the CFRP strands: steel pipe anchors filled with expansive grout, vertical casting in a jig for alignment, and targeting rupture in the free gauge length. Bar diameters varied across the project, so pipe diameter was adjusted to maintain a reasonable grout thickness and ensure a robust bond.

F.3.2 Preparation Notes Specific to GFRP Bars

The overall procedure mirrored that for CFRP strands, with the following practical adaptations:

1. Pipe selection and fit
    - For each GFRP bar size, steel pipes were selected to provide a small but consistent annular gap for grout (typically 0.20 to 0.30 in.).
    - Too tight a fit can lead to insufficient grout, whereas too loose a fit increases the risk of voids and eccentricity.

2. Anchor length
   - Anchor lengths were chosen to be comparable to those used for strands, adjusted for bar diameter and expected load level, so that failure occurred in the free length (Table A - 2).
3. Surface condition in the anchor region
   - Sand-coated or ribbed GFRP bars generally provided good bond with the expansive grout without additional steps. If needed, only loose dust or contaminants were removed.
4. Grouting and curing
   - The same expansive grout was adopted for GFRP bars.
   - As with strands, curing periods of at least 7 days were used, with longer curing giving more consistent results.

F.3.3 Gripping and Grip Pressure for GFRP Bars

GFRP specimens were gripped in contoured pipe grips similar to those used for the CFRP strands. However, because bar diameters and expected peak loads varied, the optimal grip pressure depended on both bar size and the test machine. In this project, smaller bars generally required lower grip pressures than the 0.6 in. CFRP strand specimens, and once appropriate values were established, they were kept constant for each bar size for the remainder of the test program. Table A - 2 summarizes the combination of bar size, pipe size, and approximate grip pressure used in this project, which can serve as a practical starting point for future testing.

Table A - 2. Recommended grip pressures for tension tests

Material	Diameter	Anchor Length (in.)	Grip Pressure (psi)
GFRP	No. 3	15 - 18	800
	No. 4		1,300
	No. 5		1,800
	No. 6	18	2,500
	No. 8		3,800
CFRP	0.6 in.		3,500

F.4. Practical Recommendations and Checklist

Based on the experience gained during this project, the following practical recommendations are offered for preparing FRP specimens for tension testing:

1. Aim for failure in the free gauge length
   - Any failure inside the anchor, at the pipe edge, or due to pipe rupture should be treated as invalid, and the specimen preparation procedure should be reviewed.

2. Use expansive grout for anchors
    - Expansive cementitious grouts marketed for controlled demolition provided reliable bond and helped avoid slip failures observed with non-expansive or epoxy grouts.
3. Control alignment at every step
    - Use simple jigs to center the FRP bar or strand in the pipe while grouting.
    - After curing, visually confirm concentricity and, if possible, correct any obvious misalignments before testing.
4. Calibrate grip pressures carefully
    - Start from conservative (lower) grip pressures and gradually increase until slip is eliminated, without deforming the pipes.
    - Document the final grip pressure used for each FRP size and pipe combination.
5. Allow adequate curing time
    - Minimum 7 days of laboratory curing is recommended before testing. Longer curing times may further reduce unintended failure modes.
6. Ensure robust safety measures
    - FRP failures are brittle and can be explosive. Always use protective shields (e.g., glass or polycarbonate enclosures) around the gauge region, restrict access to the immediate vicinity of the specimen, and follow appropriate lab safety protocols.
7. Maintain a preparation and test log
    - Record for each specimen: FRP type and size, lot number, pipe geometry, grout type, curing time, grip pressure, and failure mode. This information is invaluable for diagnosing issues and refining procedures.

Appendix G. SUPPLEMENTARY BEND TESTS ON CFRP SPIRALS

G.1. Overview

As discussed in Chapter 3, the 0.28 in. CFRP spirals used in the 24 in. square piles at Harkers Island were tested at their bend locations as part of the project-level QA/QC program. Those tests, conducted on 19 square spirals with an r/d ratio of 2.2, showed that the mean bend strength was about 41% of the ultimate tensile strength of a straight companion portion, in close agreement with the empirical JSCE [26] expression for FRP bends. At the same time, the adopted r/d = 2.2 is smaller than the minimum r/d = 3.0 currently specified for GFRP bars in ASTM D7957 [18], and there is still no ASTM standard dedicated to CFRP reinforcement.

These observations prompted follow-up discussions with the NCDOT Steering and Implementation Committee and with Tokyo Rope USA, the CFRP manufacturer. It was acknowledged that the absence of a CFRP-oriented standard is a key source of inconsistency, and that the tight bend radius used at Harkers Island was driven primarily by Japanese practice, in which r/d = 2.2 is acceptable. To better understand the implications of bend radius and surface treatment for CFRP spirals, a supplemental experimental program was carried out beyond the original QA/QC scope of this project. This appendix summarizes that additional work. The goals are to:

- Re-test CFRP spirals with r/d = 2.2 under controlled conditions to confirm the original QA/QC findings.
- Evaluate a second group of spirals with an increased bend radius (r/d = 3.0), aligned with GFRP criteria.
- Assess whether a new surface treatment developed by the manufacturer has any measurable influence on bend strength.
- Provide a richer experimental basis for future CFRP bend-strength requirements and test standards.

Unless otherwise noted, the test concept, loading configuration, and data collection procedures are identical to those described in Chapter 3 for the original spiral tests.

G.2. Experimental Program and Specimen Groups

The broader experimental program on CFRP spiral bends comprised two phases, which are summarized here:

Phase 1 – Square CFRP spirals (QA/QC program, r/d = 2.2)

- Geometry: 18 in. square spirals used in the Harkers Island piles.
- Product: 0.28 in. uni-strand CFRP spiral (bends formed prior to curing).
- Sampling: 19 spirals randomly selected from 19 different production lots delivered to the precast plant.
- Purpose: project-level QA/QC; results reported in Chapter 3 and referenced here for comparison.

Phase 2 – Rectangular CFRP spirals (supplemental program, r/d = 2.2 and 3.0)

- Geometry: 32 × 18 in. rectangular spirals produced specifically for this study.

- Product: same 0.28 in. CFRP spiral, with two variants: (i) original surface treatment, and (ii) enhanced surface treatment intended to improve bond and durability.
- Bend radius: half of the spirals with r/d = 2.2 (≈ 0.62 in. inside radius). Half with r/d = 3.0 (≈ 0.84 in. inside radius), consistent with the minimum inside bend diameter in ASTM D7957 [18] for GFRP bars in the same size range.
- Total: 22 spirals, equally divided among r/d and surface-treatment combinations.

To accommodate the larger rectangular geometry, the concrete block dimensions used in Phase 2 were increased from those in the QA/QC program to 24 × 10 × 6 in., while preserving the same conceptual layout (two concrete blocks, one side debonded, tension applied by hydraulic jacks). Similarly, all concrete used in this appendix had a target compressive strength of 35 MPa supplied by a local ready-mix plant.

Figure A - 51 shows new specimens being fabricated, and Figure A - 52 illustrates a specimen just before testing. For Phase 2, the orthogonality and bend radius of each spiral were verified. Both parameters appear to be compliant.

Figure A - 51. Specimen preparation for bent bar tests – Phase 2

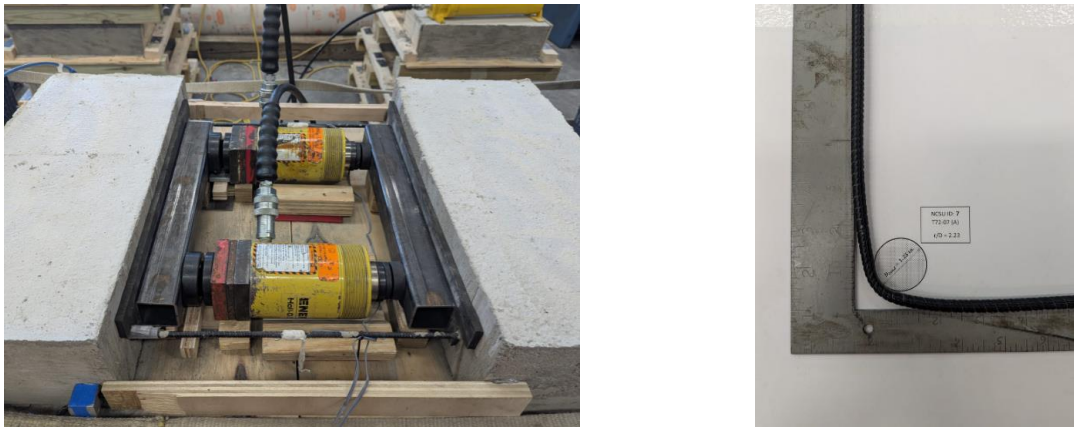

Figure A - 52. Test setup – Phase 2

G.3. Test Configuration and Practical Challenges

Because of the larger geometry and higher loads expected in Phase 2 (due to increasing the r/d ratio), the following practical issues became more pronounced:

Block rotation and eccentricity: Phase 2 specimens exhibited noticeable rotation of the concrete blocks under loading, resulting in unintended bending of the spiral legs adjacent to the bonded block face. In several early tests, failure occurred just outside the concrete block at the straight portion rather than in the bend, making those tests unsuitable for characterizing bend strength.

Alignment sensitivity of ASTM D7914 [21] configuration: Even small geometric offsets (on the order of ¼ in.) produced sufficient eccentricity to alter the failure mode. This effect is inherent to the current ASTM D7914 [21] geometry, which requires careful alignment of two separate concrete blocks, which becomes more critical with longer specimens.

To address these issues, a series of refinements were implemented:

- Systematic inspection and shimming of the bearing surfaces of the concrete blocks.
- Use of steel plates, rubber pads, and alignment guides to reduce local stress concentrations.
- Installation of spherical bearings on both ends to accommodate minor misalignments and ensure that the spirals were loaded as nearly as possible in concentric tension.

Even after these adjustments, only 12 of 22 Phase 2 specimens failed at the intended bend location, with deformations consistent with those observed in Phase 1. The sequence of a successful test, with failure at the bend, is shown in Figure A - 53. On the contrary, an unsuccessful test due to rotation and failure outside of the concrete block is presented in Figure A - 54. It is worth noting that both upward and downward rotations occurred, depending on the location of the unintended eccentric load (Figure A - 55).

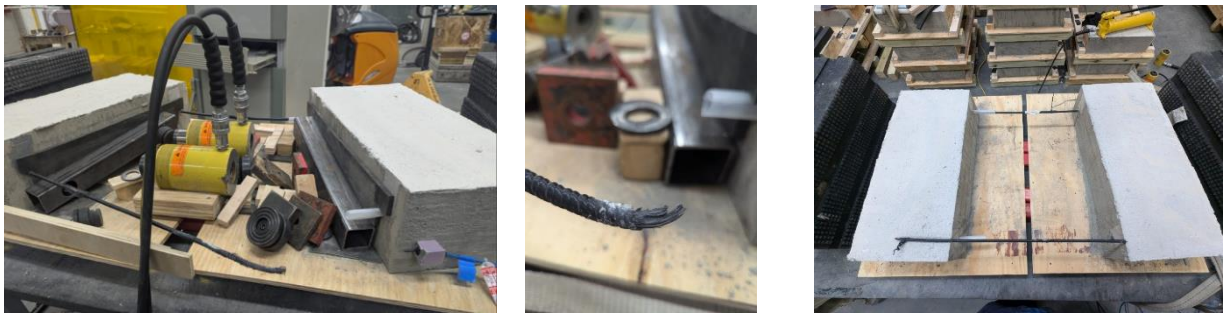

Figure A - 53. Successful failure at the bend location – Phase 2

Figure A - 54. Unsuccessful failure due to rotation – Phase 2


Figure A - 55. Downward and upward rotations – Phase 2

G.4. Experimental Results for CFRP Spirals

Phase 2 tested 22 rectangular spirals with a geometry of 32 × 18 in., divided by r/d and surface treatment. However, because of the misalignment issues described above, only 12 specimens, which failed at the bend location, are discussed in this section. The main findings for the r/d = 3.0 group are:

- Increasing the bend radius from 0.62 in. (r/d ≈ 2.2) to 0.84 in. (r/d ≈ 3.0) produced a measurable increase in mean bend strength, from about 6.5 kips to 7.2 kips, corresponding to a 9.3% increase in mean ultimate bend strength.
- The COV for ultimate bend strength increased modestly from 17% to 21%, reflecting the sensitivity to alignment.
- When normalized by the straight-bar tensile strength, the mean bend-strength ratio increased from 41% to 45%.

Again, the JSCE [26] expression matched the experimental data remarkably well for r/d = 3.0. Regarding surface treatment, no statistically meaningful difference in bend strength was observed between spirals with the original surface finish and those with the enhanced treatment. The latter is expected, as surface treatments may enhance bond properties but not necessarily strength. A summary of Phase 1 and Phase 2 results is provided in Table A-3.

Table A - 3. Summary of CFRP spiral bend-strength results (Phases 1 and 2)

Phase	FRP material	r/d	Mean rupture force at bent portion* [kip]	COV [%]	Mean rupture force of straight bar** [kip]	χ_{exp}*** [%]	χ_{JSCE}/χ_{exp}
1	CFRP	2.2	6.5	17	15.9	41	1.0
2		3.0	7.2	21		45	1.0

* Determined experimentally as part of this project.
** Values reported by manufacturer.
*** Ultimate strength comparison between bent portion and straight bar.

G.5. Implications for Bend Radius and Test Methods

1. Bend radius is the dominant parameter:

For the CFRP spiral product tested, increasing r/d from 2.2 to 3.0 increased the mean bend-strength retention from 41% to 45% of the straight-bar ultimate strength. These values are consistent with the JSCE [26] estimation, and with other researchers indicating that r/d ≈ 4.0 is associated with approximately 50% strength retention for CFRP bends [29].

2. Higher r/d ratios might be required for CFRP spirals:

If one were to target the 60% strength retention currently implied for GFRP bars in ASTM D7957 [18], the JSCE [26] expression suggests that an r/d ratio of approximately 6.0 would be required for CFRP bends. While this inference should be confirmed by additional testing, it indicates that simply adopting GFRP bend-radius limits for CFRP products may be unconservative, and that CFRP-specific bend-radius recommendations are needed.

3. ASTM D7914 geometry may be restrictive and misleading:

The testing in this appendix reinforces what other researchers have noted: the current ASTM D7914 [21] configuration is highly sensitive to small misalignments and can lead to unintended failure modes outside the bend, especially when tolerances accumulate in casting, debonding, and loading hardware. Even after substantial refinement, specimen preparation and alignment remained time-consuming.

4. L-shaped test methods offer practical advantages.

Alternative test setups based on L-shaped specimens cast into a single block, such as those adopted in CSA S807 [17], have been shown to reduce COV, simplify preparation, and produce less violent failures, making them more appealing to routine QA/QC. The results in this appendix support the recommendation in Chapter 7 that future CFRP bend-strength standards for QA/QC should favor L-shaped, self-reacting configurations wherever possible.

Appendix H. STATISTICAL TABLES

H.1. Standard Normal Distribution Table (*Taken from Devore* [27])

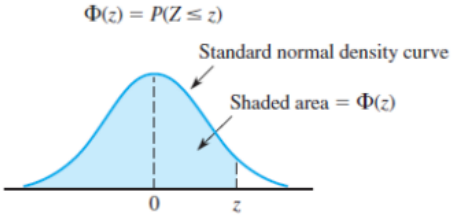

z	.00	.01	.02	.03	.04	.05	.06	.07	.08	.09
−3.4	.0003	.0003	.0003	.0003	.0003	.0003	.0003	.0003	.0003	.0002
−3.3	.0005	.0005	.0005	.0004	.0004	.0004	.0004	.0004	.0004	.0003
−3.2	.0007	.0007	.0006	.0006	.0006	.0006	.0006	.0005	.0005	.0005
−3.1	.0010	.0009	.0009	.0009	.0008	.0008	.0008	.0008	.0007	.0007
−3.0	.0013	.0013	.0013	.0012	.0012	.0011	.0011	.0011	.0010	.0010
−2.9	.0019	.0018	.0017	.0017	.0016	.0016	.0015	.0015	.0014	.0014
−2.8	.0026	.0025	.0024	.0023	.0023	.0022	.0021	.0021	.0020	.0019
−2.7	.0035	.0034	.0033	.0032	.0031	.0030	.0029	.0028	.0027	.0026
−2.6	.0047	.0045	.0044	.0043	.0041	.0040	.0039	.0038	.0037	.0036
−2.5	.0062	.0060	.0059	.0057	.0055	.0054	.0052	.0051	.0049	.0038
−2.4	.0082	.0080	.0078	.0075	.0073	.0071	.0069	.0068	.0066	.0064
−2.3	.0107	.0104	.0102	.0099	.0096	.0094	.0091	.0089	.0087	.0084
−2.2	.0139	.0136	.0132	.0129	.0125	.0122	.0119	.0116	.0113	.0110
−2.1	.0179	.0174	.0170	.0166	.0162	.0158	.0154	.0150	.0146	.0143
−2.0	.0228	.0222	.0217	.0212	.0207	.0202	.0197	.0192	.0188	.0183
−1.9	.0287	.0281	.0274	.0268	.0262	.0256	.0250	.0244	.0239	.0233
−1.8	.0359	.0352	.0344	.0336	.0329	.0322	.0314	.0307	.0301	.0294
−1.7	.0446	.0436	.0427	.0418	.0409	.0401	.0392	.0384	.0375	.0367
−1.6	.0548	.0537	.0526	.0516	.0505	.0495	.0485	.0475	.0465	.0455
−1.5	.0668	.0655	.0643	.0630	.0618	.0606	.0594	.0582	.0571	.0559
−1.4	.0808	.0793	.0778	.0764	.0749	.0735	.0722	.0708	.0694	.0681
−1.3	.0968	.0951	.0934	.0918	.0901	.0885	.0869	.0853	.0838	.0823
−1.2	.1151	.1131	.1112	.1093	.1075	.1056	.1038	.1020	.1003	.0985
−1.1	.1357	.1335	.1314	.1292	.1271	.1251	.1230	.1210	.1190	.1170
−1.0	.1587	.1562	.1539	.1515	.1492	.1469	.1446	.1423	.1401	.1379
−0.9	.1841	.1814	.1788	.1762	.1736	.1711	.1685	.1660	.1635	.1611
−0.8	.2119	.2090	.2061	.2033	.2005	.1977	.1949	.1922	.1894	.1867
−0.7	.2420	.2389	.2358	.2327	.2296	.2266	.2236	.2206	.2177	.2148
−0.6	.2743	.2709	.2676	.2643	.2611	.2578	.2546	.2514	.2483	.2451
−0.5	.3085	.3050	.3015	.2981	.2946	.2912	.2877	.2843	.2810	.2776
−0.4	.3446	.3409	.3372	.3336	.3300	.3264	.3228	.3192	.3156	.3121
−0.3	.3821	.3783	.3745	.3707	.3669	.3632	.3594	.3557	.3520	.3482
−0.2	.4207	.4168	.4129	.4090	.4052	.4013	.3974	.3936	.3897	.3859
−0.1	.4602	.4562	.4522	.4483	.4443	.4404	.4364	.4325	.4286	.4247
−0.0	.5000	.4960	.4920	.4880	.4840	.4801	.4761	.4721	.4681	.4641

(*continued*)

$\Phi(z) = P(Z \leq z)$

z	.00	.01	.02	.03	.04	.05	.06	.07	.08	.09
0.0	.5000	.5040	.5080	.5120	.5160	.5199	.5239	.5279	.5319	.5359
0.1	.5398	.5438	.5478	.5517	.5557	.5596	.5636	.5675	.5714	.5753
0.2	.5793	.5832	.5871	.5910	.5948	.5987	.6026	.6064	.6103	.6141
0.3	.6179	.6217	.6255	.6293	.6331	.6368	.6406	.6443	.6480	.6517
0.4	.6554	.6591	.6628	.6664	.6700	.6736	.6772	.6808	.6844	.6879
0.5	.6915	.6950	.6985	.7019	.7054	.7088	.7123	.7157	.7190	.7224
0.6	.7257	.7291	.7324	.7357	.7389	.7422	.7454	.7486	.7517	.7549
0.7	.7580	.7611	.7642	.7673	.7704	.7734	.7764	.7794	.7823	.7852
0.8	.7881	.7910	.7939	.7967	.7995	.8023	.8051	.8078	.8106	.8133
0.9	.8159	.8186	.8212	.8238	.8264	.8289	.8315	.8340	.8365	.8389
1.0	.8413	.8438	.8461	.8485	.8508	.8531	.8554	.8577	.8599	.8621
1.1	.8643	.8665	.8686	.8708	.8729	.8749	.8770	.8790	.8810	.8830
1.2	.8849	.8869	.8888	.8907	.8925	.8944	.8962	.8980	.8997	.9015
1.3	.9032	.9049	.9066	.9082	.9099	.9115	.9131	.9147	.9162	.9177
1.4	.9192	.9207	.9222	.9236	.9251	.9265	.9278	.9292	.9306	.9319
1.5	.9332	.9345	.9357	.9370	.9382	.9394	.9406	.9418	.9429	.9441
1.6	.9452	.9463	.9474	.9484	.9495	.9505	.9515	.9525	.9535	.9545
1.7	.9554	.9564	.9573	.9582	.9591	.9599	.9608	.9616	.9625	.9633
1.8	.9641	.9649	.9656	.9664	.9671	.9678	.9686	.9693	.9699	.9706
1.9	.9713	.9719	.9726	.9732	.9738	.9744	.9750	.9756	.9761	.9767
2.0	.9772	.9778	.9783	.9788	.9793	.9798	.9803	.9808	.9812	.9817
2.1	.9821	.9826	.9830	.9834	.9838	.9842	.9846	.9850	.9854	.9857
2.2	.9861	.9864	.9868	.9871	.9875	.9878	.9881	.9884	.9887	.9890
2.3	.9893	.9896	.9898	.9901	.9904	.9906	.9909	.9911	.9913	.9916
2.4	.9918	.9920	.9922	.9925	.9927	.9929	.9931	.9932	.9934	.9936
2.5	.9938	.9940	.9941	.9943	.9945	.9946	.9948	.9949	.9951	.9952
2.6	.9953	.9955	.9956	.9957	.9959	.9960	.9961	.9962	.9963	.9964
2.7	.9965	.9966	.9967	.9968	.9969	.9970	.9971	.9972	.9973	.9974
2.8	.9974	.9975	.9976	.9977	.9977	.9978	.9979	.9979	.9980	.9981
2.9	.9981	.9982	.9982	.9983	.9984	.9984	.9985	.9985	.9986	.9986
3.0	.9987	.9987	.9987	.9988	.9988	.9989	.9989	.9989	.9990	.9990
3.1	.9990	.9991	.9991	.9991	.9992	.9992	.9992	.9992	.9993	.9993
3.2	.9993	.9993	.9994	.9994	.9994	.9994	.9994	.9995	.9995	.9995
3.3	.9995	.9995	.9995	.9996	.9996	.9996	.9996	.9996	.9996	.9997
3.4	.9997	.9997	.9997	.9997	.9997	.9997	.9997	.9997	.9997	.9998

H.2. Student T Distribution Table (*Taken from Devore* [27])

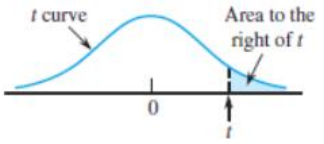

t \ ν	1	2	3	4	5	6	7	8	9	10	11	12	13	14	15	16	17	18
0.0	.500	.500	.500	.500	.500	.500	.500	.500	.500	.500	.500	.500	.500	.500	.500	.500	.500	.500
0.1	.468	.465	.463	.463	.462.	.462	.462	.461	.461	.461	.461	.461	.461	.461	.461	.461	.461	.461
0.2	.437	.430	.427	.426	.425	.424	.424	.423	.423	.423	.423	.422	.422	.422	.422	.422	.422	.422
0.3	.407	.396	.392	.390	.388	.387	.386	.386	.386	.385	.385	.385	.384	.384	.384	.384	.384	.384
0.4	.379	.364	.358	.355	.353	.352	.351	.350	.349	.349	.348	.348	.348	.347	.347	.347	.347	.347
0.5	.352	.333	.326	.322	.319	.317	.316	.315	.315	.314	.313	.313	.313	.312	.312	.312	.312	.312
0.6	.328	.305	.295	.290	.287	.285	.284	.283	.282	.281	.280	.280	.279	.279	.279	.278	.278	.278
0.7	.306	.278	.267	.261	.258	.255	.253	.252	.251	.250	.249	.249	.248	.247	.247	.247	.247	.246
0.8	.285	.254	.241	.234	.230	.227	.225	.223	.222	.221	.220	.220	.219	.218	.218	.218	.217	.217
0.9	.267	.232	.217	.210	.205	.201	.199	.197	.196	.195	.194	.193	.192	.191	.191	.191	.190	.190
1.0	.250	.211	.196	.187	.182	.178	.175	.173	.172	.170	.169	.169	.168	.167	.167	.166	.166	.165
1.1	.235	.193	.176	.167	.162	.157	.154	.152	.150	.149	.147	.146	.146	.144	.144	.144	.143	.143
1.2	.221	.177	.158	.148	.142	.138	.135	.132	.130	.129	.128	.127	.126	.124	.124	.124	.123	.123
1.3	.209	.162	.142	.132	.125	.121	.117	.115	.113	.111	.110	.109	.108	.107	.107	.106	.105	.105
1.4	.197	.148	.128	.117	.110	.106	.102	.100	.098	.096	.095	.093	.092	.091	.091	.090	.090	.089
1.5	.187	.136	.115	.104	.097	.092	.089	.086	.084	.082	.081	.080	.079	.077	.077	.077	.076	.075
1.6	.178	.125	.104	.092	.085	.080	.077	.074	.072	.070	.069	.068	.067	.065	.065	.065	.064	.064
1.7	.169	.116	.094	.082	.075	.070	.065	.064	.062	.060	.059	.057	.056	.055	.055	.054	.054	.053
1.8	.161	.107	.085	.073	.066	.061	.057	.055	.053	.051	.050	.049	.048	.046	.046	.045	.045	.044
1.9	.154	.099	.077	.065	.058	.053	.050	.047	.045	.043	.042	.041	.040	.038	.038	.038	.037	.037
2.0	.148	.092	.070	.058	.051	.046	.043	.040	.038	.037	.035	.034	.033	.032	.032	.031	.031	.030
2.1	.141	.085	.063	.052	.045	.040	.037	.034	.033	.031	.030	.029	.028	.027	.027	.026	.025	.025
2.2	.136	.079	.058	.046	.040	.035	.032	.029	.028	.026	.025	.024	.023	.022	.022	.021	.021	.021
2.3	.131	.074	.052	.041	.035	.031	.027	.025	.023	.022	.021	.020	.019	.018	.018	.018	.017	.017
2.4	.126	.069	.048	.037	.031	.027	.024	.022	.020	.019	.018	.017	.016	.015	.015	.014	.014	.014
2.5	.121	.065	.044	.033	.027	.023	.020	.018	.017	.016	.015	.014	.013	.012	.012	.012	.011	.011
2.6	.117	.061	.040	.030	.024	.020	.018	.016	.014	.013	.012	.012	.011	.010	.010	.010	.009	.009
2.7	.113	.057	.037	.027	.021	.018	.015	.014	.012	.011	.010	.010	.009	.008	.008	.008	.008	.007
2.8	.109	.054	.034	.024	.019	.016	.013	.012	.010	.009	.009	.008	.008	.007	.007	.006	.006	.006
2.9	.106	.051	.031	.022	.017	.014	.011	.010	.009	.008	.007	.007	.006	.005	.005	.005	.005	.005
3.0	.102	.048	.029	.020	.015	.012	.010	.009	.007	.007	.006	.006	.005	.004	.004	.004	.004	.004
3.1	.099	.045	.027	.018	.013	.011	.009	.007	.006	.006	.005	.005	.004	.004	.004	.003	.003	.003
3.2	.096	.043	.025	.016	.012	.009	.008	.006	.005	.005	.004	.004	.003	.003	.003	.003	.003	.002
3.3	.094	.040	.023	.015	.011	.008	.007	.005	.005	.004	.004	.003	.003	.002	.002	.002	.002	.002
3.4	.091	.038	.021	.014	.010	.007	.006	.005	.004	.003	.003	.003	.002	.002	.002	.002	.002	.002
3.5	.089	.036	.020	.012	.009	.006	.005	.004	.003	.003	.002	.002	.002	.002	.002	.001	.001	.001
3.6	.086	.035	.018	.011	.008	.006	.004	.004	.003	.002	.002	.002	.002	.001	.001	.001	.001	.001
3.7	.084	.033	.017	.010	.007	.005	.004	.003	.002	.002	.002	.002	.001	.001	.001	.001	.001	.001
3.8	.082	.031	.016	.010	.006	.004	.003	.003	.002	.002	.001	.001	.001	.001	.001	.001	.001	.001
3.9	.080	.030	.015	.009	.006	.004	.003	.002	.002	.001	.001	.001	.001	.001	.001	.001	.001	.001
4.0	.078	.029	.014	.008	.005	.004	.003	.002	.002	.001	.001	.001	.001	.001	.001	.001	.000	.000

(continued)

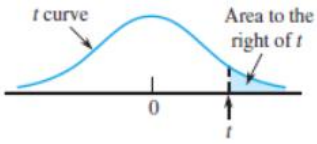

t / ν	19	20	21	22	23	24	25	26	27	28	29	30	35	40	60	120	∞ (= z)
0.0	.500	.500	.500	.500	.500	.500	.500	.500	.500	.500	.500	.500	.500	.500	.500	.500	.500
0.1	.461	.461	.461	.461	.461	.461	.461	.461	.461	.461	.461	.461	.460	.460	.460	.460	.460
0.2	.422	.422	.422	.422	.422	.422	.422	.422	.421	.421	.421	.421	.421	.421	.421	.421	.421
0.3	.384	.384	.384	.383	.383	.383	.383	.383	.383	.383	.383	.383	.383	.383	.383	.382	.382
0.4	.347	.347	.347	.347	.346	.346	.346	.346	.346	.346	.346	.346	.346	.346	.345	.345	.345
0.5	.311	.311	.311	.311	.311	.311	.311	.311	.311	.310	.310	.310	.310	.310	.309	.309	.309
0.6	.278	.278	.278	.277	.277	.277	.277	.277	.277	.277	.277	.277	.276	.276	.275	.275	.274
0.7	.246	.246	.246	.246	.245	.245	.245	.245	.245	.245	.245	.245	.244	.244	.243	.243	.242
0.8	.217	.217	.216	.216	.216	.216	.216	.215	.215	.215	.215	.215	.215	.214	.213	.213	.212
0.9	.190	.189	.189	.189	.189	.189	.188	.188	.188	.188	.188	.188	.187	.187	.186	.185	.184
1.0	.165	.165	.164	.164	.164	.164	.163	.163	.163	.163	.163	.163	.162	.162	.161	.160	.159
1.1	.143	.142	.142	.142	.141	.141	.141	.141	.141	.140	.140	.140	.139	.139	.138	.137	.136
1.2	.122	.122	.122	.121	.121	.121	.121	.120	.120	.120	.120	.120	.119	.119	.117	.116	.115
1.3	.105	.104	.104	.104	.103	.103	.103	.103	.102	.102	.102	.102	.101	.101	.099	.098	.097
1.4	.089	.089	.088	.088	.087	.087	.087	.087	.086	.086	.086	.086	.085	.085	.083	.082	.081
1.5	.075	.075	.074	.074	.074	.073	.073	.073	.073	.072	.072	.072	.071	.071	.069	.068	.067
1.6	.063	.063	.062	.062	.062	.061	.061	.061	.061	.060	.060	.060	.059	.059	.057	.056	.055
1.7	.053	.052	.052	.052	.051	.051	.051	.051	.050	.050	.050	.050	.049	.048	.047	.046	.045
1.8	.044	.043	.043	.043	.042	.042	.042	.042	.042	.041	.041	.041	.040	.040	.038	.037	.036
1.9	.036	.036	.036	.035	.035	.035	.035	.034	.034	.034	.034	.034	.033	.032	.031	.030	.029
2.0	.030	.030	.029	.029	.029	.028	.028	.028	.028	.028	.027	.027	.027	.026	.025	.024	.023
2.1	.025	.024	.024	.024	.023	.023	.023	.023	.023	.022	.022	.022	.022	.021	.020	.019	.018
2.2	.020	.020	.020	.019	.019	.019	.019	.018	.018	.018	.018	.018	.017	.017	.016	.015	.014
2.3	.016	.016	.016	.016	.015	.015	.015	.015	.015	.015	.014	.014	.014	.013	.012	.012	.011
2.4	.013	.013	.013	.013	.012	.012	.012	.012	.012	.012	.012	.011	.011	.011	.010	.009	.008
2.5	.011	.011	.010	.010	.010	.010	.010	.010	.009	.009	.009	.009	.009	.008	.008	.007	.006
2.6	.009	.009	.008	.008	.008	.008	.008	.008	.007	.007	.007	.007	.007	.007	.006	.005	.005
2.7	.007	.007	.007	.007	.006	.006	.006	.006	.006	.006	.006	.006	.005	.005	.004	.004	.003
2.8	.006	.006	.005	.005	.005	.005	.005	.005	.005	.005	.005	.004	.004	.004	.003	.003	.003
2.9	.005	.004	.004	.004	.004	.004	.004	.004	.004	.004	.004	.003	.003	.003	.003	.002	.002
3.0	.004	.004	.003	.003	.003	.003	.003	.003	.003	.003	.003	.003	.002	.002	.002	.002	.001
3.1	.003	.003	.003	.003	.003	.002	.002	.002	.002	.002	.002	.002	.002	.002	.001	.001	.001
3.2	.002	.002	.002	.002	.002	.002	.002	.002	.002	.002	.002	.002	.001	.001	.001	.001	.001
3.3	.002	.002	.002	.002	.002	.001	.001	.001	.001	.001	.001	.001	.001	.001	.001	.001	.000
3.4	.002	.001	.001	.001	.001	.001	.001	.001	.001	.001	.001	.001	.001	.001	.001	.000	.000
3.5	.001	.001	.001	.001	.001	.001	.001	.001	.001	.001	.001	.001	.001	.001	.000	.000	.000
3.6	.001	.001	.001	.001	.001	.001	.001	.001	.001	.001	.001	.001	.000	.000	.000	.000	.000
3.7	.001	.001	.001	.001	.001	.001	.001	.001	.000	.000	.000	.000	.000	.000	.000	.000	.000
3.8	.001	.001	.001	.000	.000	.000	.000	.000	.000	.000	.000	.000	.000	.000	.000	.000	.000
3.9	.000	.000	.000	.000	.000	.000	.000	.000	.000	.000	.000	.000	.000	.000	.000	.000	.000
4.0	.000	.000	.000	.000	.000	.000	.000	.000	.000	.000	.000	.000	.000	.000	.000	.000	.000